

PHOTOLUMINESCENCE AND ELECTRICAL PROPERTIES
OF IMPURITY-DOPED ZnSe LAYERS GROWN
BY MOLECULAR BEAM EPITAXY

分子線エピタキシー法により成長した不純物添加ZnSe薄膜の
フォトルミネッセンス特性と電気特性に関する研究

NOVEMBER 1991

KAZUHIRO OHKAWA



①

**PHOTOLUMINESCENCE AND ELECTRICAL PROPERTIES
OF IMPURITY-DOPED ZnSe LAYERS GROWN
BY MOLECULAR BEAM EPITAXY**

分子線エピタキシー法により成長した不純物添加ZnSe薄膜の
フォトルミネッセンス特性と電気特性に関する研究

NOVEMBER 1991

KAZUHIRO OHKAWA

CONTENTS

Acknowledgment	iii
1. Introduction: Wide band-gap II-VI compounds	1
References	9
2. Preparation of ZnSe layers by molecular beam epitaxy	14
2.1. Introduction	14
2.2. Molecular-beam epitaxial growth of ZnSe	19
2.2.1. Heteroepitaxy on GaAs substrates	19
2.2.2. Homoepitaxy	23
2.3. Doping of ZnSe	26
2.3.1. Gallium doping	26
2.3.2. Chlorine doping	27
2.3.3. Nitrogen doping with a high-purity N_2^+ ion beam	32
2.3.4. Active-nitrogen doping with a N_2 ($A^3\Sigma_u^+$) metastable beam	33
References	39
3. Characterization of ZnSe layers	44
3.1. Introduction	44
3.2. Optical measurements	46
3.3. Electrical measurements	51
References	54
4. Effect of biaxial strain on exciton luminescence from ZnSe heteroepitaxial layers	56
4.1. Introduction	56
4.2. Theoretical calculation of effect of biaxial strain	58
4.2.1. Layer-thickness dependence of lattice parameters	58

4.2.2. Valence band split due to biaxial strain	62
4.3. Effect of biaxial strain on bound exciton emissions	65
4.3.1. Temperature dependence	65
4.3.2. Layer-thickness dependence	70
4.3.3. Exciton luminescence from strain-free layers	71
References	73
5. Electrical and optical properties of Cl-doped n-type ZnSe layers	75
5.1. Introduction	75
5.2. Activation of donors and scattering mechanisms of electrons	77
5.3. Donor concentration dependence of photoluminescence properties	86
5.4. Screening and Stark effects due to donors on excitons	89
References	93
6. Electrical and optical properties of nitrogen-doped p-type ZnSe layers	95
6.1. Introduction	95
6.2. Nitrogen concentration dependence of photoluminescence properties	96
6.3. Impurity levels in nitrogen-doped homoepitaxial layers	99
6.4. Electrical properties	102
6.5. Relationships between electrical and photoluminescence properties	106
References	108
7. Conclusion	110
Appendix	115
A. Preparation of ZnSe substrates for homoepitaxy	115
B. ZnSe p-n junction LEDs	124

ACKNOWLEDGMENT

The author would like to express his deepest gratitude to Professor Taizo Masumi of University of Tokyo for his guidance and encouragement throughout the course of this work. The author wishes to make deep acknowledgment to Professors Katsumi Sakurai, Susumu Komiyama, Seiichi Kagoshima, and Makoto Gonokami of University of Tokyo and Professor Takafumi Yao of Hiroshima University for their guidance.

The author wishes to express his gratitude to Drs. Tsuneharu Nitta, Tohru Fukui and Kenji Kanai of Matsushita Electric Industrial Co., Ltd. for supporting this work and for their continuous encouragement.

The author also wishes to express his gratitude to Drs. Kiyotaka Wasa and Osamu Yamazaki of Matsushita Electric Industrial Co., Ltd. for their continuous encouragement and their helpful advice.

The author is very grateful to Dr. Tsunoe Mitsuyu for sharing his insight in many aspects of the work. He is also very grateful to Messrs. Takeshi Karasawa and Akira Ueno for their useful discussions and for performing many of the experiments.

The author would like to thank Drs. Takashi Hirao and Kentaro Setsune of Matsushita Electric Industrial Co., Ltd. for their useful advice and many insightful discussions. He would also like to thank Drs. Yoshio Manabe, Masatoshi Kitagawa, Mikihiko Nishitani, Akihisa Yoshida and Koichi Mizuno of Matsushita Electric Industrial Co., Ltd. for their useful discussions.

The author would like to thank Messrs. Suguru Nakamura, Yoshiaki Yoshioka and their members of Matsushita Technoresearch, Inc. for their contribution to x-ray and SIMS analyses.

The author thanks to all the colleagues in the laboratory for the varieties of assistance during the experiments and the other working.

CHAPTER 1

INTRODUCTION: WIDE BAND-GAP II-VI COMPOUNDS

Wide band-gap II-VI compounds such as Zn-chalcogenides and Cd-chalcogenides are excellent luminescent materials in the visible to ultraviolet spectrum region.^{1,2} These II-VI compounds have wide direct band-gaps ranging from 1.52 eV (CdTe) in infrared to 3.54 eV (ZnS) in ultraviolet, and their ternary² and quaternary alloys³ can cover all the range of the visible to ultraviolet spectrum. The spectral region, short wavelength in particular, is difficult to be achieved by III-VI compounds as shown in Fig. 1.1. Therefore, these II-VI compounds are the most promising materials for light emitters in this spectrum region.⁴ ZnSe has been studied most intensively among II-VI compounds⁵: 1) it has wide band-gap of 2.7 eV at room temperature which draws interests in possible application for efficient light-emitting diodes (LEDs) and laser diodes (LDs) in blue region;⁶ 2) large third-order nonlinear susceptibility observed in exciton phenomena⁷ will be used for the realization of nonlinear optical devices. ZnSe material parameters are shown in Table 1.1 together with the ratios of material parameters of ZnSe and GaAs to compare II-VI and III-V compounds.

Si, Ge and III-V compounds have the ability to control electron and hole concentrations by selective incorporation of donors and acceptors. Wide band-gap II-VI compounds have, however, difficulty in achieving amphoteric doping. In general, there is a tendency that the tellurides are readily doped p-type, whereas the selenides and the sulphides are doped

n-type. There are two different explanations for the difficulties in amphoteric doping. Aven,²¹ Neumark²² and Igagi²³ have insisted that the residual impurities in II-VI compounds are the main reason. However, Mandel²⁴ and Kröger²⁵ have claimed so-called self-compensation effect, because wide band-gap readily introduces vacancies in crystal to compensate carriers caused by doping. Vacancies are easily generated during crystal growth since II-VI compounds have large ionicity relative to III-V compounds.

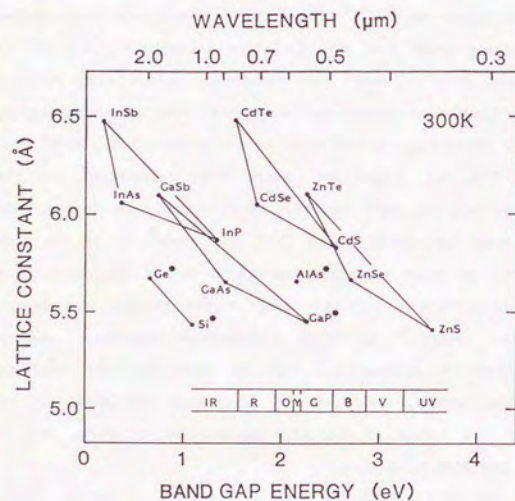


FIG. 1.1. Energy gaps and lattice constants of representative semiconductors of group VI, III-V and II-VI compounds. Symbol (*) indicates indirect band-gap semiconductors.

TABLE 1.1. Properties of ZnSe

Parameter	Value	Reference	Ratio(ZnSe/GaAs)
Crystal structure	Zinc blende		1
Lattice parameter (Å)	5.6693 (bulk, 300K)	8	1.0028
Energy gap E_g (eV)	2.715 (bulk, 300K)	9	1.9
Ionicity	0.630	10	2
Melting point (°C)	1250	11	1.01
Density ρ (g/cm ⁻³)	5.266	12	0.99
Electron effective mass m_e^*	0.16 m_0	13	2.3
Hole effective mass m_h^*	0.70 m_0	14	1.4
High-frequency dielectric constant ϵ_∞	5.9 ϵ_0	15	0.54
Static dielectric constant ϵ_s	9.14 ϵ_0	16	0.71
Exciton binding energy (meV)	21	17	5
Optical phonon energy $\hbar\omega_{LO}$ (meV)	31.7	18	0.87
Optical phonon Debye temperature θ_d (K) = $\hbar\omega_{LO}/k$	368	18	0.87
Piezoelectric coefficient e_{14} (esu/cm ²)	1.47x10 ⁴	19	0.31
Conduction band acoustic deformation potential E_{AC} (eV)	4.2	20	0.54
Valence band acoustic deformation potential E_{AC} (eV)	4.0	20	0.51
Longitudinal velocity of sound v_s (cm/s)	4.44x10 ⁵	12	0.9

Understanding of physical properties of II-VI compounds is necessary to achieve amphoteric doping. Photoluminescence (PL) measurement is one of the most powerful methods to obtain physical information from high-resistivity impurity-doped II-VI compounds. PL measurement with high resolution is possible at low temperature due to the small thermal disturbance. Excitons are created under these circumstances. When the exciton is in the vicinity of an impurity, the total energy of the system is reduced. Therefore it is energetically favorable for the exciton remain near the impurity; the exciton becomes "bound" to the impurity. Increase in binding energy of an exciton depends on a species of the impurity. Bhargava²⁶ and Dean et al.²⁷ have shown donor ionization energies in ZnSe through the investigation of bound exciton emissions as shown in Table 1.2. The ionization energy is mostly determined by dielectric constant and electron effective mass of ZnSe, and the dependence on donor species is very weak. In case of acceptors, the ionization energy depends on the species of impurities as summarized in Table 1.3. Acceptors have, as a rule, large ionization energy relative to donors due to the heavier effective mass of a hole. PL measurement provides detailed information about impurity levels understanding of which will greatly contribute to realize to amphoteric doping of II-VI compounds.

GaAs has been widely used as a substrate for ZnSe epitaxial growth³⁴ because of small lattice mismatch. Although a single emission peak of excitons bound to donors or acceptors was observed for single crystal of ZnSe,³⁵ heteroepitaxial layers of ZnSe on GaAs showed two bound excitonic emission lines with which were related to donors³⁶ and acceptors³⁷. Crystallographic difference between homoepitaxy and heteroepitaxy arises from lattice mismatch and differential thermal contraction. Even the small lattice mismatch influences the early stage of ZnSe epitaxial growth. Mitsuhashi et al.³⁸ have shown that a thin ZnSe

TABLE 1.2. Ionization energies for various donor impurities in ZnSe.

Donor	Ionization energy (meV)	References
B	25.6	26
Al	25.6	27
Ga	27.2	27
In	28.2	27
F	28.8	27
Cl	26.2	26
Hydrogen model	28.8	28

TABLE 1.3. Ionization energies for various acceptor impurities in ZnSe.

Acceptor	Ionization energy (meV)	References
Li	114	29
Na	102	30
Cu	650	31
Ag	430	26
Au	550	26
N	111	32
P	84	33
As	110	26
Hydrogen model	108	26

layer is coherently grown on a GaAs substrate with tetragonal distortion. Yao et al.³⁹ have pointed out that difference in thermal contraction causes large biaxial tensile strain in thick ZnSe layers on cooling below the growth temperature. Pikus et al.⁴⁰ have derived a general expression of the orbital-strain Hamiltonian of Si and Ge under uniaxial strain. Asai et al.⁴¹ have estimated the valence band split of III-V compound biaxially strained by lattice mismatch from the Pikus' theory. In the case of II-VI/III-V heteroepitaxy, calculation of biaxial strain at low temperature (same as that of PL measurements) is necessary to investigate the effect of biaxial strain on PL properties. There is, however, no measurement or theoretical calculation of low-temperature lattice parameters of biaxially strained ZnSe heteroepitaxial layers.

In low-temperature PL measurements, high-purity, n- and p-type ZnSe layers exhibit intense free exciton emission (E_x), neutral donor-bound exciton emission (I_2) and neutral acceptor-bound exciton emission (I_1), respectively. Relatively pure ZnSe layers have been grown by molecular beam epitaxy (MBE)⁴² and metal-organic chemical vapor deposition (MOCVD)⁴³ using ultra-high-purity source materials. Undoped ZnSe layers show high resistivity ($> 10^4 \Omega\text{cm}$ at 300 K), indicating residual donor concentration is very low. The intensity of I_2 emission increases with the increase in donor concentration.⁴⁴ Heavily-doped n-type ZnSe will have many ionized donors and free electrons which cause Stark and screening effects on excitons.^{45,46} The effects have been observed for samples with high carrier concentration greater than the critical concentration for Mott transition⁴⁷ (N_M). Doping with group III elements can yield n-type ZnSe.⁴⁸⁻⁵⁰ Free electron concentrations of Ga-doped⁴⁹ and Al-doped⁵⁰ ZnSe were limited to the mid 10^{17} cm^{-3} . Since the concentration of the Mott transition for ZnSe is $N_M = 5.6 \times 10^{17} \text{ cm}^{-3}$ (see Sec. 5.2), the properties and behavior of excitons in degenerated ZnSe are

left to be examined as a subject of our interest.

Group I and V elements act as acceptors in ZnSe. The ionization energy becomes larger for heavier hole effective mass. The smallest ionization energy is obtained for phosphorus at 84 meV. Even this value is greater than the thermal energy at room temperature $kT = 26 \text{ meV}$, which implies small thermal activation of acceptors even at room temperature. This would be a severe problem in achieving low-resistivity p-type ZnSe. Another problem of phosphorus doping is the creation of deep levels which is observed in PL measurement.⁵¹ Phosphorus doping was not realized p-type conduction. Several doping techniques have realized p-type ZnSe.^{18,52-56} Nishizawa et al.⁵³ have reported on Li-doped p-type ZnSe bulk grown by the temperature difference method under controlled vapor pressure in 1985. P-type conduction was confirmed for Li-doped ZnSe films grown by MBE⁵⁷ and MOCVD⁵⁸. Free hole concentration was, however, limited to the order of 10^{15} cm^{-3} . Haase et al.⁵⁹ and Sasaki et al.⁶⁰ have shown that the Li atoms in ZnSe are very diffusive during growth. Diffusion of dopants causes difficulty in forming p-n junctions. Zhu et al.⁶¹ have first reported on successful suppression of Li diffusion by delta-doping technique in MBE growth. Further study will be needed to obtain low-resistivity Li-doped p-type ZnSe. As Stutius⁶² has pointed out, nitrogen (N) is the most promising element as a p-type dopant in ZnSe because the diffusion of N is expected to be small and may not form deep levels. Park et al.⁶³ reported the formation of shallow acceptors in N-doped ZnSe grown by MBE under large N_2/NH_3 overpressures. Observation of p-type conduction has not been achieved partly due to low sticking coefficients of N_2 and NH_3 molecules. Mitsuyu et al.⁴³ have pointed out that the increase in sticking coefficient is necessary for providing a sufficient doping of nitrogen.

There still remains some important issues to be resolved. PL

properties of ZnSe, the effect of biaxial strain on bound exciton emission in particular, are not well understood. Screening and Stark effects in ZnSe has not been observed so far since degenerated ZnSe have not been obtained. Electrical properties of ZnSe are not satisfactorily controllable: 1) free electron concentration of n-type ZnSe is limited to the order of 10^{17} cm^{-3} ; 2) incorporation of N into ZnSe is too little to obtain p-type conduction. If amphoteric doping into ZnSe is achieved, it will provide blue light-emitters and a new concept of doping for other wide band-gap II-VI compounds.

PL and electrical properties of low-resistivity p-type and n-type ZnSe will be clarified in this thesis. High-quality ZnSe epitaxial layers and successful amphoteric doping are crucial for the understanding of these properties. Details of the preparation technique are described in Chapter 2. ZnSe homoepitaxial layers obtained were strain-free and had good crystallinity.⁶⁴⁻⁶⁶ Degenerated n-type ZnSe has been grown by Cl doping.^{66,67} Low-resistivity p-type ZnSe was accomplished by active-nitrogen doping.^{18,66,68-72} Chapter 3 shows characterization of doped ZnSe. PL properties of doped ZnSe heteroepitaxial layers are discussed in chapter 4. The chapter will present the effect of biaxial strain on bound exciton luminescence.^{37,66,73} Electron transport phenomena in Cl-doped ZnSe are described in chapter 5. This chapter also discusses optical properties of fully degenerated n-type ZnSe. Chapter 6 will present relationships between electrical and optical properties of N-doped p-type ZnSe.^{18,66,68-70} Chapter 7 concludes the thesis by summarizing PL and electrical properties of impurity-doped ZnSe layers.

From the point of view of a device, Cl and active-nitrogen doping are new practical techniques to obtain low-resistivity n- and p-type ZnSe layers. Dry etching is also a novel treatment of ZnSe substrates for homoepitaxy which gives ZnSe epitaxial layers with good crystallinity. Not

only these novel techniques give new scientific information of ZnSe, but the techniques will make it possible to fabricate LEDs and LDs by using wide band-gap II-VI compounds. Fabrication of blue LEDs and its characteristics are described in appendix. These are the first blue LEDs with good optical and electrical properties.

References

- 1 B. Ray, in "II-VI Compounds", (Pergamon, Oxford, 1969).
- 2 Y.S. Park, and B.K. Skin, in "Electroluminescence" edited by J.I. Pankove (Springer, Berlin, 1977), pp. 135-170.
- 3 T. Ido, J. Electron. Mater. **9**, 869 (1980).
- 4 T. Yao, IEICE Technical Report, EFM-86-31, p. 79.
- 5 J. Gutowski, N. Presser, and G. Kudlek, Phys. Stat. Sol. (a) **120**, 11 (1990).
- 6 T. Yao, Y. Makita, and S. Maekawa, Appl. Phys. Lett. **35**, 97 (1979).
- 7 T. Saiki, K. Takeuchi, T. Mitsuyu, K. Ohkawa, and M. Kuwata-Gonokami, to be published in Appl. Phys. Lett. (1991).
- 8 H.P. Singh, and B. Dayal, Phys. Status Solidi. **23**, K93 (1967).
- 9 Y. Shirakawa, and H. Kukimoto, J. Appl. Phys. **51**, 2014 (1980).
- 10 J.C. Phillips, in "Bonds and Bands in Semiconductors", (Academic Press, New York, 1973).
- 11 M.R. Lorenz, in "Physics and Chemistry of II-VI compounds", edited by M. Aven and J.S. Prener, (North-Holland, Amsterdam, 1967), Chap. 3.
- 12 W.H. Gust, J. Appl. Phys. **53**, 4843 (1982).
- 13 J.L. Merz, H. Kukimoto, K. Nassau, and J.W. Shiever, Phys. Rev. B **6**, 545

- (1972).
- 14 B. Segall, in "Physics and Chemistry of II-VI Compounds" edited by M. Aven and J.S. Prener, (North-Holland, Amsterdam, 1967), Chap. 1.
 - 15 D.T.F. Marple, *J. Appl. Phys.* **35**, 539 (1964).
 - 16 D.A. Berlincourt, H. Jaffe, and L.R. Shiozawa, *Phys. Rev.* **129**, 1009 (1963).
 - 17 G.E. Hite, D.T.F. Marple, M. Aven, and B. Segall, *Phys. Rev.* **156**, 850 (1967).
 - 18 K. Ohkawa, and T. Mitsuyu, *J. Appl. Phys.* **70**, 439 (1991).
 - 19 D.A. Berlincourt, D.R. Curran, and H. Jaffe, "Physical Acoustics, Vol. 1", edited by Mason, (Academic Press, London, 1964), p. 182.
 - 20 H.E. Ruda, *J. Appl. Phys.* **59**, 1220 (1986); *ibid.* **59**, 3516 (1986).
 - 21 M. Aven, in "II-VI Semiconducting Compounds" edited by D.G.Thomas (Benjamin, New York, 1967), pp. 1232-1259.
 - 22 G.F. Neumark, *J. Appl. Phys.* **51**, 3383 (1980).
 - 23 K. Igaki, *Solid State Physics* **17**, 97 (1982).
 - 24 G. Mandel, *Phys. Rev.* **134**, A1073 (1964).
 - 25 F.A. Kröger, *J. Chem. Phys. Solids* **26**, 1707 (1965).
 - 26 P.J. Dean, D.C. Herbert, C.J. Werkhoven, B.J. Fitzpatrick, and R.N. Bhargava *Phys. Rev. B* **23**, 4888 (1981).
 - 27 R.N. Bhargava, *J. Cryst. Growth* **59**, 15 (1982).
 - 28 J.L. Merz, H. Kukimoto, K. Nassau, and J.W. Schiever, *Phys. Rev. B* **6**, 545 (1964).
 - 29 J.L. Merz, K. Nassau, and J.W. Schiever, *Phys. Rev. B* **8**, 1444 (1973).
 - 30 Y. Yamada, T. Taguchi, and A. Hiraki, *Inst. Phys. Conf. Ser. No 95: Chapter 6*, paper presented at Int. Conf. "Shallow Impurities in Semiconductors" (Lingköping, Sweden, 1988), p. 377.
 - 31 P.J. Dean, *Czech. J. Phys. B* **30**, 272 (1980).
 - 32 P.J. Dean, W. Stutius, G.F. Neumark, B.J. Fitzpatrick, and R.N. Bhargava, *Phys. Rev. B* **27**, 2419 (1983).
 - 33 K. Kosai, B.J. Fitzpatrick, H.G. Grimmeiss, R.N. Bhargava, and G.F. Neumark, *Appl. Phys. Lett.* **35**, 194 (1979).
 - 34 R.L. Gunshor, and L.A. Kolodziejski, *IEEE J. Quantum Electron.* **24**, 1744 (1988).
 - 35 M. Isshiki, *J. Cryst. Growth* **86**, 615 (1988).
 - 36 T. Yao, Y. Makita, and S. Maekawa, *Jpn. J. Appl. Phys.* **20**, L741 (1981).
 - 37 K. Ohkawa, T. Mitsuyu, and O. Yamazaki, *Phys. Rev. B* **38**, 12465 (1988).
 - 38 H. Mitsuhashi, I. Mitsuishi, M. Mizuta, and H. Kukimoto, *Jpn. J. Appl. Phys.* **24**, L578 (1985).
 - 39 T. Yao, Y. Okada, S. Matui, K. Ishida, and I. Fujimoto, *J. Cryst. Growth* **81**, 518 (1987).
 - 40 G.E. Pikus, and G.L. Bir, *Sov. Phys. Solid State* **1**, 1502 (1960).
 - 41 H. Asai, and K. Oe, *J. Appl. Phys.* **54**, 2052 (1983).
 - 42 T. Mitsuyu, K. Ohkawa, and O. Yamazaki, *Appl. Phys. Lett.* **49**, 1348 (1986).
 - 43 J. Wakitani, K. Yanashima, T. Yasuda, J. Yoshino, and H. Kukimoto, in *Abstracts of the Autumn Meeting of the Japan Society of Applied Physics*, 29p-PA-8, 1989.
 - 44 K. Ohkawa, T. Mitsuyu, and O. Yamazaki, *J. Appl. Phys.* **62**, 3216 (1987).
 - 45 E. Hanamura, *J. Phys. Soc. Japan* **28**, 120 (1970).
 - 46 H. Kukimoto, S. Shionoya, S. Toyotomi, and K. Morigaki, *J. Phys. Soc. Japan*, **28**, 110 (1970).
 - 47 N.F. Mott, *Phil. Mag.* **6**, 287 (1961).
 - 48 F. Kitagawa, T. Mishima, and K. Takahashi, *J. Electrochem. Soc.* **127**, 937 (1980).

- 49 T. Niina, T. Minato, and K. Yoneda, *Jpn. J. Appl. Phys.* **21**, L387 (1982).
- 50 W. Stutius, *J. Appl. Phys.* **53**, 284 (1981).
- 51 J.E. Nicholls, and J.J. Davies, *J. Phys. C* **12**, 1917 (1979).
- 52 R.J. Robinson, and Z.K. Kun, *Appl. Phys. Lett.* **27**, 74 (1975).
- 53 J. Nishizawa, R. Suzuki, and Y. Okuno, *J. Appl. Phys.* **59**, 2256 (1985).
- 54 T. Yasuda, I. Mitsuishi, and H. Kukimoto, *Appl. Phys. Lett.* **52**, 57 (1988).
- 55 A. Ohki, N. Shibata, and S. Zembutsu, *Jpn. J. Appl. Phys.* **27**, L909 (1988).
- 56 A. Taike, M. Migita, and H. Yamamoto, *Appl. Phys. Lett.* **56**, 1989 (1990).
- 57 H. Cheng, J.M. DePuydt, J.E. Potts, and T.L. Smith, *Appl. Phys. Lett.* **52**, 147 (1988).
- 58 I. Mitsuishi, J. Shibatani, M.H. Kao, M. Yamamoto, J. Yoshino, and H. Kukimoto, *Jpn. J. Appl. Phys.* **29**, L733 (1990).
- 59 H.A. Haase, H. Cheng, J.M. DePuydt, and J.E. Potts, *J. Appl. Phys.* **67**, 448 (1990).
- 60 T. Sasaki, T. Oguchi, and H. Katayama-Yoshida, in "Defect Control in Semiconductors" edited by K. Sumino, (Elsevier Science Publisher, North-Holland, 1990), pp. 959-963.
- 61 Z. Zhu, H. Mori, M. Kawashima, and T. Yao, in *Collected Abstracts of 5th International Conference on II-VI Compounds*, Tamano, Okayama, September 8-13, 1991, We1a-18.
- 62 W. Stutius, *J. Cryst. Growth* **59**, 1 (1982).
- 63 R.M. Park, H.A. Mar, and N.M. Salansky, *J. Appl. Phys.* **58**, 1047 (1985).
- 64 K. Ohkawa, T. Karasawa, A. Yoshida, T. Hirao, and T. Mitsuyu, *Appl. Phys. Lett.* **54**, 2553 (1989).
- 65 K. Ohkawa, T. Karasawa, and T. Mitsuyu, *J. Vac. Sci. Technol. B* **9**, 1934 (1991).

- 66 K. Ohkawa, A. Ueno, and T. Mitsuyu, to be published in *J. Cryst. Growth* (1992).
- 67 K. Ohkawa, T. Mitsuyu, and O. Yamazaki, *J. Appl. Phys.* **62**, 3216 (1987).
- 68 K. Ohkawa, T. Karasawa, and T. Mitsuyu, in *Abstracts of 6th International Conference on Molecular Beam Epitaxy*, San Diego, August 1990, PIII-21.
- 69 K. Ohkawa, T. Karasawa, and T. Mitsuyu, *Jpn. J. Appl. Phys.* **30**, L152 (1991).
- 70 K. Ohkawa, T. Karasawa, and T. Mitsuyu, *J. Cryst. Growth* **111**, 797 (1991).
- 71 K. Ohkawa, A. Ueno, and T. Mitsuyu, to be published in *Jpn. J. Appl. Phys.* December (1991).
- 72 K. Ohkawa, and T. Mitsuyu, to be published in *J. Lumin.*
- 73 K. Ohkawa, T. Mitsuyu, and O. Yamazaki, *J. Cryst. Growth* **86**, 329 (1988).

CHAPTER 2

PREPARATION OF ZnSe LAYERS BY MOLECULAR BEAM EPITAXY

2.1. Introduction

II-VI compounds epilayers have been grown by means of sputtering,¹ liquid phase epitaxy (LPE),² vapor phase epitaxy (VPE),³ molecular beam epitaxy (MBE)⁴ and metal-organic chemical vapor deposition (MOCVD)⁵ (the expression MOVPE [metal-organic vapor phase epitaxy] is often used synonymously and sometimes preferred to emphasize the epitaxial growth). These are very promising techniques for the preparation of high-quality thin films, which is obviously desirable from a device point of view. In spite of high melting point of ZnSe 1250 °C, typical growth temperature of ZnSe by MBE⁶ and MOCVD⁷ is as low as 280 - 370 °C. These techniques of MBE and MOCVD are characterized as low-temperature and nonequilibrium processes. Low-temperature growth techniques are expected to minimize contamination and the self-compensation effects.⁸

The author has employed MBE process for the growth of ZnSe due to several reasons: 1) ultrahigh vacuum will prevent epitaxial layers from contamination introduced by the growth chamber; 2) material properties can be controlled by the beam intensities of constituent elements and dopants; 3) the lower growth temperature will prevent the formation of vacancy; 4) the surface can be observed by reflection high-energy electron diffraction (RHEED) during the growth; and 5) an epitaxial layer is suitable for device fabrication. MBE growth of II-VI compounds was first reported by

Smith et al.⁹ in 1975. They had studied the surface morphology of II-VI compounds [ZnSe, ZnTe and Zn(SeTe)] layers on GaAs substrates. Yao et al.¹⁰ have succeeded in the growth of ZnSe layers having good crystallinity with smooth surface texture. Most of the work involving the MBE growth of ZnSe has employed GaAs as substrate material. GaAs is an attractive substrate material for several reasons: 1) GaAs takes the zinc blende crystal structure; 2) GaAs has a relatively small lattice mismatch with ZnSe (0.28 %); 3) GaAs is readily available with high quality at a low cost; and 4) surface preparation techniques for MBE are established. The crystallinity of heteroepitaxial ZnSe layers depends on the layer thickness but a FWHM is limited to 95 arc s for the thick layers after lattice relaxation. Some attempts have been made to improve the quality of heteroepitaxial layers. Gunshor et al.¹¹ have grown ZnSe layer/GaAs layer on GaAs substrate, and they have shown that heterovalent interface state density is very low compared with the case without GaAs epitaxial layer. Kamata et al.¹² and Matsumura et al.¹³ reported on lattice matched ZnS_xSe_{1-x} alloy on GaAs, and have showed better crystallinity was possible. The FWHM of ZnSe bulk single crystal could reach 15 arc s¹⁴ which cannot be easily achieved by ZnSe heteroepitaxial layers on GaAs substrates.

Homoepitaxy using the substrates with high crystallinity has, therefore, the potential to provide strain-free ZnSe layers with better crystallinity.¹⁵⁻¹⁸ A major problem in homoepitaxy is the preparation of the ZnSe substrate surface. The damaged layer caused by polishing for the fabrication of ZnSe substrates¹⁹ should be removed. However, surface smooth enough for epitaxial growth cannot be obtained by simple chemical etching due to Se residue often observed after the etching.¹⁸ It is very difficult to remove the polishing damage with smooth surface in chemical etching. Clausen et al.²⁰ have performed reactive ion etching of ZnSe

layer on GaAs to fabricate micro-sized structures. The dry etching will be a promising technique to remove polishing damage for homoepitaxy.

To achieve amphoteric doping of ZnSe, the first step is the growth of high-purity intrinsic ZnSe. The intrinsic semiconductor of ZnSe will exhibit high resistivity. As-grown ZnSe bulk exhibited high resistivity ($> 10^6 \Omega\text{cm}$) not because of high purity but defects caused by so-called self-compensation effect.²¹ MBE and MOCVD are low-temperature growth techniques which are expected to suppress the self-compensation effect.⁸ Undoped ZnSe layers grown by these epitaxial growth techniques, however, exhibit n-type conduction with carrier concentration of 10^{16}cm^{-3} . Ga diffusion into ZnSe epilayer from GaAs substrate is one of the causes of extrinsic donor impurities.²² However, Qui et al.²³ have shown that there is no Ga diffusion at growth temperature of conventional MBE: two monolayers of coherent zinc blende Ga_2Se_3 exists at ZnSe/GaAs heterointerface. Kobayashi²⁴ observed Ga diffusion at the temperature higher than 400 °C. Yoneda et al.²⁵ indicated that undoped high-resistivity ZnSe layers can be grown by MBE using highly purified source materials. It was found that high-resistivity and high-quality intrinsic ZnSe was obtained using ultra-high purity source materials²⁶ of Zn and Se for the MBE growth. Wakitani et al.²⁷ showed that donor impurity also came from the source gases in the case of MOCVD. These results suggest that intrinsic ZnSe with high resistivity is possible by using ultra-high purity source materials both in MBE and in MOCVD.

Incorporation of group III elements produces shallow donors. Statius²⁸ reported on Al-doped n-type ZnSe grown by MOCVD. Kitagawa et al.²⁹ reported in 1980 that Ga-doped ZnSe grown by MBE had resistivity of 0.07 Ωcm . Indium doping into ZnSe was also attempted,^{30,31} but they did not report n-type conduction. Electron concentration in both Al and Ga doping cases has been limited in the order of 10^{17}cm^{-3} . Heavier doping

has resulted in decrease of carrier concentration together with quenching of band-edge photoluminescence (PL) emission.³² Considering these previous works, ultimate carrier concentration by the doping with group III elements may be the order of 10^{17}cm^{-3} . Thus group VII elements are very attractive as a new n-type dopant. Group VII elements, however, have not been investigated as donors.

Group I elements such as Li and Na produce shallow acceptors in ZnSe when they substitutionally replace Zn lattice sites, and Group V elements on the Se lattice sites also act as shallow acceptor. In 1971, Park et al.³³ reported on p-type conduction in Li-doped ZnSe crystal grown both from the vapor phase and from the melt. Its carrier concentration was as low as 10^9cm^{-3} , and resistivity was $10^8 \Omega\text{cm}$. Nishizawa et al.³⁴ showed that carrier concentration of Li-doped ZnSe single crystal could reach the order of 10^{15}cm^{-3} . Unfortunately, Li impurities in ZnSe are very diffusive at the growth temperatures.³⁵ It is very difficult to dope Li atoms in the intended region such as a p-n junction. Na is a shallow acceptor with the ionization energy of 102 meV.³⁶ Neutral acceptor-bound exciton emission (I_1) was observed for Na-doped ZnSe in low-temperature PL measurement,^{36,37} indicating that Na atoms act as shallow acceptors in ZnSe. However, p-type conduction was not reported in literature. Phosphorus has the smallest acceptor-ionization energy of 84 meV which is the advantage of higher activation in ZnSe. Yao et al.³⁸ and Ohkawa et al.³⁹ attempted the growth of P-doped ZnSe by MBE, and P-doped ZnSe exhibited I_1 emission at 2.7914 eV. MBE-grown P-doped ZnSe did not show deep-level emission related to P acceptors. Deep-level emission around 1.9 eV was, however, observed from P-doped ZnSe grown by a modified Bridgmann technique⁴⁰ and MOCVD⁴¹. Reinberg et al.⁴⁰ identified the origin of deep-level emission as P_{Se} center by using electron paramagnetic resonance. Phosphorus is an attractive

dopant for its small ionization energy, but p-type conduction was not observed. Shibli et al.⁴² incorporated As into MBE-grown ZnSe in the range of 10^{17} - 10^{21} atoms/cm³ using Zn₃As₂ as the As source. As-doped ZnSe layers also did not exhibit p-type conduction.

Recent reports show steady improvement of electrical characteristics of p-type ZnSe. In 1988, Yasuda et al.⁴³ reported on p-type ZnSe with the highest carrier concentration of 9×10^{17} cm⁻³, the p-type ZnSe layers on GaAs were grown by MOCVD using Li₃N as a dopant of Li and N acceptors. Suemune et al.⁴⁴ measured hole concentrations around 7×10^{15} cm⁻³ in N-doped (using NH₃) lattice-matched ZnS_{0.06}Se_{0.94}/GaAs epitaxial layers grown by MOCVD. Jin et al.⁴⁵ have reported the p-type conduction in bulk ZnSe by nitrogen ion implantation followed by rapid thermal annealing. These recent reports of p-type conduction were achieved by using nitrogen as an acceptor. Stutius⁴⁶ has pointed out that nitrogen is the most promising element for p-type dopant of ZnSe. Doping of N in MBE process is very difficult because of the low-sticking coefficient of N₂ and NH₃ molecules. Park et al.⁴⁷ reported the MBE growth of N-doped ZnSe under N₂ overpressure of about 10^{-4} Torr. Their ZnSe layers exhibited strong donor-acceptor pair emission (DAP) at low-temperature PL measurement, but p-type conduction was not observed. This result indicates that N₂ molecules at the ground state are dissociated into N atoms on the ZnSe surface and are incorporated as shallow acceptors, but it is difficult to provide sufficient amount of N atoms as dopant due to low-sticking coefficient of N₂. Further study to enhance sticking coefficient of nitrogen is important.

The main purposes of the works presented in this chapter are: 1) preparation of high-quality ZnSe layers both in heteroepitaxy and in homoepitaxy;⁴⁸⁻⁵¹ 2) growth of low-resistivity n-type ZnSe having carrier concentration higher than 10^{17} cm⁻³;^{51,52} and 3) MBE growth of p-type

ZnSe.^{51,53-58}

2.2. Molecular-beam epitaxial growth of ZnSe

2.2.1. Heteroepitaxy on GaAs substrates^{48,52}

MBE system used in this study is shown in Fig. 2.1. The system is a conventional (but not commercial) one, consisting of a cryo-pump, a liquid-N₂ shroud, RHEED and a quadrupole mass spectrometer (QMS). The background pressure was about 10^{-10} Torr. The fluxes of the elements were measured by a quartz oscillator placed in the position of the substrate. This system has several ports for Knudsen cells (K-cells). Unintended impurities²⁷ (such as the halogenides) in source material is a severe problem for doping experiments. The K-cell is, therefore, specially designed for group II and VI elements to purify the source materials. The K-cells have a small orifice with 0.2-2 mm of diameter. Since the small orifice makes it possible to heat the sources to higher temperature compared with the conventional open-type cell, the halogenides have large vapor pressure in the K-cell. Vapor of impurities in source materials is exhausted by a vacuum pump during the early stage of heating. Same purification was also observed in a heat-pipe oven technique for the generation of Ca vapor;⁵⁹ impurities such as Na and chlorides have large vapor pressures and were exhausted by a pump. Using this purification by the K-cell and by high-purity source materials, the MBE growth of high-purity ZnSe layers have been attained.²⁶

The GaAs substrates used were undoped semi-insulating wafers with (100) orientation. The substrate was first cleaned in trichlorethylene, acetone and methanol to remove organic contamination. The substrate was

then etched by 6 μm in $\text{H}_2\text{SO}_4:\text{H}_2\text{O}_2:\text{H}_2\text{O} = 5:1:1$ solution at 50 $^\circ\text{C}$ for 2 min to remove polishing damage resulting from cutting and polishing of wafers. Before growth, the substrate was thermally cleaned at 600 $^\circ\text{C}$ for 10 min under ultrahigh vacuum to remove oxide layer. Source materials used were elemental Zn and Se both with a purity of "6N super" grade. Typical source temperatures were 440 and 240 $^\circ\text{C}$ for Zn and Se, respectively. At these temperatures, Zn beam consists of Zn atoms, and Se beam consists of polyatomic Se species (Se_n ; $n = 2,5,6,7,8$). Beam flux intensities of Zn and

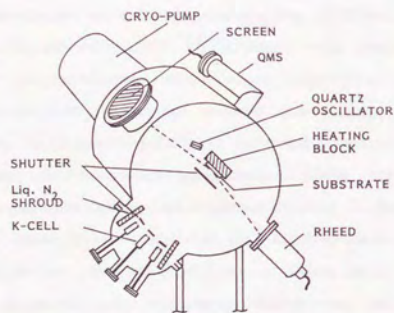


FIG. 2.1. Schematic of Molecular-beam epitaxy system.

Se were about 1.5 and 3.0 $\text{\AA}/\text{s}$, respectively. The beam intensities in atomic number were $J_{\text{Zn}} = J_{\text{Se}} = 1 \times 10^{15}$ atoms/(cm^2s). The growth rate was kept at 2 $\text{\AA}/\text{s}$. Typical growth temperature (T_g) during the growth was 325 $^\circ\text{C}$.

Growth-temperature dependence of electrical and optical properties was investigated to optimize the growth temperature. Ga-doped ZnSe layers on GaAs substrates were grown by MBE with various growth temperatures.

(Details of the growth procedure of the Ga-doped ZnSe layers are described in Sec. 2.3.1) Every sample was grown with the same condition except T_g . The T_g dependence of PL and electrical properties is shown in Fig. 2.2. Hall mobility at room temperature (μ_{RT}) is almost constant for wide T_g range, but the highest Hall mobility at 77 K ($\mu_{77\text{K}}$) was obtained for the layer grown at around $T_g = 300\text{-}325$ $^\circ\text{C}$. The carrier concentration

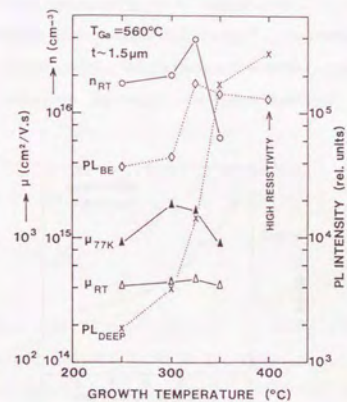


FIG. 2.2. Growth-temperature dependence of PL and electrical properties of n-type Ga-doped ZnSe.

(n_{RT}) showed the maximum value at $T_g = 325$ $^\circ\text{C}$. Band-edge emission (PL_{BE}) at 2.68 eV (462 nm) ascribed to DF emission⁶⁰ has its maximum intensity at around $T_g = 325$ $^\circ\text{C}$, and a broad deep-level emission (PL_{DEEP}) at around 2.1 eV (590 nm) increases rapidly and surpasses the band-edge emission above 350 $^\circ\text{C}$. Consequently the optimum growth

temperature may be around 325 °C; this temperature yields high Hall mobility with high carrier concentration, and strong band-edge PL emission with well-suppressed deep-level PL emission. A possible explanation for these results is that an epitaxial layer grown at 325 °C has good crystallinity. Degraded crystallinity probably introduces deep levels which may act as carrier-traps and scattering centers for free electrons and may be the origins of deep-level PL emissions.

Crystallinity of the layers was evaluated by double-crystal x-ray diffraction measurements. Figure 2.3 shows full widths at half-maximum (FWHMs) of rocking curves measured for ZnSe layers with a variety of layer thicknesses. Since the lattice constant of bulk ZnSe is larger than

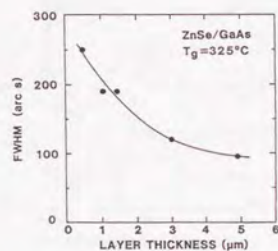
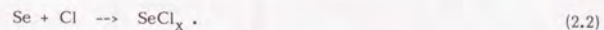


FIG. 2.3. FWHMs of x-ray rocking curves for ZnSe layers plotted as a function of layer thickness.

that of GaAs by 0.28 % at room temperature, the lattice of ZnSe epitaxial layer relaxes with increasing layer thickness. It is found that FWHM reaches 95 arc s at the layer thickness of 4.9 μm whose lattice is fully relaxed. This value is considerably smaller than 250 arc s of MOCVD-grown ZnSe layers.¹²

2.2.2. Homoepitaxy⁴⁹⁻⁵¹

A boule of ZnSe single crystal was sliced parallel to the (100) plane. The substrates were mechanically polished and degreased in trichlorethylene, acetone and methanol. Since as-polished substrates have polishing damage extending to a few microns in depth,¹⁹ the ZnSe substrates were etched by 10 μm in depth to remove the polishing damage. The dry etching was carried out in an etching system with parallel electrodes by introducing BCl₃ (99.9999 %) as a reactive gas. The pressure was 60 mTorr at 1.1 W/cm² of radio-frequency (rf) power density. The ZnSe substrates were positioned on a quartz plate on the cathode which was cooled by a flow of water. ZnSe reacts with BCl₃ plasma, as follows



Both Zn and Se are able to be etched by BCl₃ plasma because zinc chlorides and selenium chlorides have large vapor pressure⁶¹ even at room temperature. The dry-etched substrates exhibited mirror-like surface morphology even after 10-μm etching. The Se residue often observed on chemically etched surface did not exist.

Low-temperature PL spectra from as-polished and dry-etched ZnSe substrates are shown in Fig. 2.4. Dry etching caused drastic changes in PL spectrum: 1) intensity of DAP emission from dry-etched substrate is one order of magnitude larger than that from as-polished substrate; 2) exciton emissions such as E_x at 2.804 eV (442.2 nm), I₂ at 2.798 eV (443.1 nm) and I₁ at 2.793 eV (443.9 nm) clearly appear and peak intensities of those emissions are two orders of magnitude larger. The polishing damage would

have many nonradiative centers that is supposed to act as deep levels. Thus, these changes in the PL properties show that the polishing damage is eliminated by dry etching. FWHM of a (400) rocking curve for the as-polished substrate was about 40 arc s, and it decreased to 20 arc s after the dry etching. This remarkable improvement is consistent with the change in the PL spectra.

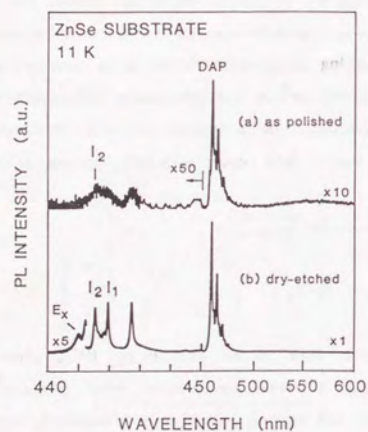


FIG. 2.4. 11-K PL spectra obtained from (a) as-polished ZnSe substrate and (b) 10- μ m etched ZnSe substrate.

Although dry etching eliminates polishing damage, it creates plasma damage on a subsurface of the substrates.⁶² The plasma damage probably consists of ion-induced lattice damage and a residual chloride layer. Dry-etched substrates, furthermore, need a subsequent thermal etching process. Typical thermal etching condition adopted was 600 °C for 10 min. Plasma

X-RAY
TOPOGRAPH

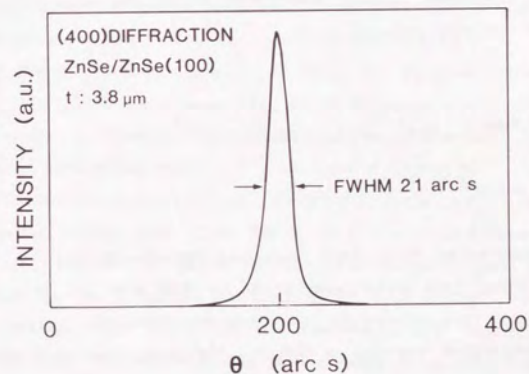


FIG. 2.5. X-ray topograph of (224) diffraction and x-ray rocking curve of the (400) diffraction obtained from an undoped ZnSe homoepitaxial layer with 3.8 μ m thickness.

damage would be decomposed at this temperature. Details of conditions of dry etching and thermal etching will be described in Appendix A.

Crystallinity of homoepitaxial layers was evaluated by means of x-ray topograph and double-crystal x-ray diffraction as shown in Fig. 2.5. Overall x-ray topograph of the (224) diffraction shows the homoepitaxial layer to be uniform, i.e., there is no strain and no grain boundary such as a twinning. A FWHM of the homoepitaxial layer is as narrow as 21 arc s. This value is the narrowest FWHM ever obtained for ZnSe epitaxial layers prepared by MBE and MOCVD. The homoepitaxy using our treatment provides II-VI compounds epitaxial layers with almost the same crystalline quality as III-V compounds epitaxial layers.

2.3. Doping of ZnSe

2.3.1. Gallium doping^{48,63}

GaAs substrates used were undoped, semi-insulating and (100) oriented. Ga-doped ZnSe layers were grown by MBE with Zn, Se and Ga beams. The beam flux ratio of Zn to Se was approximately $J_{Zn}/J_{Se} = 1$. The growth temperature was kept at 325 °C. The growth rate was about 2 Å/s. Ga doping level was controlled by the temperature of the K-cell containing elemental Ga (purity 99.9999 %). Electron concentration obtained was less than $6 \times 10^{17} \text{ cm}^{-3}$. The Ga-doped ZnSe layers used for PL measurement had carrier concentration less than $1 \times 10^{17} \text{ cm}^{-3}$, and layer thicknesses were in the range 0.5-5 μm. Ga-doped ZnSe layers with carrier concentration higher than this level show strong deep-level emission. Ga-doped ZnSe layers with this doping level is suitable for the investigation of band-edge PL emission since low-temperature PL spectrum is dominated

by neutral donor-bound exciton emission (I_x), and deep-level emission is negligible.

2.3.2. Chlorine doping⁵²

The MBE growth was performed on semi-insulating (100) GaAs or (100) ZnSe substrates. The purity of ZnCl_2 powder used for the chlorine doping was 99.999 %. The beam flux ratio in number of atoms of Zn to Se was kept at unity. The doping level of Cl was controlled by temperature of the K-cell containing ZnCl_2 . ZnCl_2 cell temperature (T_{Cl}) was varied from 150 to 250 °C. Estimated pressure of ZnCl_2 in the K-cell varies from 10^{-6} to 10^{-3} Torr.⁶⁴ In most cases, the layer thickness was fixed to about 2 μm in order to eliminate the influence of the difference in biaxial strain on exciton luminescence which will be discussed in Chapter 4.

Electrical properties of Cl-doped layers were measured at temperature ranging from 77 to 333 K by means of Hall measurement (see Sec. 3.3). Figure 2.6 shows carrier concentration, Hall mobility and resistivity at 300 K plotted as functions of T_{Cl} . Undoped layers exhibited high resistivity above a limit of the measurement ($10^4 \Omega\text{cm}$). It was found that the carrier concentration can be controlled in a wide range by ZnCl_2 cell temperature. The carrier concentration increases with T_{Cl} and corresponds with the feature of ZnCl_2 vapor pressure shown in Fig. 2.6 with a broken line. In comparison with Al-doped²⁸ or Ga-doped³² ZnSe layers previously reported, Cl-doping has greatly improved the carrier concentration and the resistivity of the ZnSe layer: $2.2 \times 10^{19} \text{ cm}^{-3}$ and $1.4 \times 10^{-3} \Omega\text{cm}$ at $T_{Cl} = 250 \text{ °C}$, respectively. In a heavy doping region around $T_{Cl} = 250 \text{ °C}$, the carrier concentration is somewhat lower than a value expected from the ZnCl_2 vapor pressure line. This indicates that

some of the incorporated Cl atoms do not act as donors, but presumably form complex centers. Hall mobility tends to decrease with increasing the doping level owing to impurity scattering, but still at large value of $200 \text{ cm}^2/(\text{Vs})$ at high doping level.

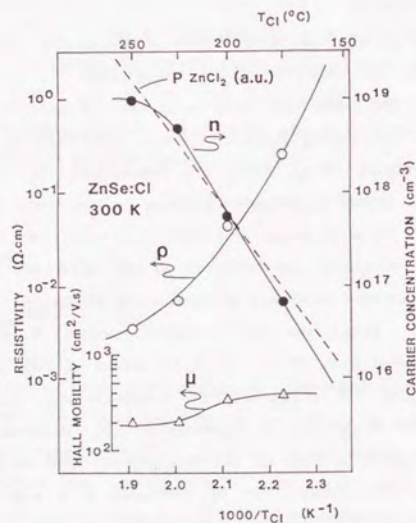


FIG. 2.6. Electrical property of Cl-doped ZnSe layers at 300 K as functions of ZnCl_2 cell temperature. The dashed line represents the vapor pressure of the ZnCl_2 .

The Cl-doped ZnSe layers exhibited mirrorlike surface morphology for the unaided eye even in the heaviest doping level. Figure 2.7 shows a Nomarski microphotograph (the surface roughness is emphasized in the photograph) of a Cl-doped ZnSe layer with $n_{300\text{K}} = 5.2 \times 10^{17} \text{ cm}^{-3}$. The photograph shows that the surface is slightly wavy, but similar morphology is observed for undoped layers.



FIG. 2.7. Nomarski microphotograph of surface of a Cl-doped ZnSe layer with $n_{300\text{K}} = 5.2 \times 10^{17} \text{ cm}^{-3}$.

The crystallinity of the doped layers was examined by double-crystal x-ray diffraction. The lattice parameters perpendicular to the surface (a_1) and FWHMs of (400) x-ray rocking curves from Cl-doped layers with various doping levels are plotted in Fig. 2.8, as a function of carrier concentration. Influence of doping was scarcely observed for $n_{300\text{K}} < 10^{17} \text{ cm}^{-3}$. However, in the heavier doping region $n_{300\text{K}} > 10^{18} \text{ cm}^{-3}$, there is a tendency for both lattice parameter and FWHM to increase. Such behavior is also observed for Ga-doped MBE ZnSe.³² It is assumed that an excess incorporation of Cl atoms results in a formation of lattice

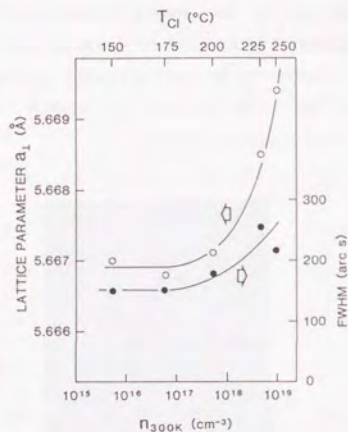


FIG. 2.8. Lattice parameter a_1 and FWHM of x-ray rocking curve for ZnSe layers with 2- μm thickness plotted as a function of carrier concentration.

defects involving vacancies and their complexes which cause the lattice dilatation and disorder.

Diffusion of dopants is significant for characteristics and long-term stability of junction devices. The diffusion of Cl atoms during growth was evaluated by a secondary ion-mass-spectroscopy (SIMS) analysis. The sample analyzed by SIMS has a multilayer structure, i.e., undoped ZnSe (0.6 μm)/n-ZnSe ($T_{\text{Cl}} = 200^\circ\text{C}$, 0.6 μm)/n⁺-ZnSe ($T_{\text{Cl}} = 250^\circ\text{C}$, 0.6 μm)/GaAs substrate. Figure 2.9 shows the in-depth profiles of Cl, As and ZnSe. The signals of As and ZnSe indicate the GaAs substrate region and the ZnSe

layer region, respectively. A steplike profile of the Cl concentration was clearly observed which coincides well with the structure of the sample. Diffusion length is defined by abruptness that is defined as a distance where the intensity varies from 84 % to 16 % of its maximum. Although the abruptness of Cl is as small as 370 \AA , the value includes a considerable error by knock-on and a mixing effect caused by collision of the energetic Cs⁺ primary ions with 14.5 keV. The real diffusion of Cl atoms in ZnSe during the MBE growth will be considerably smaller than 370 \AA .

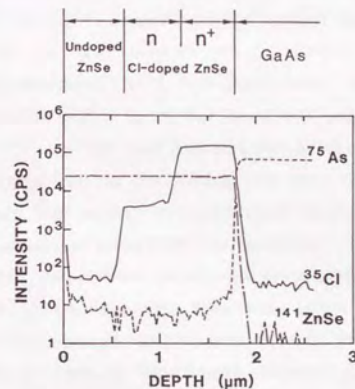


FIG. 2.9. In-depth profile of Cl, As and ZnSe signals in SIMS.

It is found that the ratio of the Cl concentration in the n⁺ layer to that in the n layer is about 30 in Fig. 2.9. On the other hand, the ratio in carrier concentration should be 18 according to the results shown in Fig. 2.6. This result indicates that a considerable amount of Cl atoms in the heavily doped layer is inactive. The implication of this fact agrees

well with the results in electrical and crystallographic properties of heavily-doped layers.

2.3.3. Nitrogen doping with a high-purity N_2^+ ion beam⁵³

Low-energy nitrogen ion doping has been attempted for the first time^{26,53} because sticking coefficient of nitrogen on ZnSe is very low. The ion gun system used has a mass separator to generate a high-purity N_2^+ molecular-ion beam. Typical kinetic energy of an ion was 300 eV, and typical ion current density at the substrate was less than 0.5 nA/cm^2 [$= 6 \times 10^9 \text{ atoms/(cm}^2\text{s)}$]. GaAs substrates were simultaneously irradiated with Zn, Se and N_2^+ beams. The beam flux ratio of Zn to Se was approximately $J_{Zn}/J_{Se} = 1$. The growth temperature was 325 °C. The growth rate was kept at 2 Å/s. The layer thicknesses are in the range of 0.05-5 μm. N concentration calculated from the ion current and the growth rate is about 10^{17} cm^{-3} or less. Since the high-purity ion beam made it possible to suppress unintended donor incorporation, N-doped ZnSe layers obtained have shown strong I_1 emission with well-suppressed I_2 and DAP emissions (see Fig. 4.1 (b)) in low-temperature PL measurement. However, p-type conduction was not observed for these N-doped ZnSe layers because crystallinity of these layers was degraded by ion damage under heavy doping condition attempting to realize p-type conduction. N-doped ZnSe layers with low doping level $< 10^{17} \text{ cm}^{-3}$ exhibit as good crystallinity as undoped layers. Since the lightly-doped ZnSe layers show excellent PL spectra that are dominated by I_1 emission, the layers are suitable for the investigation of band-edge PL emission.

2.3.4 Active-nitrogen doping with a N_2 ($A^3\Sigma_u^+$) metastable beam^{51,54-58}

Based on the results of the previous section, we have attempted, for the first time, a new doping method using active-nitrogen beam during the MBE growth.⁵⁴ The kinetic energy of an active nitrogen is the order of thermal energy. Low-damage doping was, therefore, expected with this method compared with the ion doping.

The active-nitrogen beam source is mounted on the MBE chamber. The beam is generated from an electrical discharge created by inductively-coupled rf excitation at 13.56 MHz by using N_2 and NH_3 gases as nitrogen source.

Optical emission spectra obtained from N_2 and NH_3 plasma are shown in Fig. 2.10. Every peak of the spectrum from N_2 plasma has been assigned as the second ($C^3\Pi_u \rightarrow B^3\Pi_g$) and the first ($B^3\Pi_g \rightarrow A^3\Sigma_u^+$) positive emission bands of a N_2 molecule. These excited states of a N_2 molecule are shown in Fig. 2.11. Any radiative transition of a N atom⁶⁵ was not detected. The N_2^+ ionic radiative transition ($B^2\Sigma_u^+ \rightarrow X^2\Sigma_g^+$ at 391 nm)²⁸ was not observed except for the low-pressure discharge. Even if N_2^+ molecular ions exist, the ions could not go out from the aperture due to the plasma sheath. Strong H atomic lines (the Balmer series $H_{\alpha, \beta, \gamma}$) were observed in the spectrum of NH_3 plasma. Other emission peaks shown in Fig. 2.10 (b) are assigned as the first and second positive emission bands of a N_2 molecule. Nitrogen-related emissions in both cases are N_2 molecular transitions ($C^3\Pi_u \rightarrow B^3\Pi_g \rightarrow A^3\Sigma_u^+$). Considering the life times of each state in Table 2.1, active nitrogens which can reach the substrate are only N_2 ($A^3\Sigma_u^+$) metastables. Nitrogen species responsible for doping are presumably active nitrogen of N_2 ($A^3\Sigma_u^+$) metastable. Sticking coefficient of unexcited N_2 ($X^1\Sigma_g^+$) is low, but that of the active nitrogen is high. Thus, nitrogen concentration of the ZnSe layers grown by active-

nitrogen doping has reached $1 \times 10^{19} \text{ cm}^{-3}$.

The vibrational temperature of N_2 molecules at the $\text{C}^3\Pi_u$ state was evaluated to be about 4500 K from the second positive emission bands of the spectrum in Fig. 2.10 (a). Its rotational temperature can be estimated from classical equipartition of energy to be the same value as kinetic energy. The kinetic energy equals to the temperature of the rf discharge cell around 1100 K, as the pressure in the cell would be greater than 1 mTorr. Thus the active nitrogen has the total thermal energy (kinetic, rotational and vibrational energies) of about 0.6 eV. The total kinetic

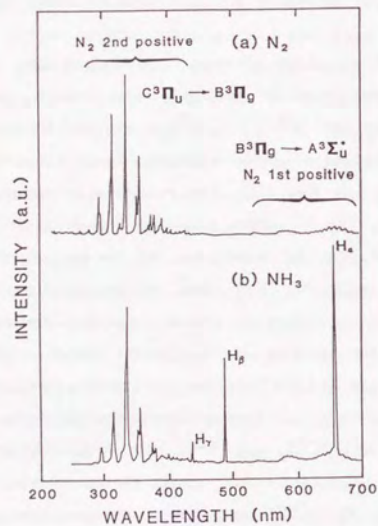


FIG. 2.10. Optical emission spectra from (a) N_2 plasma and (b) NH_3 plasma in an active-nitrogen beam source.

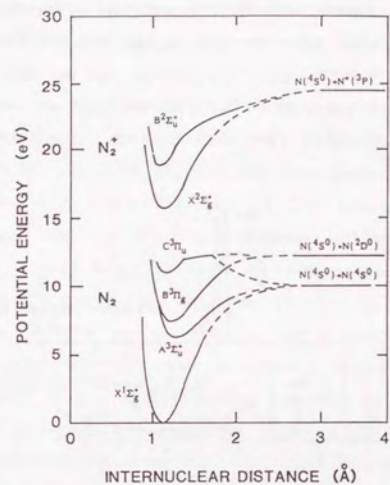


FIG. 2.11. Potential energy curves for N_2 and N_2^+ .

TABLE 2.1. Life times of spontaneous emission for active-nitrogen molecules.

State of N_2 molecule	Life time	References
$\text{A}^3\Sigma_u^+$	2.0 s	29
$\text{B}^3\Pi_g$	1.3 μs	29
$\text{C}^3\Pi_u$	40 ns	30

energy is fairly low compared with the ion energy of about 300 eV in the ion doping, indicating that active-nitrogen doping is a low-damage doping process.

Figure 2.12 (a) shows typical PL spectrum from an undoped ZnSe heteroepitaxial layer on GaAs substrate at 12 K. It is found that the

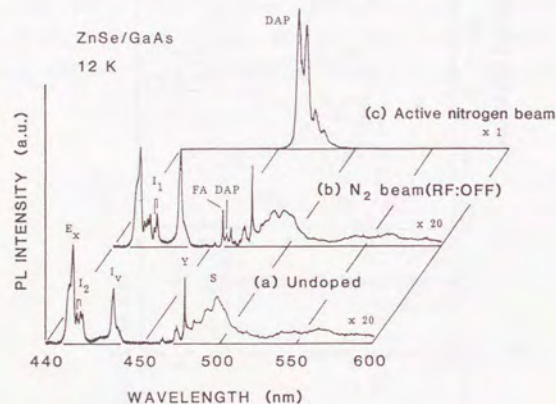


FIG. 2.12. 12-K PL spectra from (a) undoped ZnSe, (b) lightly N-doped ZnSe grown by irradiation of N_2 beam without rf discharge and (c) p-type ZnSe:N grown by active-nitrogen doping.

undoped ZnSe layer exhibits a dominant E_x emission at 2.801 eV, well-suppressed I_2 emissions at 2.798 and 2.796 eV, and so-called Y emission at 2.602 eV which is supposed to be related to dislocations⁶⁶⁻⁶⁸, indicating that high-quality single-crystal layers with low donor and acceptor densities have been obtained. A lightly N-doped ZnSe layer on GaAs was

grown by irradiation of the N_2 gas beam without rf discharge during MBE growth. The flow rate of N_2 gas was 2.0 sccm, so the background pressure of the MBE chamber was about 2×10^{-5} Torr. The PL spectrum from the sample is shown in Fig. 2.12 (b). The PL spectrum is almost the same as that of the undoped ZnSe shown in Fig. 2.12 (a) except for weak I_1 emissions at 2.792 and 2.790 eV, radiative recombination of a free electron and an acceptor hole (FA) at 2.711 eV and DAP emission at 2.696 eV. This result indicates that the sticking coefficient of N_2 molecule at $X^1\Sigma_g^+$ ground state is very low. The same N_2 source creates active nitrogen beam when the rf power (100 W) is on with the same N_2 flow. Drastic change in PL spectrum was observed for the N-doped ZnSe layers grown by using the active nitrogen beam as shown in Fig. 2.12 (c): strong DAP emission at 2.681 eV and weak (0.1 % of the intensity of DAP emission) I_1 emission were observed, and deep-level emission was not observed. This strong DAP emission indicates that the active nitrogen of a N_2 ($A^3\Sigma_u^+$) metastable have higher sticking coefficient compared with N_2 at the ground state, and the active nitrogen is doped into ZnSe as shallow acceptors. Further study is needed for the understanding of the mechanism of the dissociation of a N_2 ($A^3\Sigma_u^+$) metastable into N atomic acceptors in ZnSe. In the case of NH_3 gas for active-nitrogen doping, features of the PL spectrum are almost the same as that for N_2 gas except for deep-level emission around 2.15 eV (580 nm). Hydrogen would be responsible for the deep levels. N_2 gas is probably superior to NH_3 gas as a source of active nitrogen.

The diffusion of N atoms under our growth condition (325 °C, 4 hours) was evaluated by SIMS analysis. The sample analyzed has a multilayer structure, i.e., N-doped/undoped/GaAs. Figure 2.13 shows the in-depth profile of N concentration that coincided with the structure of the sample. The ^{94}Se N peak in the ZnSe/GaAs heterointerface was due to the

same mass peak of ^{94}SeO ; namely, an oxide layer residue would exist at the heterointerface. The mixing effect and sputtering-induced surface roughness were the cause of the Se signal in the GaAs substrate region as shown in Fig 2.13. It was found that the diffusion length of N atoms in ZnSe at the growth condition was less than $0.1\ \mu\text{m}$ which is much less than that of Li atoms.³⁵

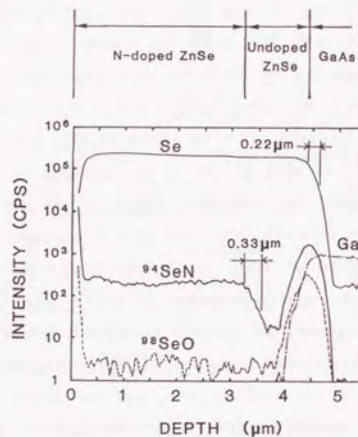


FIG. 2.13. SIMS analysis of N-doped ZnSe ($3.2\ \mu\text{m}$)/undoped ZnSe ($1.2\ \mu\text{m}$)/GaAs structure.

References

- 1 K. Wasa, and S. Hayakawa, *Jpn. J. Appl. Phys.* **12**, 408 (1973).
- 2 S. Fujita, H. Mimoto, and T. Noguchi, *J. Cryst. Growth* **45**, 281 (1978).
- 3 T. Muranoi, and M. Furukoshi, *Jpn. J. Appl. Phys.* **22**, L517 (1983).
- 4 R.L. Gunshor, and L.A. Kolodziejski, *IEEE J. Quantum Electron.* **24**, 1744 (1988).
- 5 J.B. Mullin, S.J.C. Irvine, J. Giess, and A. Royle, *J. Cryst. Growth* **72**, 1 (1985).
- 6 T. Yao, M. Ogura, S. Matsuoka, and T. Morishita, *Jpn. J. Appl. Phys.* **22**, L144 (1983).
- 7 A. Yoshikawa, T. Okamoto, T. Fujimoto, K. Onoue, S. Yamaga, and H. Kasai, *Jpn. J. Appl. Phys.* **29**, L225 (1990).
- 8 T. Taguchi, and B. Ray, in "Progress in Crystal Growth and Characterization Vol. 6" edited by B.R. Pamplin, (Pergamon, Oxford, 1983).
- 9 D.L. Smith, and V.Y. Pickhardt, *J. Appl. Phys.* **46**, 2366 (1975).
- 10 T. Yao, S. Amano, Y. Makita, and S. Maekawa, *Jpn. J. Appl. Phys.* **15**, 1001 (1976).
- 11 R.L. Gunshor, L.A. Kolodziejski, M.R. Melloch, M. Vaziri, C. Choi, and N. Otsuka, *Appl. Phys. Lett.* **50**, 200 (1987).
- 12 A. Kamata, K. Hirahara, M. Kawachi, and T. Beppu, in Extended Abstracts of the 17th Conference on Solid State Devices and Materials (The Japan Society of Applied Physics, Tokyo, 1985), p. 233.
- 13 N. Matsumura, M. Tsubokura, J. Saraie, and Y. Yodogawa, *J. Cryst. Growth* **86**, 311 (1988).
- 14 J. Nishizawa, K. Itoh, Y. Okuno, and F. Sakurai, *J. Appl. Phys.* **57**, 2210 (1985).

- 15 R.M. Park, H.A. Mar, and N.M. Salansky, *J. Vac. Sci. Technol. B* **3**, 1637 (1985).
- 16 K. Menda, I. Takayasu, T. Minato, and M. Kawashima, *J. Cryst. Growth* **86**, 342 (1988).
- 17 T. Yodo, T. Koyama, and K. Yamashita, *J. Cryst. Growth* **86**, 273 (1988).
- 18 M. Ohishi, K. Ohmori, Y. Fujii, H. Saito, and S. Tiong, *J. Cryst. Growth* **86**, 324 (1988).
- 19 K. Ueda, T. Koyama, K. Yamashita, K. Kumata, N. Takayama, and H. Hashimoto, in Abstracts of the Autumn Meeting of the Japan Society of Applied Physics, 6p-X-12, 1988.
- 20 E.M. Clausen, Jr., H.G. Craighead, M.C. Tamargo, J.L. deMiguel, and L.M. Schiavone, *Appl. Phys. Lett.* **53**, 690 (1988).
- 21 G. Handel, *Phys. Rev. A* **134**, 1073 (1964).
- 22 T. Muranoi, and M. Furukoshi, *Thin Sol. Films* **86**, 307 (1981).
- 23 J. Qui, D.R. Menke, M. Kobayashi, R.L. Gunshor, Q.-D. Qian, D. Li, and N. Otsuka, *J. Cryst. Growth* **111**, 747 (1991).
- 24 N. Kobayashi, *Jpn. J. Appl. Phys.* **27**, L1597 (1988).
- 25 K. Yoneda, Y. Hishida, T. Toda, H. Ishii, and T. Niina, *Appl. Phys. Lett.* **45**, 1300 (1984).
- 26 T. Mitsuyu, K. Ohkawa, and O. Yamazaki, *Appl. Phys. Lett.* **49**, 1348 (1986).
- 27 J. Wakitani, K. Yanashima, T. Yasuda, J. Yoshino, and H. Kukimoto, in Abstracts of the Autumn Meeting of the Japan Society of Applied Physics, 29p-PA-8, 1989.
- 28 W. Stutius, *Appl. Phys. Lett.* **38**, 352 (1981).
- 29 F. Kitagawa, T. Mishima, and K. Takahashi, *J. Electrochem. Soc.* **127**, 937 (1980).
- 30 T. Yao, T. Sera, Y. Makita, and S. Maekawa, *Surf. Sci.* **86**, 120 (1979).
- 31 M. Isshiki, T. Yoshida, K. Igaki, Y. Hayashi, and Y. Nakano, *J. Phys. C: Solid State Phys.* **19**, 4375 (1986).
- 32 T. Niina, T. Minato, and K. Yoneda, *Jpn. J. Appl. Phys.* **21**, L387 (1982).
- 33 Y.S. Park, P.M. Hemenger, and C.H. Chung, *Appl. Phys. Lett.* **18**, 45 (1971).
- 34 J. Nishizawa, K. Itoh, Y. Okuno, and F. Sakurai, *J. Appl. Phys.* **57**, 2210 (1985).
- 35 H. Cheng, J.M. DePuydt, J.E. Potts, and M.A. Haase, *J. Cryst. Growth* **95**, 512 (1989).
- 36 Y. Yamada, T. Taguchi, and A. Hiraki, *Inst. Phys. Conf. Ser. No 95: Chapter 6*, paper presented at Int. Conf. "Shallow Impurities in Semiconductors" (Lingköping, Sweden, 1988), p. 377.
- 37 J.L. Merz, K. Nassau, and J.W. Shiever, *Phys. Rev. B* **8**, 1444 (1973).
- 38 T. Yao, and Y. Okada, *Jpn. J. Appl. Phys.* **25**, 821 (1986).
- 39 K. Ohkawa, T. Karasawa, and T. Mitsuyu, in Abstracts of the Autumn Meeting of the Japan Society of Applied Physics, 1989, 29p-PA-13.
- 40 A.R. Reinberg, W.C. Holton, M. de Wit, and R.K. Watts, *Phys. Rev. B* **3**, 410 (1971).
- 41 W. Stutius, *Appl. Phys. Lett.* **40**, 246 (1982).
- 42 S.M. Shibli, M.C. Tamargo, B.J. Skromme, S.A. Schwarz, C.L. Schwartz, R.E. Nahory, and R.J. Martin, *J. Vac. Sci. Technol. B* **8**, 187 (1990).
- 43 T. Yasuda, I. Mitsuishi, and H. Kukimoto, *Appl. Phys. Lett.* **52**, 57 (1988).
- 44 I. Suemune, K. Yamada, H. Masato, Y. Kanda, Y. Kan, and M. Yamanishi, *Jpn. J. Appl. Phys.* **27**, L2195 (1988).
- 45 M.K. Jin, T. Yasuda, and J.L. Merz, in Abstracts of the Spring Meeting

- of the Materials Research Society, 1991, p.282 (N 6.3).
- 46 W. Stutius, *J. Cryst. Growth* **59**, 1 (1982).
- 47 R.M. Park, H.A. Mar, and N.M. Salansky, *J. Appl. Phys.* **58**, 1047 (1985).
- 48 K. Ohkawa, T. Mitsuyu, and O. Yamazaki, in Abstracts of the Spring Meeting of the Japan Society of Applied Physics, 1a-Y-4, 1986.
- 49 K. Ohkawa, T. Karasawa, A. Yoshida, T. Hirao, and T. Mitsuyu, *Appl. Phys. Lett.* **54**, 2553 (1989).
- 50 K. Ohkawa, T. Karasawa, and T. Mitsuyu, *J. Vac. Sci. Technol.B* **9**, 1934 (1991).
- 51 K. Ohkawa, A. Ueno, and T. Mitsuyu, to be published in *J. Cryst. Growth* (1992).
- 52 K. Ohkawa, T. Mitsuyu, and O. Yamazaki, *J. Appl. Phys.* **62**, 3216 (1987).
- 53 K. Ohkawa, T. Mitsuyu, and O. Yamazaki, *J. Cryst. Growth* **86**, 329 (1988).
- 54 K. Ohkawa, T. Karasawa, and T. Mitsuyu, in Abstracts of 6th International Conference on Molecular Beam Epitaxy, San Diego, August 1990, PIII-21
- 55 K. Ohkawa, T. Karasawa, and T. Mitsuyu, *J. Cryst. Growth* **111**, 797 (1991).
- 56 K. Ohkawa, and T. Mitsuyu, to be published in *J. Lumin.*
- 57 K. Ohkawa, T. Karasawa, and T. Mitsuyu, *Jpn. J. Appl. Phys.* **30**, L152 (1991).
- 58 K. Ohkawa, and T. Mitsuyu, *J. Appl. Phys.* **70**, 439 (1991).
- 59 K. Ohkawa, Master Thesis, The University of Tokyo, 1985.
- 60 Y. Shirakawa, and H. Kukimoto, *J. Appl. Phys.* **51**, 2014 (1980).
- 61 Handbook of Chemistry and Physics (CRC press, Florida), pp. D-197-198.
- 62 L.H. Connick, A. Bhattacharyya, K.N. Ritz, and W.L. Smith, *J. Appl. Phys.* **64**, 2059 (1988).
- 63 K. Ohkawa, T. Mitsuyu, and O. Yamazaki, in Abstracts of the Spring Meeting of the Japan Society of Applied Physics, 1a-Y-3, 1986.

- 64 F.H. Keneshea, and D. Cubicciotti, *J. Chem. Phys.* **40**, 191 (1964).
- 65 A.R. Filippelli, F.A. Sharpton, C.C. Lin, and R.E. Murphy, *J. Chem. Phys.* **76**, 3597 (1982).
- 66 T. Taguchi, T. Kusao, and A. Hiraki, *J. Cryst. Growth* **72**, 46 (1985).
- 67 J. Saraie, N. Matsumura, M. Tsubokura, K. Miyagawa, and N. Nakamura, *Jpn. J. Appl. Phys.* **28**, L108 (1989).
- 68 K. Shahzad, J. Petruzzello, D.J. Olego, D.A. Cammack, and J.M. Gaines, *Appl. Phys. Lett.* **57**, 2452 (1990).

CHAPTER 3

CHARACTERIZATION OF ZnSe LAYERS

3.1. Introduction

ZnSe layers are mainly characterized by optical, electrical and crystallographic measurements. In attempting to achieve an understanding of these properties it is necessary to relate them to basic parameters of the materials. Optical, electrical and crystallographic properties are related to the electronic structure and the crystal structure. For instance, photoluminescence (PL) measurement, which is the representative technique of the optical measurements, gives basic physical parameters such as band gap, impurity levels, defects and crystallinity. We must understand each physical property from every measurement self-consistently.

Optical measurement has two ways; observation of emission of light from materials and observation of absorption of light. Photoluminescence is the optical radiation emitted by a physical system resulting from excitation to a nonequilibrium state by irradiation with light. PL measurement is one of the most important basic research tools for studying II-VI compounds. There are several techniques such as low-temperature PL, time-resolved PL and photoluminescence excitation. Low-temperature PL properties yield physical information of II-VI compounds about impurity levels,^{1,2} defects³⁻⁶ and so on. We have shown the correlation between intensity of free exciton emission (E_x) in low-

temperature PL and crystallinity measured by double-crystal x-ray diffraction.^{7,8} Bhargava et al.⁹ identified branches of donor-acceptor pair emission (DAP) by time-resolved PL measurement. Shirakawa et al.¹⁰ have measured temperature dependence of the free exciton energy by photoluminescence excitation spectra. Exciton resonance dip is observed in reflection spectrum at low temperature.¹¹ E_x emission can be confirmed by the exciton resonance dip in the reflection spectrum.

Electrical properties of semiconductors, the ones resulting from doping in particular, are very important. When doped-semiconductor layers are conductive, electrical properties are measured by means of Hall effect. However, capacitance-voltage (C-V) measurement¹² will be convenient for characterization of high-resistivity semiconductors. Hall measurement is generally performed by the van der Pauw configuration.^{13,14} The result gives information about majority carrier, its concentration, Hall mobility and resistivity. The activation of impurities and the carrier scattering mechanism are understood by temperature and carrier-concentration dependences of these properties.^{15,16} Ohmic contact to n-type ZnSe is easy to be attained with In-Hg alloy. Ohmic contact to p-type ZnSe, however, is difficult to form. DePuydt et al.¹⁷ reported that the large resistance between Au electrodes deposited by evaporation was due to contact resistance rather than large sample resistivity, and the electrodes formed a rectifying rather than an ohmic contact. Hall measurement is suitable for thin films, but C-V measurement is able to evaluate thick films and bulk, and give net acceptor ($N_A - N_D$) or net donor ($N_D - N_A$) concentration.

Crystallinity of ZnSe layers is evaluated by conventional x-ray diffraction, double-crystal x-ray diffraction and x-ray topograph measurements. Lattice constant is measured by both x-ray diffraction analyses. Full width at half-maximum (FWHMs) of rocking curves from

double-crystal x-ray diffraction evaluates quality of crystals. X-ray topograph of overall layers shows uniformity of strain, grain boundary and twinning boundary.⁸

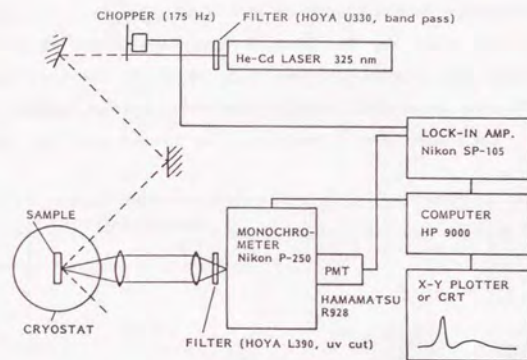
Direct measurement of elements is possible by a secondary ion-mass-spectroscopy (SIMS). Intentionally or unintentionally doped impurities are observed by this analysis. Diffusion of impurity is also evaluated by in-depth profile.

Talystep is widely used for the measurement of surface roughness and layer thickness.¹⁸ Overall surface roughness is observed by Nomarski microscope. Nomarski microscopy is a white-light interference phase-contrast technique sensitive to tens of angstroms or less of surface relief.¹⁹

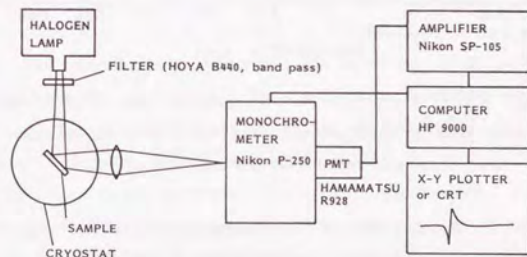
This chapter describes details of PL, reflection and Hall measurements of II-VI compound layers.

3.2. Optical measurements

Measurement systems for PL and reflection spectra are shown in Fig. 3.1 (a) and (b), respectively. PL measurements were made at liquid-helium temperature 4.2 K to 300 K using the cryostat. The PL was excited by the 325-nm line from a He-Cd laser. The excitation power density was about 0.1 W/cm^2 [$= 1.6 \times 10^{17}$ photons/(cm^2s)]. The PL spectra were recorded using a monochromator with a 25-cm focal length. The resolution was about 0.07 nm (0.4 meV at 440 nm). Reflection spectra were measured as follows. Surface of samples was irradiated with light from a halogen lamp. The irradiated light was broad blue light created by using a band-pass filter shown in Fig. 3.1 (b), which suppresses the increase of temperature of a sample by useless light such as red and ultraviolet light. The angle of light



(a)



(b)

FIG. 3.1. Schematics of the instrumentation necessary for (a) photoluminescence and (b) reflection measurements.

incident to the normal face was 45° . The reflected light was led to the above monochromator with the resolution of 0.07 nm.

Figure 3.2 shows the PL spectrum from lightly-doped ZnSe layer on GaAs substrate. The measurement was made at 11 K; the low temperature makes it possible to observe a highly-resolved spectrum without thermal disturbance. Each peak has a recombination center such as impurities,

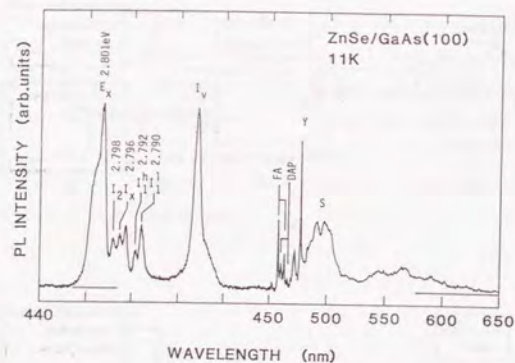


FIG. 3.2. 11-K photoluminescence spectrum from a lightly-doped ZnSe layer on GaAs substrate. Horizontal scale for excitonic emission region (440-450 nm) is magnified.

defects and so on. Analysis of PL emissions related to donors and/or acceptors gives a direction of the investigation of amphoteric doping of II-VI compounds. Excitonic emissions are observed at low-temperature PL measurement since the binding energy of an electron and a hole is larger than the thermal energy of 11K. Using the hydrogen model, the binding energy (E_n) and exciton diameter (r_n) are given by

$$E_n = - \frac{\mu e^4}{2 (4\pi\epsilon_s)^2 \hbar^2} \cdot \frac{1}{n^2}, \quad (3.1)$$

$$r_n = \frac{4\pi\epsilon_s \hbar^2}{\mu e^2} n^2, \quad (3.2)$$

where μ is a reduced mass, e is the electronic charge, ϵ_s is the static dielectric constant, and n is integer. By using the values listed in Table 1.1, the equation for ZnSe is obtained as

$$E_n = - 21/n^2 \quad [\text{meV}]. \quad (3.3)$$

At the ground state, $E_1 = - 21$ meV and $r_1 = 37 \text{ \AA}$ were obtained by calculation. Because of the large binding energy of 21 meV compared with the thermal energy (kT) of less than 1 meV at 11 K, excitons can exist at the temperature. Figure 3.3 is a schematic representation of different types of excitonic transitions. E_x emission is a recombination emission from an exciton which moves freely in crystal. Photon energy of E_x emission is smaller than band-gap energy (E_g) by the binding energy of E_n . Under certain circumstances, the binding energy of an exciton is increased by the presence of a point defect such as a neutral or ionized impurity. Energy is the fundamental criterion that determines whether or not an exciton can be trapped on an impurity. When the exciton is nearby an impurity, the total energy of the system is reduced (corresponding to an increase in the binding energy of the exciton). Therefore it is energetically favorable for the exciton to remain near the defect; the exciton becomes "bound" to the impurity. Energy difference between E_x emission and bound exciton emission is small, but it is possible to

discriminate the emissions only at low temperature. Peak energy of bound exciton emission depends on species of impurities. Neutral acceptor-bound exciton emission (I_1), neutral donor-bound exciton emission (I_2) and ionized donor-bound exciton emission (I_3) were observed in different energies with the difference of a few meV or less.^{1,2} Furthermore, it is possible to identify an element species of a donor or an acceptor.^{1,2} These analyses were successful for bulk crystals. Analysis of characteristics of thin films or heteroepitaxial layers needs further investigation.

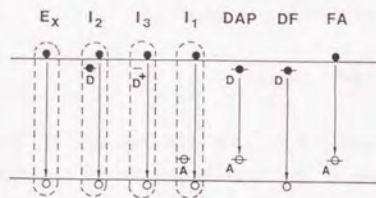


FIG. 3.3. Schematic representation of donor- and acceptor-related radiative recombinations in II-VI compounds. Dashed line indicates a excitonic state.

Other radiative transitions can be observed in the spectrum in Fig. 3.2. Representative emissions are DAP emission, recombination emission between a donor electron and a free hole (DF), and recombination emission between a free electron and an acceptor hole (FA). The origin of DAP emission is well understood as the recombination between an electron trapped at a donor and a hole trapped at an acceptor. Once the electron and the hole recombine, the final transition energy is renormalized due to the Coulombic interaction between the two bare charged impurities left behind. The resultant emission energy is given by²⁰

$$\hbar\omega_{\text{DAP}} = E_g - (E_A + E_D) + e^2/(4\pi\epsilon_0 R), \quad (3.4)$$

where R is the pair separation, and E_A and E_D are the acceptor and donor ionization energies, respectively. DF emission is the recombination between an electron trapped at a donor and a free hole in the valence band. Thermal energy of a free hole is almost constant of 3.5 meV at high temperature region (> 100 K)^{21,22} since the effective mass of a hole is as heavy as $0.7m_0$. The emission energy is given by^{21,22}

$$\hbar\omega_{\text{DF}} = E_g - E_D + 3.5 \text{ meV}. \quad (3.5)$$

FA emission is the recombination between a free electron in the conduction band and a hole trapped at an acceptor. Since the effective mass of an electron is as small as $0.16m_0$, thermal energy is then given by $\frac{1}{2}kT$.²³ Therefore, FA emission energy is given by

$$\hbar\omega_{\text{FA}} = E_g - E_A + \frac{1}{2} kT. \quad (3.6)$$

Using these equations (3.4-6), E_A , E_D and the Coulombic term can be calculated by inserting the experimental values of DAP, DF and FA emission energies.

3.3. Electrical measurements^{24,25}

Electrical properties of samples were measured in a temperature range from 77 to 333 K by Hall measurement with the van der Pauw method.^{13,14}

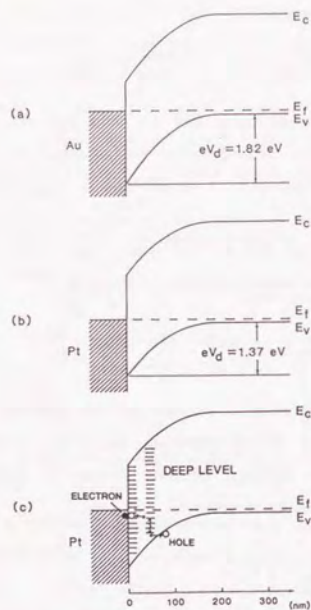


FIG. 3.4. Energy band diagram of the junction of p-type ZnSe and metals, (a) Au, (b) Pt and (c) Pt on sputter-etched area.

Ohmic contact to n-type ZnSe layers was made by depositing drops of an In-Hg alloy followed by annealing in Ar- H_2 (10%) gas at 320 °C for 30 s. Ohmic contact to p-type ZnSe, however, is very difficult to form because every metal has a lower Fermi level compared with p-type ZnSe. Figure 3.4 shows bending of ZnSe valence band at the junction with Au and Pt. We have employed, for the first time, Pt as the electrode material

for p-type ZnSe²⁵ because its Fermi level is closer to that of ZnSe than that of Au. The structure of the Pt electrode is shown in Fig. 3.5. The conditions of etching and Pt deposition for Pt electrodes are described in Table 3.1. Fabrication procedure of a Pt electrode is the removal of the p-type ZnSe layer to a depth of 1000 Å with 1 mm diameter by Ar plasma to create deep centers for carrier recombination followed by the deposition of Pt by sputtering. Rectifying characteristic has existed among

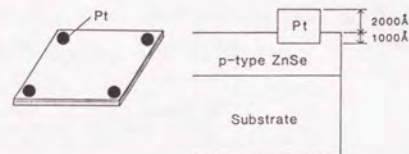


FIG. 3.5. Schematic illustration of the van der Pauw method and cross-section of Pt electrode on a p-type ZnSe layer.

Pt electrodes, but current density between Pt electrodes was 10 times greater than that in the case of evaporated Au electrodes without plasma etching. Since large resistance between the Au electrodes was due to contact resistance, our Pt electrodes reduced contact resistance by one order of magnitude. The mechanism of the Pt contacts sputter-deposited on an Ar plasma-etched surface is shown in Fig. 3.4 (c). The Ar sputtering would make deep levels in band gap of the surface ZnSe. Free holes will recombine with electrons from Pt in the deep levels.

TABLE 3.1. Plasma etching and Pt deposition

	Etching	Pt deposition
Substrate temperature	Room temperature (Water cooled)	Room temperature (Water cooled)
Sputtering gas	Ar (100%)	Ar (100%)
Gas pressure	20 mTorr	20 mTorr
Input power	20 W (rf)	300 W (rf)
Rate	30 Å/min	150 Å/min

References

- ¹ P.J. Dean, and J.L. Merz, *Phys. Rev.* **178**, 1310 (1969).
- ² K. Shahzad, D.J. Olego, C.G. Van de Walle, and D.A. Cammack, *J. Lumin.* **46**, 109 (1990).
- ³ T. Taguchi, and T. Yao, *J. Appl. Phys.* **56**, 3002 (1984).
- ⁴ T. Taguchi, T. Kusao, and A. Hiraki, *J. Cryst. Growth* **72**, 46 (1985).
- ⁵ J. Saraie, N. Matsumura, M. Tsubokura, K. Miyagawa, and N. Nakamura, *Jpn. J. Appl. Phys.* **28**, L108 (1989).
- ⁶ K. Shahzad, J. Petruzzello, D.J. Olego, D.A. Cammack, and J.M. Gaines, *Appl. Phys. Lett.* **57**, 2452 (1990).
- ⁷ K. Ohkawa, T. Karasawa, A. Yoshida, T. Hirao, and T. Mitsuyu, *Appl. Phys.*

Lett. **54**, 2553 (1989).

- ⁸ K. Ohkawa, T. Karasawa, and T. Mitsuyu, *J. Vac. Sci. Technol.* **B 9**, 1934 (1991).
- ⁹ R.N. Bhargava, R.J. Seymour, B.J. Fitzpatrick, and S.P. Herko, *Phys. Rev. B* **20**, 2419 (1983).
- ¹⁰ Y. Shirakawa, and H. Kukimoto, *J. Appl. Phys.* **51**, 2014 (1980).
- ¹¹ T. Yao, Y. Okada, S. Matsui, K. Ishida, and I. Fujimoto, *J. Cryst. Growth* **81**, 518 (1987).
- ¹² T. Marshall, S. Colak, and D. Cammack, *J. Appl. Phys.* **66**, 1753 (1989).
- ¹³ L.J. van der Pauw, *Philips Res. Rept.* **13**, 1 (1958).
- ¹⁴ L.J. van der Pauw, *Philips Tech. Rev.* **20**, 220 (1958/59).
- ¹⁵ H.E. Ruda, *J. Appl. Phys.* **59**, 1220 (1986).
- ¹⁶ H.E. Ruda, *J. Appl. Phys.* **59**, 3516 (1986).
- ¹⁷ J.M. DePuydt, M.A. Haase, H. Cheng, and J.E. Potts, *Appl. Phys. Lett.* **55**, 1103 (1989).
- ¹⁸ W.A. Pliskin, and S.J. Zanin, in "Handbook of Thin Film Technology", edited by L.I. Maissel, and R. Glang, (McGraw-Hill, New York, 1970), Chap. 11.
- ¹⁹ G. Nomarski, and A.R. Weill, *Rev. Metall.* **52**, 121 (1955).
- ²⁰ F. Williams, *Phys. Stat. Sol.* **25**, 493 (1968).
- ²¹ H. Barry Bebb, and E.W. Williams, in *Semiconductors and Semimetals Vol. 8*, edited by R.K. Willardson and A.C. Beer, (Academic Press, New York, 1972), p. 182.
- ²² M. Kitagawa, *Doctoral Thesis*, Kyoto Univ. (1982).
- ²³ D. Berlincorvt, H. Jaffe, and L.R. Shiozawa, *Phys. Rev.* **129**, 1009 (1963).
- ²⁴ K. Ohkawa, T. Mitsuyu, and O. Yamazaki, *J. Appl. Phys.* **62**, 3216 (1987).
- ²⁵ K. Ohkawa, T. Karasawa, and T. Mitsuyu, *Jpn. J. Appl. Phys.* **30**, L152 (1991).

CHAPTER 4

EFFECT OF BIAxIAL STRAIN ON EXCITON LUMINESCENCE FROM ZnSe HETEROEPITAXIAL LAYERS

4.1. Introduction

Lattice mismatch and difference in thermal expansion coefficients greatly affect physical properties of II-VI compounds heteroepitaxial layers. Investigation of these effects is necessary for understanding the fundamentals of heteroepitaxy and their application for heterojunction and superlattices.

GaAs has been widely used as a substrate for ZnSe epitaxial growth because of small lattice mismatch of 0.28 % at room temperature. This lattice mismatch of small amount, however, influences early stage of ZnSe epitaxial growth. X-ray diffraction measurements show that thin ZnSe layer is coherently grown on a GaAs substrate with tetragonal distortion.^{1,2} With increasing layer thickness, the lattice parameter perpendicular to the (100) heterointerface (a_1) approaches the lattice parameter of bulk ZnSe, indicating a relaxation of the mismatch distortion. The lattice parameter a_1 becomes smaller than the bulk value for layers thicker than 1-1.5 μm . Yao et al.² have indicated that the thick layers suffer biaxial tensile stress produced by differences in thermal contraction between ZnSe and GaAs during the cooling from the growth temperature to room temperature.

The strain produced by the lattice mismatch and the differential

thermal contraction have influences not only on crystallinity but also on optical properties of heteroepitaxial layers. Pikus et al.³ have derived a general expression of the orbital-strain Hamiltonian of Si and Ge under uniaxial strain. Asai et al.⁴ have showed that the valence band of zincblende-type material shifts and splits into light- and heavy-hole branches by the biaxial strain. Dean⁵ has pointed out that the shift of PL emission from ZnSe heteroepitaxial layers is due to the lattice mismatch between ZnSe and GaAs. Yao et al.² have ascribed the two exciton resonance dips in reflection spectra from ZnSe layers with different thicknesses (which are equivalent to different strains) to the two branches of the valence band. A new I_x emission appears at a lower energy position of conventional neutral donor-bound exciton emission (I_2) in low-temperature photoluminescence (PL) spectra from ZnSe/GaAs heteroepitaxial layers.⁶ The origin of I_x emission would be neutral donor-bound exciton emission, but the species of the donor was unknown so far.^{2,6} Potts et al.⁷ and Mar et al.⁸ have observed that the peak energy of so-called I_x emission varied with a small change of ZnSe lattice parameter. Their discussions were made using the lattice parameter at room temperature in spite of low temperature for PL properties. Strain at the same temperature with optical measurements is necessary for the quantitative calculation of effect of the strain on optical properties.⁹

Low-temperature PL spectra from n-type ZnSe layers were dominated by I_x emission.⁶ We have succeeded, for the first time, in the growth of acceptor-doped ZnSe layers with dominant neutral acceptor-bound exciton emission (I_1).¹⁰ Since these layers showed strong bound exciton emission with other emission being well-suppressed, other radiative transitions are negligible, implying that the qualitative discussion of the change in intensities of bound exciton emissions is possible. ZnSe single crystals exhibit a single bound exciton emission,¹¹ but these ZnSe/GaAs

heteroepitaxial layers showed two peaks in each bound exciton emission. For instance, Ga-doped ZnSe layers showed two peaks consisting of neutral donor-bound exciton emission (I_2) and I_x emissions.¹² Peak energy of I_2 emission was almost the same as that of single crystal¹¹, but the I_x emission appeared at lower-energy side of I_2 emission by a few meV and had strong intensity relative to I_2 emission. Same feature was also observed in I_1 emission from our N-doped ZnSe layers.⁹ Peak energy of I_1 emission from our N-doped ZnSe had a different energy of that from N-doped ZnSe homoepitaxial layers grown by liquid phase epitaxy (LPE)¹³. Different peak energy of I_1 emission also indicates a possibility that unintended impurities are incorporated into ZnSe layers in spite of our careful growth. Understanding of the origins of two peaks both in I_1 and in I_2 emissions is very important for amphoteric doping.

4.2. Theoretical calculation of effect of biaxial strain

4.2.1. Layer-thickness dependence of lattice parameters⁹

Strain in the layer can be evaluated by a measurement of lattice parameter or a Raman scattering measurement¹⁴. Measurement of the lattice parameter a_1 of ZnSe layers was made by conventional x-ray diffraction. Figure 4.1 shows the a_1 of ZnSe layers plotted as a function of layer thickness at room temperature and 12 K. The room-temperature lattice parameter was obtained experimentally, but the a_1 at 12 K is calculated values.

Layer-thickness dependence of lattice parameters at low temperature has been derived by postulating the following mechanisms about the heteroepitaxy to calculate the a_1 at 12 K. Three states of temperatures

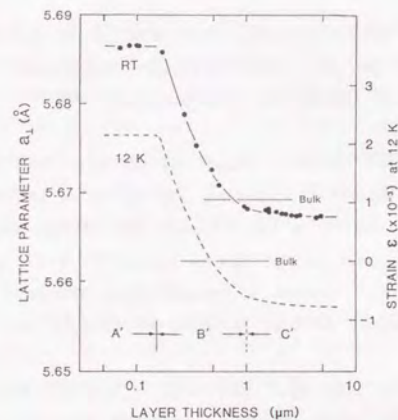


FIG. 4.1. Lattice parameter a_1 and strain ϵ of ZnSe layers plotted as a function of layer thickness at room temperature and 12 K. (Solid line connects the experimental data points (RT), and dashed line is calculated on (12 K).)

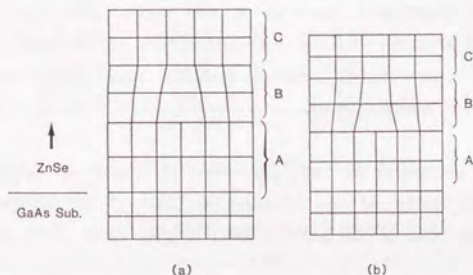


FIG. 4.2. Schematic model for the deformation of ZnSe lattice grown on GaAs substrate (a) at growth temperature, and (b) at room and low temperature.

are defined: the growth temperature (= 600 K) state, the room-temperature (= 300 K) state for the x-ray diffraction measurement and the low-temperature (= 12 K) state for the PL measurement.

[Growth temperature 600 K] Figure 4.2 (a) shows ZnSe lattice on GaAs substrate at the growth temperature. The layers of the early stages of the growth are coherent to the substrate and tetragonally deformed by compressive stress due to the lattice mismatch. Since dislocations are induced in region B beyond a certain layer thickness (i.e., critical thickness),¹ the lattice structure of ZnSe will change into cubic gradually (region C).

[Room temperature 300 K] The layer is biaxially stretched at room temperature since tensile stress is produced by the differences in thermal contraction between ZnSe and GaAs on cooling below the growth temperature. This stress makes the a_1 of thick layer smaller than that of bulk ZnSe in region C'.

[Low temperature 12 K] Both lattices of ZnSe and GaAs shrink gradually with decreasing temperature, and biaxial strain increases with decreasing temperature due to the differences in thermal contraction mechanism of which is the same as bimetal. Thus larger tensile stress exists in region C' of thick layers.

Lattice parameter of ZnSe layers at 12 K can be calculated with the above mechanism for the heteroepitaxy. The a_1 of coherent, i.e., thin (< 0.15 μm) ZnSe layer on the GaAs substrate is given by^{1,4}

$$a_1 = a_{\text{GaAs}} + \frac{C_{11} + 2C_{12}}{C_{11}} (a_{\text{bulk}} - a_{\text{GaAs}}) \quad (4.1)$$

where C_{11} and C_{12} are the elastic stiffness constants of ZnSe and the a_{bulk} is the lattice parameter of bulk ZnSe. Using C_{11} and C_{12} in Table 4.1, the lattice parameter of the coherent ZnSe layer can be evaluated as $a_1 = 5.688 \text{ \AA}$ at 300 K. This value is in quite good agreement with our experimental value of $a_1 = 5.687 \text{ \AA}$ at room temperature and other experimental values.^{1,19} In this case, the ZnSe lattice parameter a_* (which is parallel to the heterointerface) takes the value of the GaAs lattice parameter.

TABLE 4.1. Values of lattice parameters of ZnSe and GaAs, and of elastic stiffness constants for ZnSe at different temperatures (12, 300, and 600 K).

Temperature (K)	Lattice parameters of bulk (\AA)		Elastic stiffness constants of ZnSe (10^{11} dyn/cm ²)	
	GaAs	ZnSe	C_{11}	C_{12}
600	5.6639	5.6841		
300	5.6533	5.6693	8.59	5.06
12	5.6479	5.6623	8.88	5.27
Reference	15,16	17	18	18

Influence of the differential thermal contraction is remarkable on lattice parameters of thick (> 1 μm) ZnSe layers. The following assumptions were made to evaluate the influence of the differential thermal contraction: 1) the lattice parameter of region C where is away from the heterointerface has the bulk value of ZnSe at the growth temperature; 2) a_* of the layers approaches that of GaAs when being cooled from the growth temperature to room temperature. These assumptions

can give an equation

$$\frac{a_{\text{GaAs}}(300\text{K}) - a_{\text{GaAs}}(600\text{K})}{a_{\text{GaAs}}(600\text{K})} = \frac{a_r(300\text{K}) - a_{\text{bulk}}(600\text{K})}{a_{\text{bulk}}(600\text{K})} \quad (4.2)$$

The equation gives $a_r(300\text{K}) = 5.674 \text{ \AA}$ for thick layers. By replacing a_{GaAs} in Eq. (4.1) with a_r , $a_1(300\text{K}) = 5.665 \text{ \AA}$ for thick layers is obtained. This calculated $a_1(300\text{K})$ for thick layers is in good agreement with the experimental value of 5.667 \AA in Fig. 4.1.

By applying the same type of equations as (4.1,2) to low temperature (12 K), $a_1(12\text{K})$ for thin and thick ZnSe layers were obtained as 5.679 and 5.655 \AA respectively. The manner of $a_1(12\text{K})$ relaxation at moderate thickness is presumably identical for that of $a_1(300\text{K})$. The lattice parameter $a_1(12\text{K})$ is calculated as a function of ZnSe layer thickness as shown in Fig. 4.1 (dashed line). The 12-K lattice parameter of ZnSe heteroepitaxial layers on GaAs substrates has been calculated for the first time. Since ZnSe/GaAs heteroepitaxy is among the most common and important ones,²⁰ the low-temperature lattice parameter is useful to discuss physics at low temperature such as optical properties. Furthermore this procedure will give insight into the layer-thickness dependence of any heteroepitaxy at any temperature.

4.2.2. Valence band split due to biaxial strain⁹

The effective Hamiltonian formalism of Pikus³ can be used to describe the exciton problem. The exciton Hamiltonian can be expressed as

$$H = H_{v,0} + H_{v,\epsilon} + H_C + H_{\text{exciton}} \quad (4.3)$$

where $H_{v,0}$ is the zero-pressure mixing of the three p-like valence bands, $H_{v,\epsilon}$ is the strain-dependent mixing of the valence bands, H_C describes the conduction-band energy, and H_{exciton} is the valence hole - conduction electron interaction. The operator $H_{v,\epsilon}$ which represents the interaction between the valence bands due to strain can be determined from symmetry considerations by combining the strain tensor ϵ_{ij} with the angular momentum operator J , as described by Pikus.³ For zinc blende symmetry,

$$H_{v,\epsilon}^{ZB} = -a(\epsilon_{xx} + \epsilon_{yy} + \epsilon_{zz}) - 3b(J_x^2\epsilon_{xx} + J_y^2\epsilon_{yy} + J_z^2\epsilon_{zz}) + 6d/3^{3/2}([J_y J_z]\epsilon_{yz} + [J_x J_z]\epsilon_{xz} + [J_x J_y]\epsilon_{xy}) \quad (4.4)$$

where the parameter a is the hydrostatic deformation potential, and the quantities b and d are the shear deformation potentials appropriate to strain of tetragonal and rhombohedral symmetries, respectively. The valence band at the Γ point of the unstrained ZnSe layer consists of a fourfold $P_{3/2}$ multiplet ($J = 3/2$, $m_j = \pm 3/2, \pm 1/2$). Under biaxial compressive or tensile stress parallel to $[010]$ and $[001]$ (parallel to the heterointerface), the valence band is split into a heavy-hole branch ($J = 3/2$, $m_j = \pm 3/2$) and a light-hole branch ($J = 3/2$, $m_j = \pm 1/2$).^{4,5} From Eq. (4.4), band-gap shifts at the Γ point with biaxial stress are given by^{4,7}

$$\begin{aligned} \Delta E_0^{\text{hh}} &= -2a \frac{C_{11}-C_{12}}{C_{11}} \epsilon + b \frac{C_{11}+2C_{12}}{C_{11}} \epsilon, \\ \Delta E_0^{\text{lh}} &= -2a \frac{C_{11}-C_{12}}{C_{11}} \epsilon - b \frac{C_{11}+2C_{12}}{C_{11}} \epsilon. \end{aligned} \quad (4.5)$$

Here ΔE_0^{hh} and ΔE_0^{lh} are energy shifts of the band gaps between conduction band and valence band for the heavy- and the light-hole branches, respectively. The parameter ϵ is the magnitude of the strain

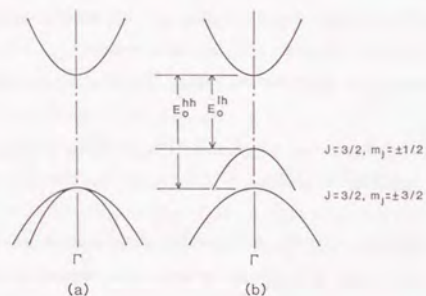


FIG. 4.3. Schematic representation of (a) unstrained band structure and (b) biaxial tensile-stressed band structure.

component. The ϵ is defined to be positive for compressive strain. Inserting $a = -3.0$ eV, $b = -1.2$ eV (Ref. 21), and the values of Table 4.1, the following results at 12 K were obtained:

$$\Delta E_0^{hh} = -0.19 \epsilon \quad [\text{eV}], \quad (4.6)$$

$$\Delta E_0^{lh} = 5.06 \epsilon \quad [\text{eV}]. \quad (4.7)$$

These equations show the features of band-gap shifts. Band structures of ZnSe near the Γ point under unstrained and strained conditions are shown in Fig. 4.3. The energy shift of the heavy-hole branch of the valence bands is almost independent of the strain, but the energy shift of the

light-hole branch is fairly dependent on the strain. For the biaxial stress parallel to heterointerface, nonzero components of the strain tensor are^{4,22}

$$\epsilon = -\epsilon_{xx} = -\epsilon_{yy} = \frac{C_{11}}{2C_{12}} \epsilon_{zz}, \quad (4.8)$$

$$\epsilon_{zz} = \frac{a_1 - a_{\text{bulk}}}{a_{\text{bulk}}}.$$

The strain in ZnSe layers can be derived by inserting the lattice parameter a_1 at 12 K in Fig. 4.1. For example, strains in thin ($< 0.15 \mu\text{m}$) and thick ($> 2 \mu\text{m}$) layers are 2.13×10^{-3} and -7.89×10^{-4} , respectively. The point where $\epsilon = 0$ is around $0.5 \mu\text{m}$. The difference between a_1 and a_{bulk} in the thick region at 12 K is much larger than the difference at room temperature, as shown in Fig. 4.1. Effect of the strain produced by the differential thermal contraction cannot be ignored at low temperature.

4.3. Effect of biaxial strain on bound exciton emissions

4.3.1. Temperature dependence⁹

The typical low-temperature PL spectra of our undoped,²³ N-doped¹⁰ and Ga-doped¹² ZnSe layers are shown in Fig. 4.4. The PL spectrum of the undoped ZnSe layer exhibits strong free exciton emission (E_x) with weak I_2 emission and suppressed deep-level emission, indicating good crystalline quality and high-purity of undoped ZnSe layers. The PL spectrum from N-doped ZnSe layers grown by high-purity N_2^+ ion doping

exhibited strong I_1 emission and weak ($1/40$ of I_1 emission) DAP emission around 2.70 eV (460 nm). This result suggests that the donor contamination introduced by the doping process is very little. The PL spectrum from Ga-doped ZnSe layer is dominated by I_x and I_2 emission with E_x emission.

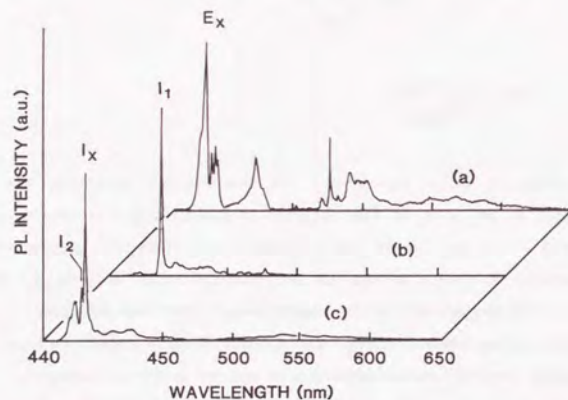


FIG. 4.4. Photoluminescence spectra of ZnSe layers on GaAs: (a) undoped, (b) N-doped and (c) Ga-doped. (a) was measured at 12 K, and (b) and (c) were measured at 4.2 K.

Figure 4.5 shows PL spectra in the excitonic emission region for N-doped ZnSe layer at different temperatures (4.2, 10 and 22 K). The weak E_x emission and the dominant neutral acceptor-bound exciton emission are observed in the spectrum at 4.2 K. The upper energy emission at 2.792 eV (444.05 nm) grows up with increasing temperature. The higher energy branch of I_1 emissions (I_1^{hh}) and I_2 emissions might be luminescence from bound excitons consisting of a heavy hole and an electron, and the lower

branch of I_1 emissions (I_1^{lh}) and the I_x emission (defined as I_2^{lh}) might be luminescence from bound excitons consisting of a light hole and an electron.

The ratio I_1^{lh}/I_1^{hh} of various samples are constant at a given temperature as shown in Fig. 4.6 and the ratio I_1^{lh}/I_1^{hh} is about 1.8 in thick ($> 1.5 \mu\text{m}$) N-doped ZnSe layers at 12 K and also in thick ($> 1.5 \mu\text{m}$)

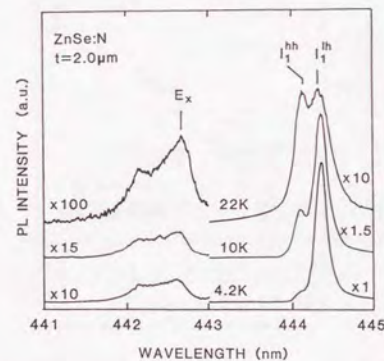


FIG. 4.5. Temperature dependence of the excitonic emission from N-doped ZnSe with layer thickness 2.0 μm .

Ga-doped ZnSe layers at 4.2 K. This proportional relation of the I_2^{hh} ($= I_2$) and I_2^{lh} ($= I_x$) suggests that the I_2 and I_x originate from same Ga-donor species. The result also indicates that the I_1^{hh} and I_1^{lh} originate from same N-acceptor species.

The Arrhenius plots of the PL intensity ratio I_1^{lh}/I_1^{hh} and I_2^{lh}/I_2^{hh} are shown in Fig. 4.7. PL intensities of the I_1^{hh} (or I_2^{hh}) emission and

the I_1^{lh} (or I_2^{lh}) emission would be in proportion to the populations of heavy and light holes in the split valence bands, respectively. The transition possibility of exciton recombination corresponding to a heavy hole is A (= constant) times larger than that of a light hole. These assumptions are shown in equations $I^{hh} = CAN^{hh}$ and $I^{lh} = CN^{lh}$ where I^{hh} and I^{lh} are PL intensities for the heavy-hole branch and the light-hole

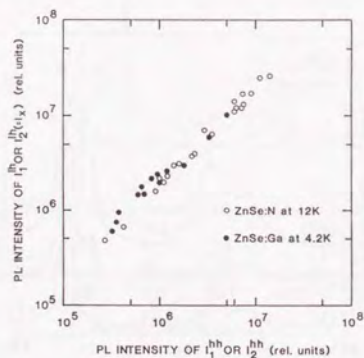


FIG. 4.6. Plots of intensities of I_1^{lh} vs I_1^{hh} and I_2^{lh} vs I_2^{hh} of ZnSe layers with various layer thicknesses (1.5-5 μm).

branch, respectively, and N^{hh} and N^{lh} are populations of heavy and light holes, respectively, C is a proportionality constant. Then the Arrhenius equation is given by

$$I^{lh}/I^{hh} = \exp(E_a/kT)/A, \quad (4.9)$$

where E_a is an activation energy. The plot of the ratio I_1^{lh}/I_1^{hh} in Fig.

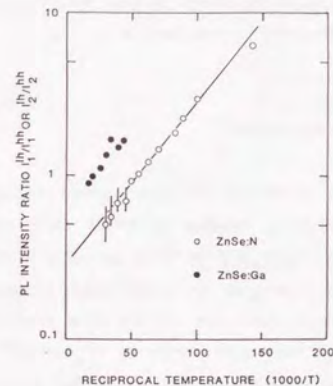


FIG. 4.7. Temperature dependence of the ratios I_1^{lh}/I_1^{hh} and I_2^{lh}/I_2^{hh} . Thickness of these N-doped and Ga-doped ZnSe layers are 2.0 and 4.8 μm , respectively. Solid line has activation energy 2.0 meV.

4.7 gives $A = 3.5$ and $E_a = 2.0$ meV. In the case of the ratio I_2^{lh}/I_2^{hh} , $A = 1.5$ and $E_a = 2.0$ meV were obtained. The result also shows that the activation energy E_a equals the difference in energy of the I_1^{hh} emission (2.792 eV) and the I_1^{lh} emission (2.790 eV) in Fig. 4.5. This result reveals that the I^{hh} and I^{lh} are originated from heavy and light hole branches of the valence band, respectively, and that a hole is thermally excited from a lower-energy state to a higher-energy state. The ratio I^{lh}/I^{hh} depends on the E_a and temperature as seen in Eq. (4.9). The difference in energy of the I_1^{lh} emission and the I_1^{hh} emission is almost constant for layers thicker than 1.5 μm as shown in Fig. 4.8, indicating that E_a is constant for thick layers; the dependence on layer thickness is similar to

that of the biaxial strain as shown in Fig. 4.1. The result suggests that the E_a is originated from the valence band split.

4.3.2. Layer-thickness dependence⁹

N-doped ZnSe homoepitaxial layer grown by LPE is reported to exhibit a single peak of I_1 emission at 2.7921 eV.¹³ No split of the peak is observed since the layer is free from strain ($\epsilon = 0$). I_1 emission from heteroepitaxial ZnSe layers, on the other hand, shows two distinct peaks I_1^{lh} and I_1^{hh} positions of which are shifted from that of I_1 emission from homoepitaxial layers. The energy shift of I_1^{lh} and I_1^{hh} can be calculated by using the Eqs. (4.6-8). Figure 4.8 shows the dependence of the peak energies on layer thickness for both I_1^{lh} and I_1^{hh} . The peak energy of I_1^{lh} shifts to higher energy for thinner ZnSe layers. The peak shift of I_1^{hh} is much smaller than that of I_1^{lh} emission. The calculated peak energies are in good agreement with the peak energies of the I_1^{lh} and I_1^{hh} emissions. In addition, similar property was also observed in the I_2^{lh} and the I_2^{hh} emissions of the Ga-doped ZnSe layers. It can be concluded that the I_1^{lh} and I_2^{lh} emissions from N-doped and Ga-doped ZnSe layers are luminescence from the light-hole exciton bound to a N-acceptor and a Ga-donor, respectively, and the I_1^{hh} and I_2^{hh} emissions are luminescence from the heavy-hole exciton bound to a N-acceptor and a Ga-donor, respectively.

In case of heteroepitaxial semiconductor layers, both the I_1 and I_2 emissions split into heavy- and light-hole branches by the biaxial strain due to lattice mismatch and differences in thermal contraction. This result implies that unintended impurities or defects are not introduced in ZnSe/GaAs heteroepitaxy.

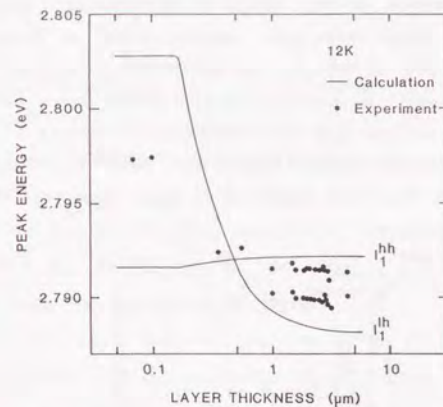


FIG. 4.8. Variation of excitonic peak energies in the 12-K PL spectra of the N-doped ZnSe layers of varying thickness. Solid lines are calculated peak energies of the I_1^{lh} and I_1^{hh} emissions. The I_1^{hh} emission is not discernible in the spectra of thinner layers.

4.3.3. Exciton luminescence from strain-free layers²⁴⁻²⁷

Strain-free ZnSe layers have been obtained by homoepitaxy.²³⁻²⁷ Excitonic emission spectra from undoped,²⁴ N-doped²⁵ and Cl-doped²⁶ ZnSe layers in both cases of homoepitaxy and heteroepitaxy are shown in Fig. 4.9. In the case of homoepitaxy, E_x , I_1 and I_2 emissions show single peaks at 2.804, 2.7931 and 2.7980 eV for undoped, N-doped and Cl-doped layers, respectively. The single peak confirms that the valence band does not

split without strain. In the ZnSe/GaAs heteroepitaxy, these emissions exhibit double peaks whose peak energies depend on biaxial strain in ZnSe layers. Figure 4.9 confirms the applicability of the Eqs. (4.6,7) that the light-hole branch is relatively sensitive to the strain, but the heavy-hole branch is not sensitive. The positions of strain-free PL peaks for undoped, N-doped and Cl-doped homoepitaxial layers are, therefore, almost the same as the heavy-hole branch of PL peaks from the heteroepitaxial layers.

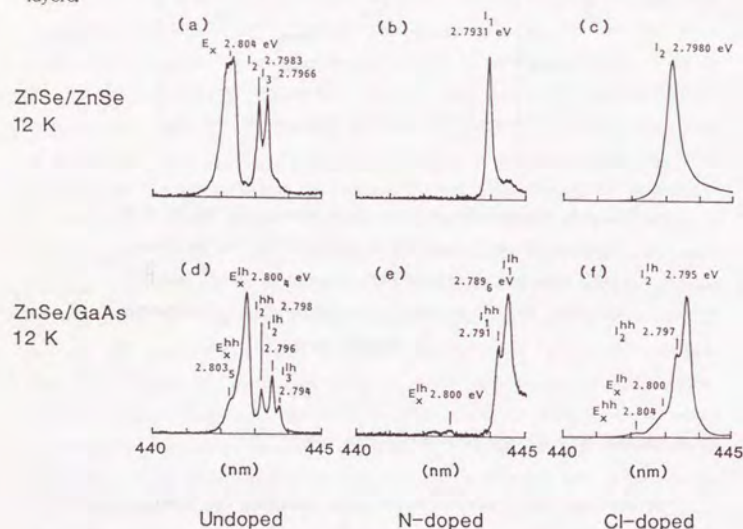


FIG. 4.9. Excitonic emission spectra (440-445 nm) from (a) undoped, (b) N-doped and (c) Cl-doped ZnSe homoepitaxial layers, and (d) undoped, (e) N-doped and (f) Cl-doped ZnSe heteroepitaxial layers at 12 K.

References

- H. Mitsuhashi, I. Mitsuishi, M. Mizuta, and H. Kukimoto, *Jpn. J. Appl. Phys.* **24**, L578 (1985).
- T. Yao, Y. Okada, S. Matsui, K. Ishida, and I. Fujimoto, *J. Cryst. Growth.* **81**, 518 (1987).
- G.E. Pikus, and G.L. Bir, *Sov. Phys. Solid State* **1**, 1502 (1960).
- H. Asai, and K. Oe, *J. Appl. Phys.* **54**, 2052 (1983).
- P.J. Dean, *Phys. Stat. Sol. (a)*, **81**, 625 (1984).
- T. Yao, Y. Makita, and S. Maekawa, *Jpn. J. Appl. Phys.* **20**, L741 (1981).
- J.E. Potts, H. Cheng, S. Mohapatra, and T.L. Smith, *J. Appl. Phys.* **61**, 333 (1987).
- H.A. Mar, and R.M. Park, *J. Appl. Phys.* **60**, 1229 (1986).
- K. Ohkawa, T. Mitsuyu, and O. Yamazaki, *Phys. Rev. B* **38**, 12465 (1988).
- K. Ohkawa, T. Mitsuyu, and O. Yamazaki, *J. Cryst. Growth.* **86**, 329 (1988).
- M. Isshiki, *J. Cryst. Growth* **86**, 342 (1988).
- K. Ohkawa, T. Mitsuyu, and O. Yamazaki, in *Abstracts of the Spring Meeting of the Japan Society of Applied Physics*, 1a-Y-3, 1986.
- P.J. Dean, W. Stutius, G.F. Neumark, B.J. Fitzpatrick, and R.N. Bhargava, *Phys. Rev. B* **27**, 2419 (1983).
- D.J. Olego, K. Shahzad, J. Petruzzello, and D.A. Cammack, *Phys. Rev. B* **36**, 7674 (1987).
- Y.S. Touloukian, R.K. Kirby, R.E. Taylor, and T.Y.R. Lee, in *Thermophysical Properties of Matter*, edited by Y.S. Touloukian (Plenum, New York, 1977), Vol. 13.
- J.B. Mullin, B.W. Straughan, C.M.H. Driscoll, and A.F.W. Wiloughby, in

- "Institute of Physics Conference Series", (IOP, Bristol, 1975), Vol. 24.
- 17 H.P. Singh, and B. Dayal, *Phys. Status Solidi* **23**, K93 (1967).
 - 18 B.H. Lee, *J. Appl. Phys.* **41**, 2984 (1970).
 - 19 A. Kamata, K. Hirahara, M. Kawachi, and T. Beppu, in *Extended Abstracts of the 7th Conference on Solid State Devices and Materials* (The Japan Society of Applied Physics, Tokyo, 1985), p. 233.
 - 20 R.L. Gunshor, and L.A. Kolodziejski, *IEEE J. Quantum Electron.* **24**, 1744 (1988).
 - 21 D.W. Langer, and R.N. Euwema, *Phys. Rev. B* **2**, 4005 (1970).
 - 22 G.H. Olsen, C.J. Nuese, and R.T. Smith, *J. Appl. Phys.* **49**, 5523 (1978).
 - 23 K. Ohkawa, T. Karasawa, A. Yoshida, T. Hirao, and T. Mitsuyu, *Appl. Phys. Lett.* **54**, 2553 (1989).
 - 24 K. Ohkawa, T. Karasawa, and T. Mitsuyu, *J. Vac. Sci. Technol. B* **9**, 1934 (1991).
 - 25 K. Ohkawa, and T. Mitsuyu, *J. Appl. Phys.* **70**, 439 (1991).
 - 26 K. Ohkawa, A. Ueno, and T. Mitsuyu, to be published in *J. Cryst. Growth*.
 - 27 K. Ohkawa, and T. Mitsuyu, to be published in *J. Lumin.*

CHAPTER 5

ELECTRICAL AND OPTICAL PROPERTIES OF Cl-DOPED n-TYPE ZnSe LAYERS

5.1. Introduction

Low-temperature photoluminescence (PL) spectra from n-type ZnSe heteroepitaxial layers are dominated by neutral donor-bound exciton emission (I_2) having two peaks that are ascribed not to two different impurities but to the split of the valence band to heavy- and light-hole branches. The result in the previous chapter shows that high-quality n-type ZnSe heteroepitaxial layers show two intense I_2 emissions.

Intrinsic ZnSe should exhibit high resistivity and well-suppressed I_2 emission. Although as-grown ZnSe bulk exhibited high resistivity, it is not due to high purity but due to defects caused by so-called self-compensation effect.¹ Before 1984, undoped ZnSe layers grown by molecular beam epitaxy (MBE)² or by metal-organic chemical vapor deposition (MOCVD)³ also exhibited n-type conduction with carrier concentration of 10^{16} cm^{-3} . Thus electrical properties of MBE-grown or MOCVD-grown ZnSe layers were poor. Recently, Yoneda et al.⁴, Mitsuyu et al.⁵ and Wakitani et al.⁶ have indicated that undoped high-resistivity ZnSe layers are possible to be grown by MBE using highly purified source materials. It was found that n-type conduction in undoped ZnSe layers was due to donor contamination of source materials. Intrinsic ZnSe layers obtained have shown high resistivity ($> 10^4 \Omega\text{cm}$) and dominant free exciton emission (E_x) in low-temperature PL measurement.⁴⁻⁶ Strong E_x emission indicates

good crystalline quality of the layer.⁷

Stutius⁸ reported on Al-doped n-type ZnSe grown by MOCVD in 1981. Kitagawa et al.⁹ reported in 1980 that Ga-doped ZnSe grown by MBE has resistivity of 0.07 Ωcm . Electron concentrations in both Al and Ga doping cases have been limited on the order of 10^{17} cm^{-3} . Heavier doping has resulted in a decrease in carrier concentration together with quenching band-edge PL emission.^{10,11} Carrier concentration of n-type ZnSe is, therefore, controlled up to the order of 10^{17} cm^{-3} . These n-type ZnSe layers were not fully degenerated. Behaviors of electron concentration and mobility are unknown since degenerated n-type ZnSe has not been obtained so far.

Low-temperature PL spectra from lightly doped ZnSe layers show I_2 emissions originated from donor species. Bhargava¹² and Dean et al.¹³ have shown donor ionization energies of group III and VII elements in ZnSe from the study of PL spectra. Yao et al.¹⁰ and Niina et al.¹¹ reported on Ga-doping level dependence of room-temperature PL properties. They indicated that over doping introduced deep levels. Optical properties of ZnSe with higher carrier concentration have never discussed so far.

Low-resistivity Cl-doped ZnSe layers were shown in Sec. 2.3.2. Electron concentration at 300 K has reached the order of 10^{19} cm^{-3} ,^{14,15} suggesting that fully generated n-type ZnSe has been attained by Cl doping. The behaviors of electrical and optical properties of degenerated ZnSe are investigated in this study. This chapter will discuss Cl-donor-concentration dependence of electrical and optical properties. Scattering mechanism of electrons in MBE-grown ZnSe hetero and homoepitaxial layers is also described here.

5.2. Activation of donors and scattering mechanisms of electrons

Electrical properties of ZnSe layers were evaluated by means of Hall measurement, i.e., the van der Pauw method^{16,17}. Electrical properties of Cl-doped ZnSe with various doping levels are shown in Table 5.1. At $T_{\text{Cl}} = 250\text{ }^\circ\text{C}$, carrier concentration attained $2.2 \times 10^{19}\text{ cm}^{-3}$. This is the highest carrier concentration ever achieved of n-type ZnSe. The value obtained shows a remarkable improvement by two orders of magnitude in comparison with Al-doped⁸ or Ga-doped¹¹ ZnSe layers previously reported.

TABLE 5.1. Dependence of electrical properties of Cl-doped ZnSe layer at 300 K on ZnCl_2 cell temperatures.

T_{Cl} [$^\circ\text{C}$]	ρ [Ωcm]	n [cm^{-3}]	μ [$\text{cm}^2/(\text{Vs})$]	
150	(2.8×10^0)	(5.3×10^{15})	(420)	
175	2.3×10^{-1}	6.6×10^{16}	400	
200	3.3×10^{-2}	5.2×10^{17}	380	
225	6.8×10^{-3}	4.7×10^{18}	200	
250	3.4×10^{-3}	9.6×10^{18}	200	
170	2.6×10^{-1}	6.0×10^{16}	400	(Homoepitaxy)
250	1.3×10^{-3}	2.2×10^{19}	210	(Homoepitaxy)

Temperature dependence of carrier concentration for different Cl doping levels are shown in Fig. 5.1. In the case of heavy doping ($T_{\text{Cl}} = 225$ and $250\text{ }^\circ\text{C}$), it is found that these carrier concentrations remain constant over a wide range of temperature (from 77 to 333 K). The concentration of Mott transition¹⁸ is given by

$$N_M = a_B^{*-3}/64 \quad (5.1)$$

$$a_B^* = a_B m_0/m_e^* = 0.530 m_0/m_e^* [\text{\AA}] \quad (5.2)$$

where a_B^* is effective Bohr radius, 30.3 \AA for the donor electron. The concentration N_M for ZnSe is $5.6 \times 10^{17} \text{ cm}^{-3}$. Since the experimental carrier

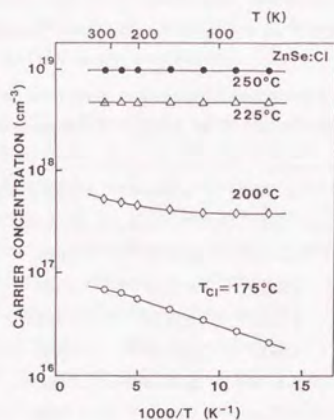


FIG. 5.1. Temperature dependence of carrier concentrations for ZnSe layers grown with various ZnCl_2 cell temperatures.

concentrations for $T_{\text{Cl}} = 225$ and 250°C are greater than N_M , the phenomenon is the Mott transition. The layers are, therefore, fully degenerate; wave function of high-density Cl donor electrons overlap and an impurity band is formed. At $T_{\text{Cl}} = 175^\circ\text{C}$ the carrier concentration

exhibited a considerable temperature dependence. In nondegenerate statistics, carrier concentration is given by¹⁹

$$\frac{n(n + N_a)}{(N_d - N_a - n)N_c} = \frac{\exp(-E_D/kT)}{g} \quad (5.3)$$

where g ($= 2$) is the degeneracy factor for donor levels, E_D is donor ionization energy, and N_d and N_a are the concentrations of donor and acceptor, respectively. N_c is the effective density of states in the conduction band and is given by¹⁹

$$N_c = 2 (2\pi m_e^* kT/h^2)^{3/2} \\ = 4.01 \times 10^{18} (T/300)^{3/2} (\text{cm}^{-3}) . \quad (5.4)$$

The donor ionization energy $E_D = 22 \text{ meV}$ and $N_D = 7.1 \times 10^{16}$ for Cl-doped ZnSe grown at $T_{\text{Cl}} = 175^\circ\text{C}$ are calculated by using Eqs. (5.3,4). This value of E_D is in good agreement with 26.2 meV determined by an optical measurement¹² for Cl donor in ZnSe.

Scattering mechanisms of carrier have two groups of phonons and defects. Polar optical phonon scattering, piezoelectric phonon scattering and acoustic phonon belong to the former group. Ionized impurity scattering and neutral impurity scattering belong to the latter group. A brief account of each of the scattering mechanisms will be given below.

(a) Polar optical phonon scattering. Polar optical phonon scattering results from the polar interaction between charged carriers and optical phonons. Because of the partially ionic character of ZnSe ionicity of which is 0.63, longitudinal optical phonons induce electrostatic potential. The expression obtained for the dependence of mobility on polar

longitudinal optical phonon scattering is given by²⁰

$$\mu_{po} = 89.9 \frac{m_0^{3/2}}{m^{*3/2}} \frac{1}{\epsilon_0/\epsilon_\infty - \epsilon_0/\epsilon_s} \frac{T^{3/2} \sinh(\theta_d/T/2)}{\theta_d^2 K_1(\theta_d/T/2)} \quad (5.5)$$

where θ_d is the Debye temperature and $K_1(x)$ is the type-II modified Bessel function. Using the values of Table 1.1, the mobility for ZnSe is obtained as follows

$$\mu_{po} = 8.97 \times 10^2 (T/300)^{3/2} \sinh(184/T)/K_1(184/T) \text{ [cm}^2\text{/(Vs)]}. \quad (5.6)$$

Equation (5.6) gives $\mu_{po} = 466$ and $6520 \text{ cm}^2\text{/(Vs)}$ at 300 and 77 K, respectively. Influence of this polar optical phonon scattering is important at room temperature.

(b) Piezoelectric phonon scattering. ZnO, CdS and CdSe are II-VI crystals which are strongly piezoelectric. Piezoelectric implies electric polarization effects induced in a crystal by the application of a mechanical stress. The mechanical stress takes the periodic form of the acoustic lattice vibrations which activate polarization fields to modify the transport properties of carriers at low temperature. The expression obtained for the dependence of mobility on piezoelectric phonon scattering is given by²¹

$$\mu_{pe} = 1.05 C_{11} (\epsilon_s/\epsilon_0)^2 e_{14}^{-2} (m^*/m_0)^{-3/2} T^{-1/2}. \quad (5.7)$$

Equation (5.7) gives μ_{pe} for ZnSe by using ZnSe parameters in Table 1.1 as follows,

$$\mu_{pe} = 3.15 \times 10^5 (T/300)^{-1/2} \text{ [cm}^2\text{/(Vs)]}. \quad (5.8)$$

μ_{pe} decreases with increasing temperature. However, the value at 300 K is as large as $3.15 \times 10^5 \text{ cm}^2\text{/(Vs)}$.

(c) Acoustic phonon scattering. This is based on a wave phenomenon. The vibration of atoms deforms the potential energy configuration of the atoms and leads to small vibrations in the energy gap. The variation in the energies of the conduction and valence band edges resulting from the vibrational motion is localized; these changes in potential energy of the carriers. Hence the mobility of electron is modified by the effect of lattice vibrations according to²²

$$\mu_{ac} = \frac{2(2\pi)^{1/2}}{3} \frac{eh^4 \rho v_s^2}{E_{AC}^2 m^{*5/2}} (kT)^{-3/2} \quad (5.9)$$

where E_{AC} is conduction band acoustic deformation potential, v_s is the longitudinal velocity of sound and ρ is the density. Using the values in Table 1.1, μ_{ac} of ZnSe is given by

$$\mu_{ac} = 3.52 \times 10^4 (T/300)^{-3/2} \text{ [cm}^2\text{/(Vs)]}. \quad (5.10)$$

Equation (5.10) gives $\mu_{ac} = 3.52 \times 10^4$ and $2.71 \times 10^5 \text{ cm}^2\text{/(Vs)}$ at 300 and 77 K, respectively.

(d) Ionized impurity scattering. Ionized impurity scattering results from either deliberately introduced impurities or lattice defects (such as negative charged Zn vacancies²³) generated by non-stoichiometry of the compounds. Coulomb field of the ionized defect deflects the electron or hole from its paths in a way that depends on the sign of the charge on the scattering center. Ionized impurity scattering is particularly important

at low temperatures when the thermal motion of the lattice atoms is small. An expression derived for the mobility dominated by ionized impurity scattering in a nondegenerate material is²⁴

$$\mu_{ii} = \frac{3.28 \times 10^{15} (\epsilon_s/\epsilon_0)^2 (m^*/m_0)^{-3/2} N_i^{-1} T^{3/2}}{\ln(1+X) - X/(1+X)} \quad (5.11)$$

in ZnSe

$$= \frac{3.56 \times 10^{21}}{N_i} (T/300)^{3/2} \frac{1}{\ln(1+X) - X/(1+X)} [\text{cm}^2/(\text{Vs})] \quad (5.12)$$

where N_i and n are the ionized donor and free electron concentrations, respectively. X is defined as follows

$$X = 1.29 \times 10^{14} (m^*/m_0) (\epsilon_s/\epsilon_0) T^2/n \quad (5.13)$$

in ZnSe

$$= 1.70 \times 10^{19}/n (T/300)^2. \quad (5.14)$$

Assuming $N_i = n$, equations (5.12) and (5.14) give $\mu_{ii}(300\text{K})$ 8.58×10^3 and $1.83 \times 10^3 \text{ cm}^2/(\text{Vs})$ for samples with $n_{300\text{K}} = 1 \times 10^{17}$ and $1 \times 10^{18} \text{ cm}^{-3}$, respectively.

(e) Neutral impurity scattering. A part of ionized donor impurities recombines a free electron at low temperature. Neutral impurities scatter free electrons in the conduction band. An expression derived for the mobility by neutral impurity scattering is²⁵

$$\mu_{ni} = \frac{e}{20 a_B^* N_n} = \frac{1.43 \times 10^{22}}{N_n} \frac{m^*}{m_0} \frac{\epsilon_s}{\epsilon_0} \quad (5.15)$$

in ZnSe

$$= 2.51 \times 10^{20}/N_n \quad [\text{cm}^2/(\text{Vs})] \quad (5.16)$$

where N_n is neutral impurity concentration. Temperature dependence of μ_{ni} is caused from the temperature dependence of N_n .

The total mobility μ_{total} , which includes the five mechanisms above, is approximately²⁶

$$\mu_{\text{total}}^{-1} = \sum \mu_i^{-1} = \mu_{po}^{-1} + \mu_{pe}^{-1} + \mu_{ac}^{-1} + \mu_{ii}^{-1} + \mu_{ni}^{-1}. \quad (5.17)$$

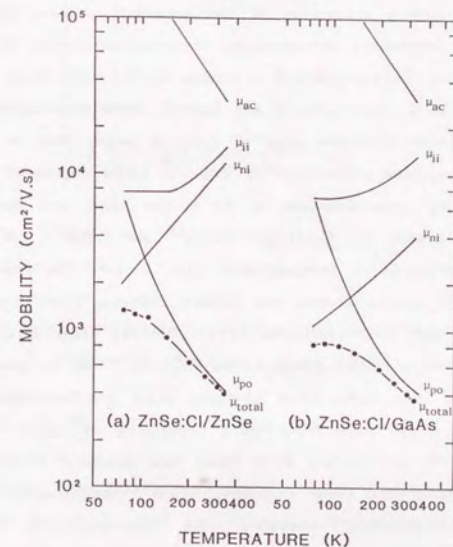


FIG. 5.2. Temperature dependence of electron mobility for Cl-doped ZnSe homoepitaxial and heteroepitaxial layers.

Figure 5.2 shows temperature dependence of Hall mobility of experiments and calculations. Samples are Cl-doped ZnSe homo and heteroepitaxial layers with carrier concentration $n_{300K} = 6 \times 10^{16} \text{ cm}^{-3}$. These layers have several features in common: 1) polar optical phonon scattering limits mobility at higher temperature; 2) neutral impurity scattering mainly affects electron mobility at lower temperature; 3) piezoelectric and acoustic phonon scatterings are negligible in this temperature region. Since lattice vibration is strong at higher temperature, phonon scatterings are dominant factor which affects the electron mobility. The effect of polar optical phonon scattering is the greatest in case of ZnSe and GaAs²⁷. With decreasing temperature, electron scattering by defects is getting effective, because lattice vibration is "frozen". Since velocity of an electron is slow, both ionized and neutral impurity scatterings deflect electrons. Electron effective mass of ZnSe is larger than in GaAs. Thus influence of impurity scatterings in ZnSe is large compared with GaAs. Neutral impurity concentrations at 77 K for homo and heteroepitaxial layers calculated from Eq. (5.15) are 1.2×10^{17} and $2.5 \times 10^{17} \text{ cm}^{-3}$, indicating that the concentration of homoepitaxial layer is low. The neutral impurity may consist of neutral donors and lattice defects. Donor concentrations (N_D) of homo and heteroepitaxial layers derived from Eqs. (5.3,4) are $7 \times 10^{16} \text{ cm}^{-3}$. Neutral donor concentration (N_D^0) at 77 K is, therefore, about $5 \times 10^{16} \text{ cm}^{-3}$ in both cases, since Cl-doped homo and heteroepitaxial layers in Fig. 5.2 show the same temperature dependence of carrier concentration at $T_{Cl} = 175 \text{ }^\circ\text{C}$ in Fig. 5.1. It is found that influence of lattice defects involves vacancies and their complex. Since homoepitaxial layers have fairly well crystallinity compared with heteroepitaxial layers, Hall mobility of the Cl-doped homoepitaxial layer has reached $1310 \text{ cm}^2/(\text{Vs})$ at 77 K.

Figure 5.3 shows temperature dependence of the Hall mobility for

different doping levels. In the case of light doping ($T_{Cl} = 175 \text{ }^\circ\text{C}$), the Hall mobility decreases with increasing temperature because of the polar optical phonon scattering. At lower temperature the mobility tends to saturate for $T_{Cl} = 175 \text{ }^\circ\text{C}$ and to decrease for $T_{Cl} = 200 \text{ }^\circ\text{C}$ owing to the ionized and neutral impurity scatterings. It is found that the Hall mobility is almost independent of temperature in the heavy doping levels

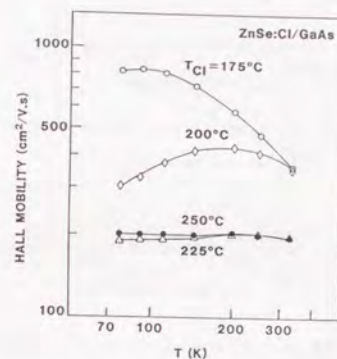


FIG. 5.3. Temperature dependence of Hall mobilities for ZnSe layers with various doping levels.

($T_{Cl} = 225$ and $250 \text{ }^\circ\text{C}$). This indicates that the mobilities of these layers are dominated by neutral impurity scattering due to both neutral donors and lattice defects. The difference between neutral impurity concentration calculated from Eq. (5.16) and neutral donor concentration, therefore, implies density of lattice defects. These defects will affect the crystallinity of Cl-doped ZnSe layers. Figure 5.4 shows influence of lattice defects ($N_n - N_D^0$) on crystallinity of the layers. With increasing

lattice defects, FWHMs of x-ray rocking curves for Cl-doped layers increase. Lattice defects in the electron scattering presumably include inactive Cl atoms observed for heavily doped ZnSe (see Sec. 2.3.2), vacancies and their complexes (Cl donor-vacancy).

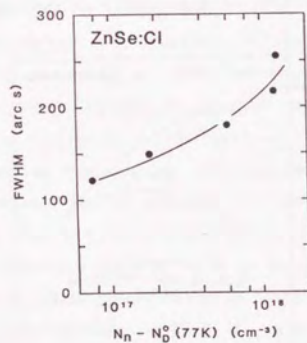


FIG. 5.4. FWHMs of x-ray rocking curves for Cl-doped ZnSe layers as a function of difference between neutral impurity concentration and neutral donor concentration at 77 K.

5.3. Donor concentration dependence of photoluminescence properties¹⁴

Photoluminescence spectra from undoped and Cl-doped ZnSe layers at room temperature (RT) are shown in Fig. 5.5. Undoped layer exhibits band-edge emission around 2.689 eV (461 nm). Deep-level emission in 500-700-nm range is scarcely observed, indicating the absence of deep centers such as the self-activated centers. For the Cl-doped ZnSe layer

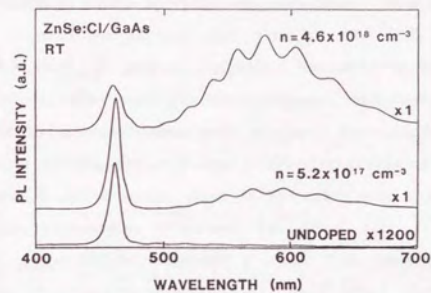


FIG. 5.5. Room-temperature PL spectra from undoped and Cl-doped ZnSe layers.

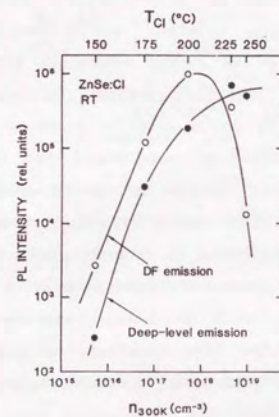


FIG. 5.6. Room-temperature PL peak intensity v.s. carrier concentration for DF and deep-level emissions from Cl-doped ZnSe layers.

with $n_{300K} = 5.2 \times 10^{17} \text{ cm}^{-3}$, the band-edge emission significantly increases; the intensity is 1600 times greater than that of the undoped layer. (Refer to the scale factor indicated in Fig. 5.5.) For $n_{300K} = 4.6 \times 10^{18} \text{ cm}^{-3}$, however, broad deep-level emission around 2.15 eV (580 nm) increases and overcomes the band-edge emission. The peak intensity of the band-edge emission and that of the deep-level emission are plotted in Fig. 5.6 as a function of carrier concentration at room temperature. It can be seen in this figure that the band-edge emission remarkably increases with increasing doping level and shows a maximum around $n_{300K} = (5-10) \times 10^{17} \text{ cm}^{-3}$. It has been found that the maximum intensity of the band-edge emission is 4 times larger than that of our Ga-doped ZnSe layers grown at the optimum condition.^{28,29} The deep-level emission also increases with increasing the doping level, but is considerably weaker than the band-edge emission even at $n_{300K} = 5.2 \times 10^{17} \text{ cm}^{-3}$. These results suggest that Cl is superior to Ga as an n-type dopant in terms of the optical property as well as the electrical property. Intensity of the band-edge emission relates to the Cl doping level as shown in Fig. 5.6. The peak energy at 2.689 eV observed at room temperature is smaller than the band-gap energy of 2.715 eV³⁰ by 26 meV, which agrees well with the Cl-donor ionization energy of 26.2 meV. Therefore, the room-temperature band-edge emission can be attributed to recombination radiation between an electron trapped at a Cl donor and a free hole in the valence band (DF). The origin of the deep-level emission is uncertain at present, but probably is related to the lattice defects such as complex centers involving Cl atoms associated with vacancies suggested in the previous section.

5.4. Screening and Stark effects due to donors on excitons

Figure 5.7 shows PL spectrum at 4.2 K measured for Cl-doped ZnSe with $T_{Cl} = 150 \text{ }^\circ\text{C}$. The peak of which is at 2.801 eV is due to the ground-state free exciton. The presence of the distinct E_x line indicates good crystallinity of this epitaxial layer. The figure shows other several

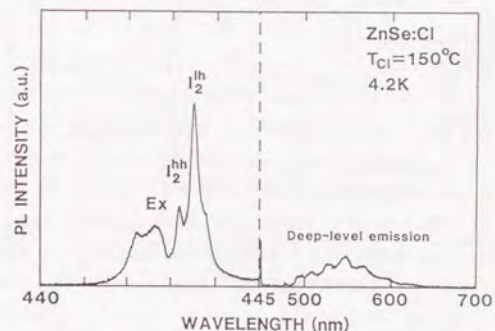


FIG. 5.7. PL spectrum measured at 4.2 K for Cl-doped ZnSe grown with the ZnCl_2 cell temperature of $150 \text{ }^\circ\text{C}$.

intense emissions; in particular, a dominant peak at 2.795 eV is the light-hole (lh) branch of I_2 emission, and 2.798-eV peak is the heavy-hole (hh) branch. The donor-acceptor pair emission (DAP) around 2.7 eV (460 nm) was not observed, indicating that there is no acceptor impurities. PL spectra in excitonic emission region measured for the sample with different doping levels are shown in Fig. 5.8. Intensity of the I_2 emission (light- and heavy-hole branches) remarkably increases in the range up to $T_{Cl} = 200 \text{ }^\circ\text{C}$. The ratio of the intensity for $T_{Cl} = 150 \text{ }^\circ\text{C}$ to that for $T_{Cl} = 200 \text{ }^\circ\text{C}$

is found to be 1 : 50. This value is in good agreement with the ratio of ZnCl_2 vapor pressure at these temperatures. This fact indicates that Cl atoms are effectively doped as shallow donors and originate I_2 emission.

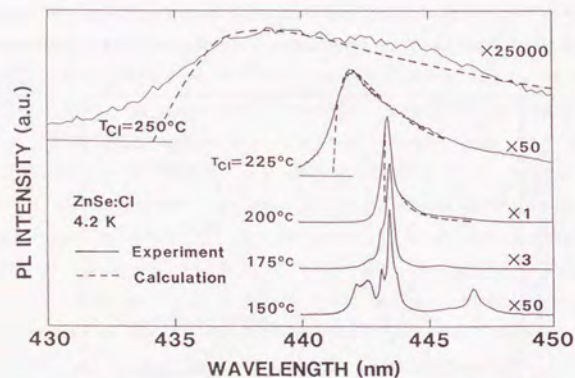


FIG. 5.8. PL spectra in excitonic region measured at 4.2 K for Cl-doped ZnSe layers. Dashed lines show calculated line shape of I_2 emission.

I_2 emission shifts toward higher energy at the heavier doping level together with asymmetric broadening with tail extending to lower energy. These phenomena are remarkable for the samples having the carrier concentration greater than that of Mott transition, i.e., $N_M = 5.6 \times 10^{17} \text{ cm}^{-3}$. A similar fact was observed by Tsang et al.³¹ for GaP crystals and by Kukimoto et al.³² for CdS crystals. The phenomena for ZnSe have been observed for the first time in this study because of the success of the growth of low-resistivity n-type ZnSe.

The observed peak shift of I_2 emission toward higher energies with increasing donor concentration corresponds to the decrease in the binding energy of the excitons.^{32,33} Further understanding of this phenomena requires consideration of the shift of band edges owing to the high density donors. Such an edge shift has been frequently discussed in relation to impurity conduction phenomenon as well as to optical transitions near band edge at high impurity concentration. However, the direct experimental evidence for it has never been reported so far. Hanamura³³ has shown that the edge shift of both the conduction and valence bands can be regarded to be negligibly small. This characteristic behavior of the binding energies of bound excitons is well interpreted in terms of the screening effect of donor electrons on excitons.

The I_2 emission is remarkably broadened beyond the excess donor concentration of Mott transition, and with increasing donor concentrations the line shape becomes quite asymmetric with a tail toward the low energy side of the peak. Such an anomalous spectral shape is not explained by the usual phonon-assisted transition. The samples involve considerable numbers of charged impurities. Then the Stark effect due to these charged impurities is of primary importance since it is dipole-monopole interaction. The following discussion shows that the observed asymmetric broadening phenomenon of I_2 emission is interpreted as being caused by this Stark Effect.

The asymmetric broadening of I_2 emission is treated theoretically in terms of the Stark effect due to charged impurities. Owing to Hanamura's theory, the energy of a bound exciton is lowered. It is assumed that among charged impurities distributed at random in the crystal only the one which is located nearest to a bound exciton contributes to the Stark effect on that bound exciton. The nearest impurity obeys the Poisson distribution. Then, the spectral line shape of the I_2 emission, expressed

by $I(E)$ in which E is the absolute value of the shift of the energy of the bound exciton which is affected by the screening effect, is given by³³

$$I(E) = CAE^{-7/4} \exp(-4/3AE^{-3/4}) \quad (5.18)$$

$$A = \pi N_i a_0^*{}^3 (4E_{i0})^{3/4}.$$

Here, N_i is the ionized impurity concentration, a_0^* and E_{i0} are the effective Bohr radius and binding energy of intrinsic exciton, respectively, and C is a proportionality constant. The fit between the experimental and theoretical spectra was tested by taking N_i as an adjustable parameter. This was done so as to obtain the best fit at the peak and at the low energy region. The results are shown in Fig. 5.8 for three samples with high donor concentrations. As is seen in the figure, the fit is quite satisfactory except for the high energy side. It can be concluded that the peculiar line shape observed for samples with high donor concentrations is due to the Stark effect of charged impurities. The ionized impurity concentrations N_i thus determined are 5.5×10^{17} , 3.0×10^{18} and $1.0 \times 10^{19} \text{ cm}^{-3}$ for samples with $T_{Cl} = 200, 225$ and $250 \text{ }^\circ\text{C}$, respectively. These samples are degenerated, samples with $T_{Cl} = 225$ and $250 \text{ }^\circ\text{C}$ in particular are fully degenerated. Since 4.2-K resistivities of these samples were almost constant, carrier concentrations may be constant. The charged impurity that causes the Stark effect is ascribed to ionized Cl donors. This result confirms that the assumption of $N_i = n$ in Eq. (5.11) is valid.

References

- ¹ G. Handel, Phys. Rev. A **134**, 1073 (1964).
- ² T. Yao, M. Ogura, S. Matsuoka, and T. Morishita, Jpn. J. Appl. Phys. **22**, L144 (1983).
- ³ S. Fujita, Y. Matsuda, and A. Sasaki, Jpn. J. Appl. Phys. **23**, L360 (1984).
- ⁴ K. Yoneda, Y. Hishida, T. Toda, H. Ishii, and T. Niina, Appl. Phys. Lett. **45**, 1300 (1984).
- ⁵ T. Mitsuyu, K. Ohkawa, and O. Yamazaki, Appl. Phys. Lett. **49**, 1348 (1986).
- ⁶ J. Wakitani, K. Yanashima, T. Yasuda, J. Yoshino, and H. Kukimoto, in Abstracts of the Autumn Meeting of the Japan Society of Applied Physics, 29p-PA-8, 1989.
- ⁷ K. Ohkawa, T. Karasawa, and T. Mitsuyu, J. Vac. Sci. Technol. B **9**, 1934 (1991).
- ⁸ W. Stutius, Appl. Phys. Lett. **38**, 352 (1981).
- ⁹ F. Kitagawa, T. Mishima, and K. Takahashi, J. Electrochem. Soc. **127**, 937 (1980).
- ¹⁰ T. Yao, and M. Ogura, in Collected Paper of MBE-CST-2, 1982, Tokyo, p.215.
- ¹¹ T. Niina, T. Minato, and K. Yoneda, Jpn. J. Appl. Phys. **21**, L387 (1982).
- ¹² R.N. Bhargava, J. Cryst. Growth **59**, 15 (1982).
- ¹³ P.J. Dean, D.C. Herbert, C.J. Werkhoven, B.J. Fitzpatrick, and R.N. Bhargava, Phys. Rev. B **23**, 4888 (1981).
- ¹⁴ K. Ohkawa, T. Mitsuyu, and O. Yamazaki, J. Appl. Phys. **62**, 3216 (1987).
- ¹⁵ K. Ohkawa, A. Ueno, and T. Mitsuyu, to be published in J. Cryst. Growth (1992).
- ¹⁶ L.J. van der Pauw, Philips Res. Rept. **13**, 1 (1958)
- ¹⁷ L.J. van der Pauw, Philips Tech. Rev. **20**, 220 (1958/59).

- 18 N.F. Mott, *Phil. Mag.*, **6**, 287 (1961).
- 19 S.S. Devlin, in "II-VI compounds" edited by M. Aven, and J.S. Prener (North-Holland, Amsterdam, 1967), p. 549.
- 20 E.M. Conwell, in "High field transport in semiconductors" (Academic Press, New York and London, 1969).
- 21 H.J.G. Meyer, and D. Polder, *Physica* **19**, 255 (1953).
- 22 J. Bardeen, and W. Shockly, *Phys. Rev.* **80**, 72 (1950).
- 23 T. Miyajima, H. Okuyama, K. Akimoto, Y. Mori, L. Wei, and S. Tanigawa, *Appl. Phys. Lett.* **59**, 1482 (1991).
- 24 H. Brooks, and C. Herring, *Phys. Rev.* **83**, 879 (1951).
- 25 C. Erginsoy, *Phys. Rev.* **79**, 1013 (1950).
- 26 J. Calaway, *Phys. Rev.* **113**, 1946 (1956).
- 27 C.M. Wolfe, G.E. Stillman, and W.T. Lindley, *J. Appl. Phys.* **41**, 3088 (1970).
- 28 K. Ohkawa, T. Mitsuyu, and O. Yamazaki, in Extended Abstracts of the 32nd Spring Meeting of the Japan Society of Applied Physics (The Japan Society of Applied Physics, Tokyo, 1986), 1a-Y-3.
- 29 K. Ohkawa, T. Mitsuyu, and O. Yamazaki, in Extended Abstracts of the 32nd Spring Meeting of the Japan Society of Applied Physics (The Japan Society of Applied Physics, Tokyo, 1986), 1a-Y-4.
- 30 Y. Shirakawa, and H. Kukimoto, *J. Appl. Phys.* **51**, 2014 (1980).
- 31 J.C. Tsang, P.J. Dean, and P.T. Landsberg, *Phys. Rev.* **173**, 814 (1968).
- 32 H. Kukimoto, S. Shionoya, S. Toyotomi, and K. Morigaki, *J. Phys. Soc. Jpn.* **28**, 110 (1970).
- 33 E. Hanamura, *J. Phys. Soc. Jpn.* **28**, 120 (1970).

CHAPTER 6

ELECTRICAL AND OPTICAL PROPERTIES OF NITROGEN-DOPED p-TYPE ZnSe LAYERS

6.1. Introduction

Although there has been plenty of reports which claimed the realization of p-type ZnSe such reports except for Li-doping have been poorly reproducible. Park et al.¹ reported in 1971 on hole concentration of $2.7 \times 10^9 \text{ cm}^{-3}$ and Hall mobility of $23 \text{ cm}^2/(\text{Vs})$ at room temperature. Nishizawa et al.² improved the hole concentration up to $3.0 \times 10^{15} \text{ cm}^{-3}$, then the mobility was $20 \text{ cm}^2/(\text{Vs})$. The highest hole concentration of Li-doped ZnSe was limited to the order of 10^{15} cm^{-3} . Preparation of highly-conductive p-type ZnSe has already been studied. Therefore, electrical and optical properties of p-type ZnSe have not been investigated in this study.

Nitrogen is the most promising element for p-type dopant of ZnSe considering the absence of formation of deep levels and no N-diffusion in ZnSe. Diffusion is one of the most important issues for device application. Doping of N in molecular beam epitaxy (MBE) process is very difficult because of the low-sticking coefficient of N_2 and NH_3 molecules. The author has achieved enhanced-incorporation of N impurities in MBE-grown ZnSe layers employing low-energy ion doping (N_2^+ , N^+).^{3,4} Although low-temperature photoluminescence (PL) showed ideal spectrum with dominant neutral acceptor-bound exciton emission (I_1) in Fig. 4.4 (b), N-doped ZnSe

layers had large resistivity. The relationship between PL and electrical properties is not well understood. To date articles of p-type ZnSe report electrical properties and/or low-temperature PL properties, but they did not discuss the relationship between these important properties. Low-temperature PL measurement reveals acceptor ionization energies,⁵⁻¹⁰ but this is not evidence of p-type conduction. Electrical properties are usually measured above 77 K. However, PL properties reported were measured below 77 K, typically 4.2 K.

Highly conductive p-type ZnSe heteroepitaxial¹¹⁻¹⁵ and homoepitaxial¹⁴⁻¹⁷ layers have been grown by MBE using active-nitrogen doping as shown in Sec. 2.3.4. The p-type ZnSe exhibits high carrier concentration and intense photoluminescence is observed even at room temperature. This chapter will discuss optical and electrical properties and their relationship.

6.2. Nitrogen-concentration dependence of photoluminescence properties

Lightly and heavily N-doped ZnSe layers have been grown by active-nitrogen doping. The lightly doped layer exhibited high resistivity of $1.5 \times 10^5 \Omega\text{cm}$ with a free hole concentration estimated at $4 \times 10^{11} \text{ cm}^{-3}$ assuming a mobility of $110 \text{ cm}^2/(\text{Vs})$. Heavily N-doped ZnSe layers showed p-type conduction with a hole concentration of $1.0 \times 10^{17} \text{ cm}^{-3}$ at 300 K. Figure 6.1 shows PL spectra from the lightly N-doped layer and the N-doped p-type layer at 12 K. The lightly N-doped ZnSe layer shows a dominant light-hole branch of I_1 emission at 2.789 eV and weak donor-acceptor pair emission (DAP) at 2.694 eV for the zero-phonon peak. The spectrum indicates that active-nitrogens are incorporated as N acceptors in ZnSe and donor concentration is very low. With increasing N acceptor

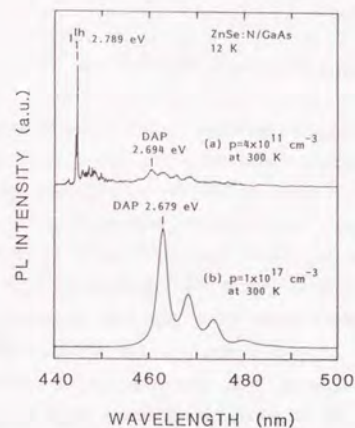


FIG. 6.1. 12-K PL spectra from (a) lightly N-doped ZnSe layers with hole concentration $4 \times 10^{11} \text{ cm}^{-3}$ and (b) N-doped p-type ZnSe layers with hole concentration of $1.0 \times 10^{17} \text{ cm}^{-3}$.

concentration, the intensity of DAP emission increased and I_1 emission decreased. Typical PL spectrum from p-type ZnSe grown by active-nitrogen doping is shown in Fig. 6.1 (b). The p-type ZnSe layer with hole concentration of $1 \times 10^{17} \text{ cm}^{-3}$ exhibits strong DAP emission at 2.679 eV. I_1 emission was very weak, of the order of 10^{-2} , compared with intensity of the DAP emission. Dominant DAP emission suggests that the p-type ZnSe layer is compensated by donors. Although conventional peak position of DAP emission is around 2.70 eV such as in Fig. 6.1 (a), p-type ZnSe grown by active-nitrogen doping shows at 2.68 eV for zero-phonon peak of DAP emission. Peak energy of DAP emission is given by Eq. (3.4) as follow,

$$\hbar\omega_{\text{DAP}} = E_g - (E_A + E_D) + e^2/(4\pi\epsilon_s R) \quad (6.1)$$

where E_g , E_A and E_D are band-gap energy, acceptor ionization energy and donor ionization energy, respectively. E_A for a N atom in the Se site (N_{Se}) is 111 meV determined by Dean et al.⁹ The last term is the Coulomb term. Since nitrogen concentration measured by secondary ion-mass-spectrometry (SIMS) is smaller than 10^{19} cm^{-3} , E_g and E_A may not be unchangeable by the alloy effect. The decrease in DAP peak energy may be due to E_D or the Coulomb term. The pair separation R decreases with increasing acceptor concentrations, and the Coulomb term will increase. The change in the Coulomb term, therefore, can not be interpreted as the decrease of $\hbar\omega_{\text{DAP}}$ by 20 meV. The decrease should be ascribed the donor ionization energy E_D . Thus E_D is as large as 50 meV. Such a deep donor is unknown so far since donor ionization energies of group III and VII elements have 25-30 meV as shown in Table 1.2. Nitrogen incorporated would be responsible for the deep donors. There are a few possible donors: (1) a N donor in the Zn site (N_{Zn}), (2) a $N_{\text{Zn}}-N_{\text{Se}}$ complex, (3) a $N_{\text{Se}}-\text{Se}$ vacancy complex, (4) an interstitial N donor. Except for donors expected at deep levels, Stark effect of ionized impurity on a donor electron and/or an acceptor hole is also possible for the low energy DAP emission of 2.68 eV. Further study will be needed to find out the reason for the 2.68-eV DAP emission.

Peak intensity of DAP emission depends on N concentration ($[N]$) evaluated by SIMS analysis as shown in Fig. 6.2. $[N]$ of every sample is greater than $1 \times 10^{18} \text{ cm}^{-3}$. Thus PL properties are dominated by DAP emission as in Fig. 6.1 (b). The maximum N concentration has reached as high as about $1 \times 10^{19} \text{ cm}^{-3}$ since an active nitrogen has a high sticking coefficient. The peak intensity of DAP emission decreases with increasing

$[N]$, indicating that nonradiative centers are induced by the doping. The sample with $[N] < 3 \times 10^{18} \text{ cm}^{-3}$ showed p-type conduction. More heavily-doped layers ($[N] > 3 \times 10^{18} \text{ cm}^{-3}$) did not exhibit p-type conduction. Considering the abrupt decrease of the DAP peak intensity around $[N] = 3 \times 10^{18} \text{ cm}^{-3}$, the carrier traps related to nonradiative centers are probably created by the overdoping.

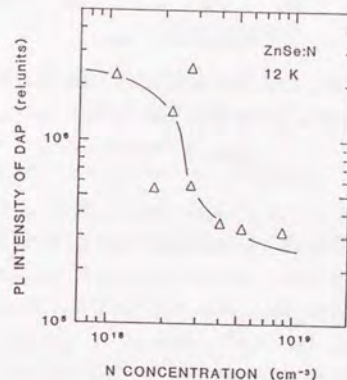


FIG. 6.2. Peak intensity of DAP emission from N-doped ZnSe layers with various N concentrations.

6.3. Impurity levels in nitrogen-doped homoepitaxial layers¹⁶

Low-temperature PL spectrum from a N-doped p-type ZnSe homoepitaxial layer with carrier concentration of $8.9 \times 10^{15} \text{ cm}^{-3}$ is shown in

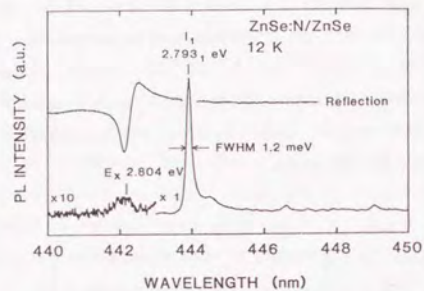


FIG. 6.3. 12-K excitonic emission and reflection spectra from N-doped p-type ZnSe homoepitaxial layer with $P_{300K} = 8.9 \times 10^{15} \text{ cm}^{-3}$.

Fig. 6.3 and 6.4. The p-type N-doped homoepitaxial layer exhibits strong I_1 and DAP emissions. Weak recombination emission between a free electron and an acceptor hole (FA) was also observed. Recombination emission between a donor electron and a free hole (DF) was not observed at 12 K, and appeared above 100 K.¹⁶ Although I_1 emission from N-doped heteroepitaxial layers is split and shift by biaxial strain and exhibit two peaks, the I_1 emission showed a single peak with narrow FWHM of 1.2 meV. The peak energy 2.7931 eV of I_1 emission is strain-free energy of I_1 emission related to a nitrogen acceptor. Weak peak at 2.804 eV is free exciton emission (E_x) which is confirmed by an exciton resonance dip in reflection spectrum in the inset of Fig. 6.3. DAP emission from the homoepitaxial layers has typical peak energy around 2.7 eV. Homoepitaxial layers have fairly good crystallinity which may suppress the creation of the deep donors.

Since homoepitaxial layers are free from strain, the peak energies

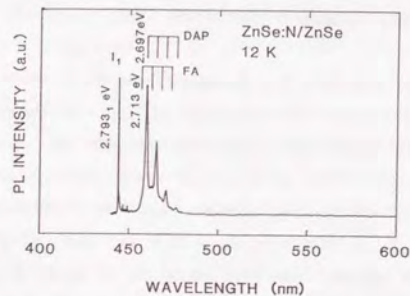


FIG. 6.4. Photoluminescence spectrum from N-doped ZnSe homoepitaxial layer at 12 K.

of DAP, FA and DF emissions are not shifted by biaxial strain. Using these peak energies, therefore, E_A and E_D in N-doped ZnSe and the Coulombic term can be calculated from Eqs. (3.5,6) as follows,

$$\hbar\omega_{DF} = E_g - E_D + 3.5 \text{ meV}, \quad (6.2)$$

$$\hbar\omega_{FA} = E_g - E_A + \frac{1}{2} kT, \quad (6.3)$$

Band-gap energy E_g is calculated by using the equation

$$E_g = E_x + 21 \text{ meV} \quad (6.4)$$

where the second term is the exciton binding energy derived from Eq. (3.3). The first term of free exciton energy E_x was obtained by Shirakawa et al.¹⁸ for the bulk ZnSe single crystal as follows,

$$E_x = 2.804 - 8.59 \times 10^{-4} T^2 / (T + 405) \text{ [eV]}. \quad (6.5)$$

Peak energies of DAP and FA emissions used were 2.697 and 2.713 eV, respectively, from 12-K PL spectrum in Fig. 6.4. Peak energy of DF emission was 2.687 eV at 300 K since DF emission was not observed in the 12-K PL spectrum from the N-doped ZnSe homoepitaxial layer. The acceptor and donor binding energies and the Coulombic term were calculated to be $E_A = 112.5$ meV, $E_D = 31.5$ meV and $e^2 / (4\pi\epsilon_s R) = 16$ meV, respectively. The acceptor ionization energy is in good agreement with the value in Table 1.3 of 111 meV determined by another optical measurement. The E_D is also a reasonable value of a shallow donor. The Coulombic term energy indicates the donor-acceptor pair separation R of about 100 Å.

6.4. Electrical properties

There are two problems in electrical measurements. The first problem is the influence of substrates. Every p-type ZnSe layers have been grown on GaAs substrates so far. In this case, there is a possibility of measuring p-type GaAs in the ZnSe/GaAs heterointerface by Zn diffusion into GaAs substrate from ZnSe layer, i.e., a Zn atom in a Ga site acts as an acceptor. The second possibility was pointed out by Neumark¹⁹ that twinning caused p-type conduction. Therefore the best way to confirm p-type ZnSe would be to measure p-type conduction in homoepitaxial layers without twinning.

The advantage of using ZnSe substrate is that electrical properties and optical properties of N-doped ZnSe layers can be measured without being affected by strain or diffusion from GaAs substrate. ZnSe substrates used were (100) oriented with high resistivity ($> 10^6 \Omega\text{cm}$) and were free

from twinning. N-doped ZnSe homoepitaxial layers exhibited p-type conduction in Hall measurement. Free hole concentration of typical N-doped ZnSe homoepitaxial layer with unoptimised doping condition was the order of 10^{16} cm^{-3} . The result provides the evidence of p-type conduction in N-doped ZnSe grown by MBE using the active-nitrogen beam.

The N concentration depended on various parameters. There is a tendency that a lower pressure of the discharge cell causes higher N

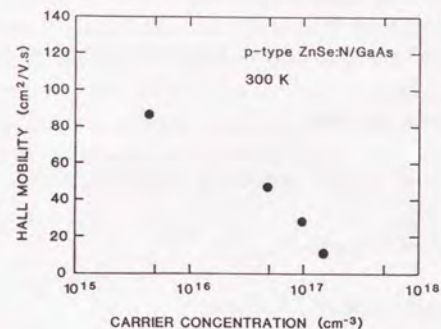


FIG. 6.5. Carrier concentration v.s. Hall mobility for p-type ZnSe layers on GaAs substrates at 300 K.

concentration and the N concentration increases with decreasing the beam flux ratio of $J_{\text{Se}}/J_{\text{Zn}}$. The pressure dependence suggests that the active nitrogen is quenched by collisions with other nitrogens at the ground state. Although the background pressure was about 1×10^{-9} Torr, the MBE chamber pressure at the active-nitrogen beam source operation was about $1 \times 10^{-7} - 3 \times 10^{-5}$ Torr where the flow rate of N_2 gas was 0.01 - 3.0 sccm. The beam flux ratio dependence indicates that acceptors incorporated by

the active-nitrogen doping substitutionally replace Se lattice sites, i.e., the acceptor is actually originated from nitrogen. The highest hole carrier concentration was as high as $1.5 \times 10^{17} \text{ cm}^{-3}$ at the optimized condition of the beam flux ratio $J_{\text{Se}}/J_{\text{Zn}}$ and the N_2 flow rate. The N-doped ZnSe showed low resistivity of $3.8 \text{ } \Omega\text{cm}$ and Hall mobility of $11 \text{ cm}^2/(\text{Vs})$. The concentration of Mott transition of p-type ZnSe is as high as $4.7 \times 10^{19} \text{ cm}^{-3}$ calculated from Eq. (5.1,2). Degenerated properties was not observed for the N-doped p-type ZnSe. Hall mobility increases with decreasing hole concentration as shown in Fig. 6.5.

Scattering mechanisms of holes are almost the same as that of electrons in Eqs. (5.5-15):

(a) Polar optical phonon scattering.

$$\mu_{\text{po}} = 9.80 \times 10^1 (T/300)^{3/2} \sinh(184/T)/K_1(184/T) \text{ [cm}^2/(\text{Vs})] \quad (6.6)$$

(b) Piezoelectric phonon scattering.

$$\mu_{\text{pe}} = 3.44 \times 10^4 (T/300)^{-1/2} \text{ [cm}^2/(\text{Vs})] \quad (6.7)$$

(c) Acoustic phonon scattering.

$$\mu_{\text{ac}} = 9.69 \times 10^2 (T/300)^{-3/2} \text{ [cm}^2/(\text{Vs})] \quad (6.8)$$

(d) Ionized impurity scattering.

$$\mu_{\text{ii}} = \frac{1.70 \times 10^{21}}{N_i} (T/300)^{3/2} \frac{1}{\ln(1+X) - X/(1+X)} \text{ [cm}^2/(\text{Vs})] \quad (6.9)$$

$$X = 7.43 \times 10^{19}/n (T/300)^2$$

(e) Neutral impurity scattering.

$$\mu_{\text{ni}} = \frac{1.10 \times 10^{21}}{N_n} \text{ [cm}^2/(\text{Vs})] \quad (6.10)$$

Phonon scatterings at 300 K give $\mu_{\text{po}} = 50.8$, $\mu_{\text{pe}} = 34400$, $\mu_{\text{ac}} = 969 \text{ cm}^2/(\text{Vs})$. Influence of polar optical phonon scattering is important for hole scattering. Many ionized impurity (including donor impurities) would exist in N-doped p-type ZnSe since PL spectra was dominated by intense DAP emission. Thus ionized impurity scattering may suppress the Hall mobility. Ionized impurity concentration N_i can be calculated by Eq. (6.9), assuming that neutral impurity scattering is negligible. Ionized acceptor concentration N_A^- and ionized donor concentration N_D^+ are derived from

$$N_i = N_A^- + N_D^+ \quad (6.11)$$

$$p = N_A^- - N_D^+ \quad (6.12)$$

The compensation ratio $\theta = N_D^+/N_A^-$ was calculated for p-type ZnSe. The compensation ratios of p-type layers with $p = 1.0$ and $1.5 \times 10^{17} \text{ cm}^{-3}$ in Fig. 6.5 were as high as 0.958 and 0.990, respectively. The compensation increases with the nitrogen density in ZnSe, and Hall mobility decreases. The donor impurities with large E_D mentioned in Sec. 6.2 presumably contribute to the compensation. Ruda²⁰ has calculated hole mobility in ZnSe by solving the Boltzmann transport equation by the variational method, and showed that ultimate limit for the hole mobility in ZnSe at 300 K was be about $110 \text{ cm}^2/(\text{Vs})$. The highest Hall mobility we obtained was $86 \text{ cm}^2/(\text{Vs})$, and the value is fairly good value of the Hall mobility in ZnSe.

6.5. Relationships between electrical and photoluminescence properties¹¹⁻¹⁷

Electrical properties are usually measured at 300 K, but the above optical properties are measured at 12 K. Higher temperature for PL measurements is necessary to discuss the relationships between electrical and PL properties.

Figure 6.6 shows temperature dependence of PL spectrum from the N-doped p-type ZnSe layers with hole concentration of $1 \times 10^{17} \text{ cm}^{-3}$ at 300 K. With increasing temperature, FA emission increases. Strong FA emission was observed even at 100 K. In the case of N-doped ZnSe that does not

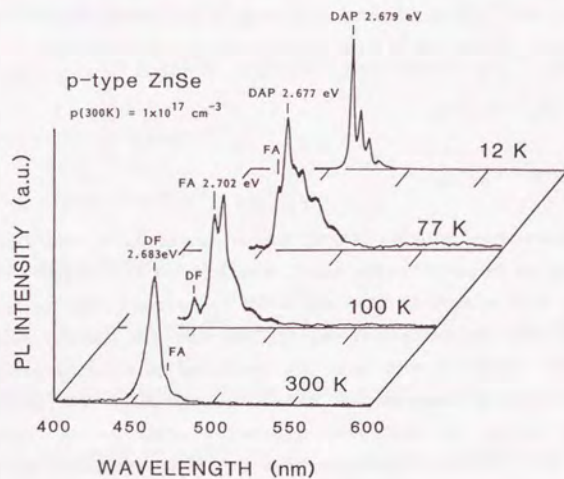


FIG. 6.6. Photoluminescence spectra from N-doped p-type ZnSe layers at various temperatures.

exhibit p-type conduction, FA emission was quenched at temperatures below 100 K.⁴ High acceptor concentration accomplished by active-nitrogen doping presumably makes FA emission more intense. N-doped ZnSe with strong FA emission above 100 K usually exhibited p-type conduction at room temperature. FA emission was observed even at 300 K as shown in Figs. 6.6

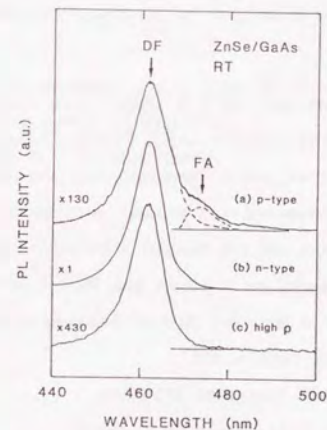


FIG. 6.7. Room-temperature PL spectra from (a) p-type, (b) n-type and (c) high-resistivity ZnSe layers.

and 6.7. Figure 6.7 shows PL spectra from N-doped p-type, Cl-doped n-type and undoped high-resistivity ZnSe layers at room temperature. The dominant peak at 2.687 eV in each sample is DF emission. Undoped ZnSe exhibits weak DF emission. Intensity of DF emission increases with increasing donor concentration. DF emission from n-type ZnSe is very strong. With respect to p-type, an emission at 2.616 eV was observed only

for p-type ZnSe. Temperature dependence of PL properties indicates that the 2.616-eV peak is FA emission. Observation of strong FA emission suggests high acceptor concentration which is an evidence of p-type ZnSe layers.

References

- ¹ Y.S. Park, P.M. Hemenger, and C.H. Chung, *Appl. Phys. Lett.* **18**, 45 (1971).
- ² J. Nishizawa, K. Itoh, Y. Okuno, and F. Sakurai, *J. Appl. Phys.* **57**, 2210 (1985).
- ³ T. Mitsuyu, K. Ohkawa, and O. Yamazaki, *Appl. Phys. Lett.* **49**, 1348 (1986).
- ⁴ K. Ohkawa, T. Mitsuyu, and O. Yamazaki, *J. Cryst. Growth* **86**, 329 (1988).
- ⁵ J.L. Merz, K. Nassau, and J.W. Shiever, *Phys. Rev. B* **8**, 1444 (1973).
- ⁶ Y. Yamada, T. Taguchi, and A. Hiraki, *Inst. Phys. Conf. Ser. No 95: Chapter 6*, paper presented at Int. Conf. "Shallow Impurities in Semiconductors" (Lingköping, Sweden, 1988), p. 377.
- ⁷ P.J. Dean, *Czech. J. Phys. B* **30**, 272 (1980).
- ⁸ R.N. Bhargava, *J. Cryst. Growth* **59**, 15 (1982).
- ⁹ P.J. Dean, W. Stutius, G.F. Neumark, B.J. Fitzpatrick, and R.N. Bhargava, *Phys. Rev. B* **27**, 2419 (1983).
- ¹⁰ K. Kosai, B.J. Fitzpatrick, H.G. Grimmeiss, R.N. Bhargava, and G.F. Neumark, *Appl. Phys. Lett.* **35**, 194 (1979).
- ¹¹ K. Ohkawa, T. Karasawa, and T. Mitsuyu, in *Abstracts of 6th International Conference on Molecular Beam Epitaxy, San Diego, August 1990, PIII-21*
- ¹² K. Ohkawa, T. Karasawa, and T. Mitsuyu, *J. Cryst. Growth* **111**, 797 (1991).
- ¹³ K. Ohkawa, T. Karasawa, and T. Mitsuyu, *Jpn. J. Appl. Phys.* **30**, L152 (1991).
- ¹⁴ K. Ohkawa, and T. Mitsuyu, to be published in *J. Lumin.*
- ¹⁵ K. Ohkawa, A. Ueno, and T. Mitsuyu, to be published in *Jpn. J. Appl. Phys.* (1991).
- ¹⁶ K. Ohkawa, and T. Mitsuyu, *J. Appl. Phys.* **70**, 439 (1991).
- ¹⁷ K. Ohkawa, A. Ueno, and T. Mitsuyu, to be published in *J. Cryst. Growth* (1992).
- ¹⁸ Y. Shirakawa, and H. Kukimoto, *J. Appl. Phys.* **51**, 2014 (1980).
- ¹⁹ G.F. Neumark, *J. Appl. Phys.* **65**, 4858 (1989).
- ²⁰ H.E. Ruda, *J. Appl. Phys.* **59**, 3516 (1986).

CHAPTER 7

CONCLUSION

In this thesis, photoluminescence and electrical properties of impurity-doped ZnSe layers have been investigated and discussed from a fundamental point of view. The breakthrough of achieving amphoteric doping which provides highly conductive p- and n-type ZnSe layers made it possible to study the physical properties of p- and n-type ZnSe layers. The results and conclusions obtained in this study are summarized as follows.

(Chapter 1)

Basic physical properties of wide band-gap II-VI compounds were described comparing with III-V compound. Difficulty in amphoteric doping of II-VI compounds was the reason why the compounds were not understood well so far.

(Chapter 2)

MBE growth and amphoteric doping of ZnSe layers were studied in detail. The optimum growth temperature of high-quality ZnSe layers was determined by electrical mobility and band-edge PL emission. ZnSe homoepitaxy was successfully achieved by the novel treatment of ZnSe substrates using dry etching with a BCl_3 plasma. The homoepitaxy provided strain-free ZnSe layers with fairly good crystallinity. A FWHM of an x-ray rocking curve reached 21 arc s that was the narrowest FWHM

ever obtained for ZnSe layers.

Ga doping for n-type and high-purity N_2^+ ion doping for p-type have supplied samples exhibiting dominant neutral donor-bound exciton emission (I_2) and dominant neutral acceptor-bound exciton emission (I_1), respectively.

Successful growth of degenerated n-type and highly conductive p-type ZnSe layers was accomplished for the first time by Cl doping and active-nitrogen doping, respectively. Electron concentration for Cl-doped ZnSe was reached the order of 10^{19} cm^{-3} where the resistivity was as low as $10^{-3} \Omega\text{cm}$. Active nitrogen generated from an rf plasma source was identified as a N_2 ($A^3\Sigma_u^+$) metastable by plasma spectroscopy. Since a N_2 molecule at the excited state has high sticking coefficient compared with that at the ground state, high-density incorporation of nitrogen was achieved. It was found by SIMS analysis that diffusion of N and Cl atoms in ZnSe during growth was negligible.

(Chapter 3)

Experimental apparatuses for PL, reflection and Hall measurements were described in this chapter. Basic optical transitions were also mentioned in detail.

There is no metal for ohmic contact to p-type ZnSe. Pt electrodes being sputter deposited on an Ar plasma-etched area was proposed for the contact. Then p-type conduction of N-doped ZnSe layers prepared by active-nitrogen doping was measured for the first time using the Pt electrodes. Drastic decrease in contact resistance to p-type ZnSe was realized by the Pt electrodes. Possible explanation of the result is that Pt had the lowest Fermi level in metals and furthermore deep levels introduced by the Ar plasma etching would act as the recombination center for current.

(Chapter 4)

The purpose of the study described in this chapter is to find out the origin of split in exciton luminescence.

Lattice parameter and biaxial strain at low temperature have been calculated, considering lattice mismatch and the difference in the thermal contraction between ZnSe and GaAs. The valence band was split into light- and heavy-hole branches by biaxial strain parallel to the heterointerface. The feature of the valence band split was in good agreement with that of the split of both I_1 and I_2 emissions observed for ZnSe heteroepitaxial layers on GaAs substrates. Comparison of impurity-doped ZnSe homo and heteroepitaxial layers confirmed the validity this theory. Temperature dependence of intensity ratio of light- and heavy-hole branches of bound exciton emission was interpreted by this theory. It was found that the I_x emission generally reported in n-type ZnSe heteroepitaxial layers was a light-hole branch of usual I_2 emission.

(Chapter 5)

The detailed study has been conducted to understand electrical and optical properties of Cl-doped n-type ZnSe layers.

Degenerated n-type ZnSe with electron concentration greater than that of Mott transition was realized for the first time by Cl doping. The highest carrier concentration has reached the order of 10^{19} cm^{-3} which is two orders of magnitude greater than that of Ga-doped ZnSe. Study of electron scattering mechanism has shown that the main scattering at high temperature is due to polar optical phonon scattering and the main scattering at low temperature is neutral impurity scattering. Since homoepitaxial layers had few lattice defects, its neutral impurity scattering was smaller compared with heteroepitaxial layers.

Effect of such high electron concentration on PL property of ZnSe was observed for the first time. I_2 emission shifted to higher energy together with asymmetric broadening with tail extending to lower energy. The phenomena were interpreted by the screening and Stark effects: the screening effect decreased the binding energy of excitons and the Poisson distribution of ionized impurities from an exciton reflected in the line shape of I_2 emission through the Stark effect. Ionized impurity concentration for degenerated ZnSe was determined by fitting theoretical calculation to the spectra obtained by experiments and the ionized impurity concentration was in good agreement with electron concentration which is equal to the ionized donor concentration.

(Chapter 6)

This chapter described the study of electrical and optical properties of N-doped p-type ZnSe layers prepared by active-nitrogen doping.

High concentration of free holes for N-doped ZnSe layers was observed in Hall measurement. The highest hole concentration at 300 K was greater than $1 \times 10^{17} \text{ cm}^{-3}$. The mobilities varied from 11 to $86 \text{ cm}^2/(\text{Vs})$ depending on hole concentration. It was found that the compensation was increased with increasing nitrogen concentration. The compensation ratio was greater than 0.9 for highly-conductive p-type ZnSe grown by active-nitrogen doping.

Anomalous zero-phonon peak energy of donor-acceptor pair emission (DAP) from N-doped p-type ZnSe was observed at 2.68 eV which was smaller than the energy commonly observed at 20 meV. The difference was explained to be due to deep donors (ionization energy 50 meV) which would be responsible for the compensation.

It was found that high N concentration greater than $3 \times 10^{18} \text{ cm}^{-3}$

introduced nonradiative centers that acted as carrier traps, thus p-type ZnSe was obtained for the N concentration less than $3 \times 10^{18} \text{ cm}^{-3}$. It was pointed out that observation of radiative recombination between a free electron and an acceptor hole (FA) at high temperature ($> 100 \text{ K}$) was the distinctive feature of p-type ZnSe. The intense FA emission indicates that many nitrogens act as acceptors.

PL properties of n-type and p-type ZnSe layers revealed the physical information about impurity levels, lattice defects and effect of strain. Electrical properties exhibited activation of impurities and scattering mechanisms in wide band-gap II-VI compounds. Information obtained for physical properties of p-type and n-type ZnSe provided a fundamental understanding of wide band-gap II-VI compounds. The breakthrough which enabled the realization of amphoteric doping of ZnSe has made it possible to use wide band-gap II-VI "compounds" as a real "semiconductor" materials for a variety of useful applications.

APPENDIX

APPENDIX A.

Preparation of ZnSe substrates for homoepitaxy

A.1. Dry etching of ZnSe^{1,2}

The dry etching was carried out in an etching system with parallel electrodes. BCl_3 gas (99.9999 %) was used as a reactive gas, and the pressure was varied from 7 to 95 mTorr at power density of 1.1 W/cm^2 of radio-frequency. The ZnSe substrates were positioned on a quartz plate on water-cooled cathode.

ZnSe can be etched by BCl_3 plasma, and the gas pressure dependence of the etching rate is shown in Fig. A.1. Mechanism of the etching would be mainly due to chemically enhanced physical sputtering,³ i.e., chlorine radicals make a chloride layer on surface, then the chloride layer is sputtered by ions which may be chlorine ions. The etching rate gradually increased with increasing the pressure, then the rate decreased abruptly above 60 mTorr. The increase in etching rate may be ascribed to increase both in the chlorine radicals and ions, and decrease in rate is due to decrease in the ion energy for sputtering because higher pressure makes the mean free path of ions shorter. The most rapid etching rate, 30-50 $\mu\text{m/h}$, was obtained at 60 mTorr. The dry-etched substrates exhibited mirror-like surface morphology even after 10- μm etching. The Se residue

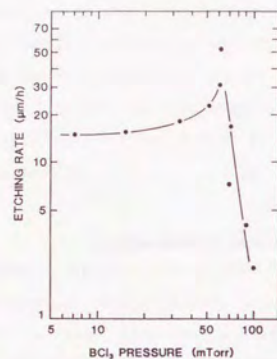


FIG. A.1. Etching rate of ZnSe v.s. BCl₃ pressures.

often observed on chemically etched surface did not exist.

Polishing damage can be observed in PL measurement since the damage has a few microns in thickness. Low-temperature PL spectra from as-polished and etched ZnSe substrates are shown in Fig. 2.5. Drastic changes were observed before and after the dry etching: intensity of the donor-acceptor pair recombination emission (DAP) increased by 10 times, exciton emissions including free exciton emission (E_x) at 442.2 nm (2.804 eV), neutral donor-bound exciton emission (I_2) at 443.1 nm (2.798 eV) and neutral acceptor-bound exciton emission (I_1) at 443.9 nm (2.793 eV) clearly appeared and the peak intensities remarkably increased by about 100 times. The polishing damage would have many nonradiative centers which might act as a deep level induced by degradation of crystallinity. Therefore, these changes observed here in the PL properties give evidence that the polishing damage was eliminated by the dry etching.

A.2. Thermal etching²

In spite of the elimination of the polishing damage, a dry etching newly creates plasma damage on a subsurface of the substrates.⁴ In this case, the plasma damage would consist of ion-induced lattice damage and a residual chloride layer. The PL analysis that can detect the polishing damage extending to a few microns in depth is impossible to appraise the subsurface, i.e., a few atomic layers. Thus quality of the subsurface was evaluated by studying a homoepitaxial layer which inherited the nature of the few upper atomic layers of the surface.

Thermal etching is a significant treatment of ZnSe substrates after dry etching. The thermal etching condition was studied by reflection high-

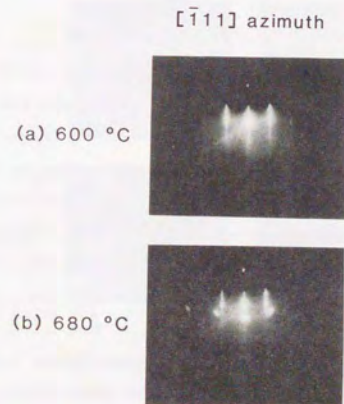


FIG. A.2. RHEED patterns along [111] direction of dry-etched ZnSe substrate at (a) 600 °C and (b) 680 °C.

energy electron diffraction (RHEED) observation. A streaked RHEED pattern from the ZnSe substrate etched at the pressure of 60 mTorr was observed before the thermal etching both at elevated and room temperature. This RHEED pattern changed to more sharp streaks by the thermal etching above 440°C. At this temperature, the plasma damage on the surface would be decomposed. Elongated streaky pattern of RHEED at 600°C is shown in Fig. A.2 (a). This pattern indicates high-quality surface. Spots shown in Fig. A.2 (b) appeared above 650°C. ZnSe was supposed to be decomposed at the temperature, then Zn islands were formed on the surface. It was found that the thermal etching was effective to obtain clean and smooth surface in the temperature range from 440 to 650°C.

A.3. Optimum etching condition²

Observation of the surface roughness was made by a Nomarski microscope. Nomarski microphotographs of ZnSe substrates and layers are shown in Fig. A.3. Scratched lines are seen on surface of as-polished substrates, but the Nomarski microscope is not able to see the polishing damage on the surface. The scratched lines were created during the polishing process. Surface morphology of the dry-etched substrates depended on the BCl_3 pressure at the dry etching. The substrates etched in 7 and 33 mTorr exhibit many circle dips and scars of the scratched lines. The dips were positioned in a row. It was found by comparison in morphology between homoepitaxial layers and those substrates that the row was on a twin boundary. On the other hand, smooth surface morphology was observed at 95 mTorr: the scars of the scratched lines and the twin boundary were not detected. The homoepitaxial layer on the substrate etched at 33 mTorr showed scaly surface morphology. It would

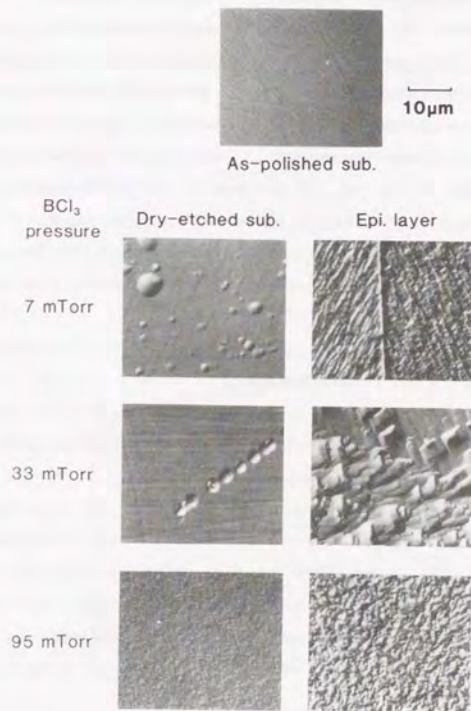


FIG. A.3. Nomarski microphotographs of as-polished ZnSe substrate, dry-etched substrates and homoepitaxial layers on the substrates etched at various BCl_3 pressures.

be intrinsic morphology of the as-grown (110) ZnSe.

Crystallinity of the substrates and homoepitaxial layers was evaluated by double-crystal x-ray diffraction analysis. Figure A.4 shows FWHMs of (220) x-ray rocking curves. The FWHM of the as-polished substrate was about 120 arc s, and it changed to 60 arc s after the dry etching. This remarkable improvement is consistent with the change in the PL spectra shown in Fig. 2.5. As a FWHM of an epitaxial layer on an as-polished substrate was 146 arc s, FWHM of the polishing damage would be at least 150 arc s. The plasma damage is too thin to measure in this x-ray analysis. The actual substrate would show the FWHM of 60 arc s. The

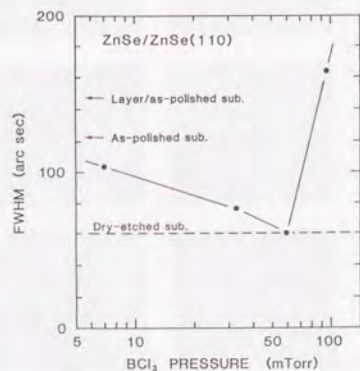


FIG. A.4. FWHMs of x-ray rocking curves of (220) diffraction for ZnSe homoepitaxial layers v.s. BCl₃ pressure at dry etching. FWHMs for as-polished substrate and homoepitaxial layer on the as-polished substrate are indicated by arrows. Dashed line shows typical FWHM for 10- μ m etched substrates.

FWHMs of the homoepitaxial layers on the dry-etched substrates depended on the BCl₃ pressure in the dry etching. In spite of the thermal etching, the residual plasma damage would exist on the subsurface. The smallest plasma damage will be caused at 60 mTorr for the effective etching of ZnSe as shown in Fig. A.1. Very little plasma damage was decomposed by the thermal etching, then FWHM of the homoepitaxial layer grown on the substrate etched at this pressure reached 60 arc s. The FWHM is as narrow as that of the substrates themselves. Higher quality of homoepitaxial layer is possible to be obtained if higher-quality ZnSe single crystals are used. (The best value of FWHM has reached 21 arc s, see Sec. 2.2.2.)

Observation of surface roughness was made by a Nomarski microscope. Nomarski microphotographs of ZnSe layers are shown in Fig. A.5. ZnSe layers on (110) GaAs and (110) ZnSe substrates show scaly surface morphology. The morphology is presumably intrinsic morphology of as-grown (110) ZnSe. Lines are observed in the homoepitaxial layer on (110) ZnSe substrate. The lines are the boundary of scaly morphology; the morphology shows different directions of scales before and after the line. The angle between the different directions is about 70°. The angle is in good agreement with angles between (100) directions on the opposite side of twinning boundaries as shown in Fig. A.6. The angle between (100)-directions is given by

$$180 - 2\text{arc cos}(3^{-\frac{1}{2}}) = 70.52^\circ . \quad (\text{A.1})$$

Therefore the line is the twinning boundary. ZnSe layers on (100) and (111) substrates exhibit smooth surface morphology. The layer on (100) substrate has good crystallinity as mention above. However the layer on (111)

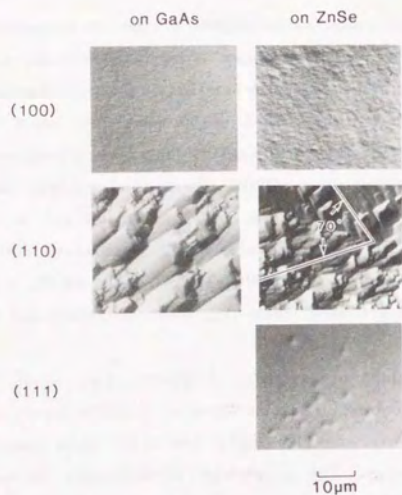


FIG. A.5. Nomarski microphotograph of ZnSe layers on GaAs and ZnSe substrates with (100), (110) and (111) orientation.

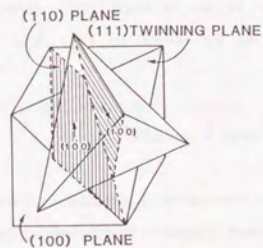


FIG. A.6. Plane indices of a zinc blende crystal with twin.

substrate has poor crystallinity. Further study will be needed for the epitaxial growth on (111) substrates. In view of application for devices, (100) epitaxial growth is promising because smooth surface and good crystallinity are obtainable.

References

- ¹ K. Ohkawa, T. Karasawa, A. Yoshida, T. Hirao, and T. Mitsuyu, *Appl. Phys. Lett.* **54**, 2553 (1989).
- ² K. Ohkawa, T. Karasawa, and T. Mitsuyu, *J. Vac. Sci. Technol. B* **9**, 1934 (1991).
- ³ R.A. Haring, A. Haring, F.W. Saris, and A.E. deVries, *Appl. Phys. Lett.* **41**, 174 (1982).
- ⁴ I.H. Connick, A. Bhattacharyya, K.N. Ritz, and W.L. Smith, *J. Appl. Phys.* **64**, 2059 (1988).

APPENDIX B

ZnSe p-n JUNCTION LEDs

B.1. MBE Growth of ZnSe p-n Junction¹

The breakthrough of achieving amphoteric doping of ZnSe was accomplished by Cl doping for n-type conduction² and active-nitrogen doping for p-type conduction. Successful doping has made it possible to fabricate devices made by II-VI compounds, especially blue light-emitting diodes (LEDs)³ and blue laser diodes (LDs)⁴.

The design of ZnSe LED structure is shown in Fig. B.1. ZnSe single-crystal substrates used were grown using a vapor transport method and were (100) oriented and n-type (treated by Zn extraction). The substrate was dry-etched by a BCl_3 plasma to remove polishing damage by $10 \mu\text{m}$ in depth.^{5,6} Prior to the growth, dry-etched ZnSe substrate was thermally etched at 600°C for 10 min under ultrahigh vacuum in a MBE chamber. The growth temperature was about 325°C . The beam flux ratio in

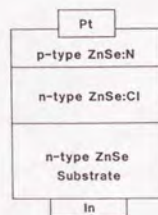


FIG. B.1. Schematic view of the cross section of a ZnSe LED.

atomic number was kept at $\text{Zn:Se} = 2:1$. A Cl-doped ZnSe layer was grown on the dry-etched substrate by MBE. Source materials used were ZnCl_2 powder, and elemental Zn and Se. The carrier concentration intended for the n-type layer was $5 \times 10^{18} \text{cm}^{-3}$. N-doped ZnSe layer was grown by using the active nitrogen doping during MBE growth. The substrate was irradiated with Zn, Se and active-nitrogen beams. Free hole concentration intended was the order of 10^{16}cm^{-3} . The p-n junction structure fabricated was p-ZnSe ($1.3 \mu\text{m}$)/n-ZnSe ($4.5 \mu\text{m}$)/n-ZnSe-substrate.

After the MBE growth, ohmic contact to the n-type ZnSe substrate was made by an In-Hg alloy followed by an annealing. The final steps of fabricating LED are sputter deposition of 1-mm Pt electrodes on p-type layer as described in Sec. 3.3.

B.2. Characteristics of ZnSe LEDs¹

Current-voltage (I-V) characteristics were measured at room temperature. The ZnSe p-n junction LEDs exhibit good rectification properties as shown in Fig. B.2 (a). The characteristics was expressed by the following equation

$$I = a [\exp(qV/nkT) - 1] . \quad (\text{B.1})$$

The equation for $n = 2$ is shown in the solid line in Fig. B.2 (b). A plot of logarithm of current against forward voltage is linear in the current range of up to 10^{-6}A , and is in good agreement with the solid line for $n = 2$. This result indicates that the current due to recombination between an electron and a hole is dominant in this range. With increasing current, the value of n increases owing to the series resistance effect.

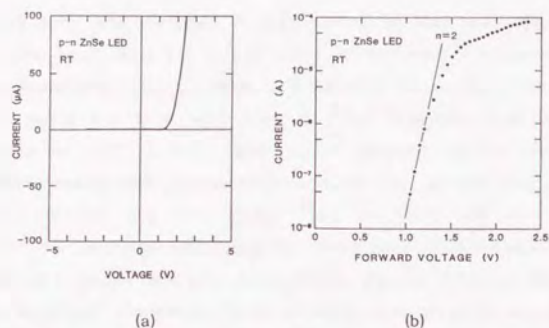


FIG. B.2. I-V characteristics of a ZnSe LED at room temperature in (a) linear scale and (b) logarithm scale for the current.

Photoluminescence (PL) spectra from the ZnSe:N/ZnSe:Cl/n-ZnSe (the LED sample) are shown in Fig. B.3. Photoluminescence observed is emitted from the N-doped ZnSe layer since the top N-doped layer is as thick as $1.3 \mu\text{m}$ for PL measurement. The 12-K PL spectrum shows strong donor-acceptor pair emission (DAP) and weak neutral acceptor-bound exciton emission (I_1). With increasing temperature, recombination emission between a free electron and an acceptor hole (FA) increased compared with DAP emission. The 77-K PL spectrum is dominated by FA emission. Peak energies of DAP and FA emissions are expressed by Eqs. (3.4,6) as follows:

$$\hbar\omega_{\text{DAP}} = E_g - (E_D + E_A) + e^2/(4\pi\epsilon_s r), \quad (\text{B.2})$$

$$\hbar\omega_{\text{FA}} = E_g - E_A + \frac{1}{2} kT. \quad (\text{B.3})$$

Using the peak energies of DAP emission at 12 K and FA emission at 77 K in Fig. B.3, the acceptor and donor ionization energies are estimated to be

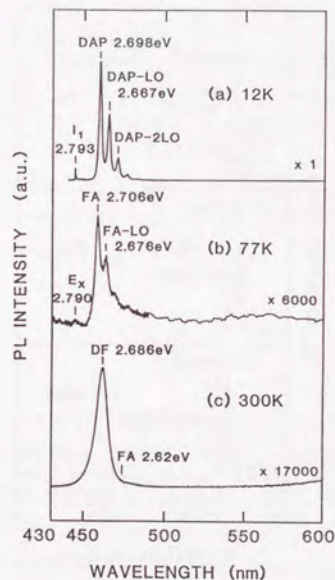


FIG. B.3. Photoluminescence spectra from a structure ZnSe:N/ZnSe:Cl/n-ZnSe-substrate at 12, 77 and 300 K.

$E_A = 111 \text{ meV}$ and $E_D = 25 - 30 \text{ meV}$, respectively. The E_A calculated is the same as the value for an N acceptor determined by Dean et al.,⁷ and the E_D also has a reasonable value as a donor impurity.

Electroluminescence (EL) spectra from the ZnSe p-n junction LED are shown in Fig. B.4. The current drawn was 0.2 mA. Comparison with the PL spectrum at 77 K leads to the assignment of 77-K EL emissions at 2.775 and 2.701 eV to be DF and FA emissions, respectively. These EL emissions

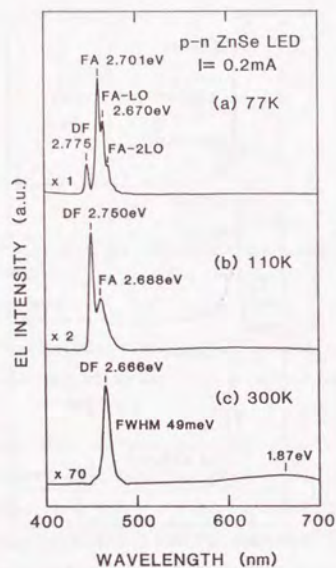


FIG. B.4. Electroluminescence spectra from a homoepitaxial ZnSe p-n junction LED at 77, 110 and 300 K.

would be generated at the p-type ZnSe region since Cl-doped ZnSe has never exhibited FA emission. FA emission gradually quenched with increasing temperature. The 110-K EL spectrum is dominated by DF emission. At room temperature of about 300 K, the EL spectrum shows strong DF emission. Since other deep-level emissions were well suppressed, the color of the light was pure blue for the unaided eye. The full width at half-maximum (FWHM) of a (400) x-ray rocking curve for the

homoepitaxial p-n junction layer was as narrow as 108 arc s, it was fairly better than 270 arc s of p-ZnSe/GaAs heteroepitaxy³. High quality of the p-n junction probably has suppressed deep-level emissions and has resulted in a narrow FWHM of 49 meV for DF emission at 300 K.

Cl doping for the formation of n-type ZnSe layers, newly developed active-nitrogen doping for p-type ZnSe layers, and excellent crystalline quality owing to homoepitaxy lead to the realization of high quality LEDs in blue region by using ZnSe for the first time.

References

- ¹ K. Ohkawa, A. Ueno, and T. Mitsuyu, in Extended Abstracts of the 1991 International Conference on Solid State Devices and Materials, Yokohama, 1991, p. 704.; to be published in Jpn. J. Appl. Phys. December (1991).
- ² K. Ohkawa, T. Mitsuyu, and O. Yamazaki, in Extended Abstracts of the 1986 International Conference on Solid State Devices and Materials, Tokyo, 1986, p. 635; J. Appl. Phys. **62**, 3216 (1987).
- ³ K. Ohkawa, T. Karasawa, and T. Mitsuyu, Jpn. J. Appl. Phys. **30**, L152 (1991).
- ⁴ K. Ohkawa, A. Tsujimura, S. Hayashi, S. Yoshii, and T. Mitsuyu, to be published in Jpn. J. Appl. Phys.
- ⁵ K. Ohkawa, T. Karasawa, A. Yoshida, T. Hirao, and T. Mitsuyu, Appl. Phys. Lett. **54**, 2553 (1989).
- ⁶ K. Ohkawa, T. Karasawa, and T. Mitsuyu, J. Vac. Sci. Technol. B **9**, 1934 (1991).
- ⁷ P.J. Dean, W. Stutius, G.F. Neumark, B.J. Fitzpatrick, and R.N. Bhargava, Phys. Rev. B **27**, 2419 (1983).

